

Structural reliability assessment of buildings subjected to wind loading

An assessment of the main bearing structure
at foundation level of dynamically sensitive
buildings designed within the Eurocode
framework

L.C. la Gasse

Structural reliability assessment of buildings subjected to wind loading

An assessment of the main bearing structure at foundation level of dynamically sensitive buildings designed within the Eurocode framework

by

L.C. la Gasse

to obtain the degree of Master of Science
in Civil Engineering, track Structural Mechanics
at the Delft University of Technology,

to be defended publicly on Thursday 29 June 2017 at 10.30 a.m.

Student number:	4147804	
Project duration:	September 19, 2016 – June 29, 2017	
Thesis committee:	Prof. dr. ir. L.J. Sluys,	TU Delft, chairman
	Dr. ir. M. A. N. Hendriks,	TU Delft
	ir. L. J. M. Houben,	TU Delft
	Prof. dr. ir. R. D. J. M. Steenbergen,	TNO, UGent
	ir. N. E. Meinen,	TNO

An electronic version of this thesis is available at <http://repository.tudelft.nl/>.

Preface

This thesis has been written as a final work in partial fulfilment for the degree of Master of Science in Civil Engineering for the master track of Structural Engineering and specialization Structural Mechanics at the Delft University of Technology. The subject of this research was formed in cooperation with TNO, the Netherlands Organisation for applied scientific research TNO, and specifically the department of Structural Reliability in Delft. They supported the development of this thesis for the entire duration of the research.

I would like to thank my entire graduation committee for their guidance and support throughout the development of the research. Thanks to Bert Sluys and Max Hendriks for their objective and critical views and their help to let me stay on track. I would like to pay special thanks to Raphaël Steenbergen for supporting me with his extensive knowledge on the subject and to Nadieh Meinen for helping me to get familiar with the subject and for providing me with helpful remarks on this thesis more than once. Furthermore I would like to thank my colleagues from both the TNO departments of Structural Reliability and Structural Dynamics for their help on the subject, but also for their interest and concern in me. I have enjoyed working among them for the past year.

Last, I would like to thank my friends and family for their support throughout my studies, but especially the last year.

Liesette la Gasse
Delft, June 2017

Abstract

Structures are considered safe, when they comply with minimum reliability requirements which are expressed by a minimum reliability index β in the Eurocodes (EN1990). However, a complete reliability assessment for every structure would be very time-consuming. Therefore in the Eurocode a partial factor approach is utilized. In this research it is investigated how the reliability of the main bearing structure of a dynamically sensitive building designed within the Eurocode framework can be assessed in a full-probabilistic way for global response to wind loading including both size and dynamic effects. The global response of buildings to wind loading as well as uncertainties in this wind load have been the subject of many research, but few reference has been made to the reliability of structures by linking both aspects. Current research provides this link and investigates the reliability of these buildings with respect to the target reliability in EN1990. For the purpose of this research the methods were developed for alongwind response at foundation level of the main bearing structure for slender high-rise buildings with a concrete core bearing structure.

First a full-probabilistic assessment procedure is developed which allows for the determination of the reliability index β of these wind-loaded structures. This procedure links and quantifies both the uncertainties in wind climate, terrain effects, global dynamic response of buildings and resistance full-probabilistically. For this purpose location-specific wind speed measurements, building shape- and terrain-specific pressure measurements and literature data are used. In this research, the combined effect of simultaneously measured pressures over both windward and leeward façade from a boundary layer wind tunnel test and the resulting dynamic alongwind buffeting response of the structure is evaluated through transient finite element analysis of a beam model. From a study on the influence of the boundary conditions at the base of the beam model, it was found that a cantilevered beam model is sufficient to derive the response at foundation level. In the reliability assessment of the main bearing structure the derived response coefficients can be incorporated directly in the stochastic wind load model. This in contrast to traditional probabilistic approaches where the global response is never addressed as such, but a combination of the modelling of the extreme pressure coefficients and a correcting size reduction and dynamic amplification factor is conventional.

To derive representative pressures to apply in the transient finite element analysis, methods to derive and evaluate both decay constant C_r and averaging constant C_T were presented. In this research and in previous research significantly lower values are derived than proposed in EN1991-1-4 and by conventional methods. The latter are therefore found to overestimate the size reduction effect.

The description of the stochastic wind load model requires the modelling of the extreme wind speeds and extreme response coefficients. For this purpose two distribution types are considered; a distribution conventional for wind engineering which requires two parameters to be fitted and a distribution which requires three parameters to be fitted. The second distribution follows the data more accurately, but is also more sensitive to individual measurements. It is recommended to maximise the amount of extreme response coefficients by methods proposed in this research to reduce the effect of statistical and sampling uncertainties. For the response coefficients derived for this research the first distribution type was found to be too conservative.

Second the proposed assessment procedure was used on a case study building to give an indication of the reliability of current designed buildings by EN1991-1-4 by means of a Level II reliability calculation. In general, the derived β -values are close to the target reliability $\beta_{\text{target}} = 3.8$ in EN1990 for standard design situations¹. Modelling the wind speed by the two parameter distribution leads to conservative reliability levels, where a three parameter distribution may only be used when sampling uncertainties are accounted for. It was found that the wind speed has the highest influence on the derived reliability levels. Therefore it is to be expected that similar reliability levels will be found for other buildings in similar wind conditions, which is the case for Dutch design situations. When conservative values for both fundamental frequency and damping are adopted in practice, a positive influence with respect to the reliability level is found.

¹Corresponds to consequence class 2 (e.g. residential and office buildings), ultimate limit state and a 50 year reference period

Contents

Preface	iii
Abstract	v
List of Figures	xi
List of Tables	xv
List of symbols	xvii
List of Latin symbols	xvii
List of Greek symbols	xix
List of abbreviations	xix
1 Introduction	1
1.1 Problem statement	1
1.2 Aim of the research	1
1.3 General scope.	2
1.4 Outline	2
I Literature review	5
2 Basics on approaches to wind loading	7
2.1 Basic description of wind	7
2.2 Davenport's wind loading chain	8
2.2.1 Wind climate.	8
2.2.2 Influence of terrain	8
2.2.3 Wind-structure interaction - Aerodynamic coefficients	9
2.2.4 Global structural response	10
2.3 Wind loading according to the Eurocode	12
2.3.1 Wind climate.	12
2.3.2 Influence of terrain	13
2.3.3 Wind-structure interaction.	14
2.3.4 Structural effects.	14
3 Approaches to global wind loading	17
3.1 Correlation of wind pressures	17
3.1.1 Correlation.	17
3.1.2 Low-pass filters	19
3.2 Dynamic response of a structure	21
3.2.1 Cantilever beam model	21
3.2.2 White noise approach	22
3.3 Davenport's approach to dynamic global wind loading	22
3.3.1 Single degree of freedom system	22
3.3.2 Cantilever beam model	24
3.4 Other approaches to dynamic global wind loading	25
3.4.1 EN1991-1-4 Annex B	25
3.4.2 EN1991-1-4 Annex C	25
3.4.3 Alternative gust response factor	26
3.5 Assumptions in global approaches	26

4	Probabilistic approaches to wind loading	29
4.1	Uncertainties in the wind loading model	29
4.1.1	Uncertainty typecasting	30
4.1.2	Summary static local wind loading uncertainties	30
4.1.3	Global dynamic wind load uncertainties	32
4.1.4	Conclusion.	35
4.2	Historical development of accounting for wind loading uncertainties	35
4.3	Method of Cook-Mayne	35
4.3.1	Full order method	36
4.3.2	'V-c method' versus 'q-c method'	37
4.3.3	Simplified method and Cook-Mayne fracture	37
4.4	Method by Davenport.	37
4.4.1	Davenport's wind loading uncertainties	37
4.4.2	Davenport's full probabilistic method	39
4.5	Probabilistic Model Code approach.	39
4.6	Structural reliability assessment procedure by Meinen (2015).	40
5	Theory on modelling of extremes	43
5.1	General description and requirements of sample data	43
5.2	Univariate theorem	43
5.3	Generalized extreme value distribution	44
5.3.1	Definition of the generalized extreme value distribution.	44
5.3.2	Block method	44
5.3.3	GEV distributions in the field of wind engineering	45
5.4	Sampling uncertainties: Bootstrap design-point method	45
II	Development of the probabilistic assessment procedure	47
6	Methodology for the assessment procedure	49
6.1	General methodology for the probabilistic assessment procedure	49
6.2	Applicability of the assessment procedure	51
6.2.1	General remarks	51
6.2.2	Load effects and combinations	51
6.2.3	Wind directionality	52
7	Method development in derivation response coefficients	53
7.1	Representative pressures	53
7.1.1	Coherence and decay constant.	54
7.1.2	Moving average filter and averaging constant	54
7.2	Response coefficients through finite element modelling	57
7.2.1	General finite element model method development	57
7.2.2	Evaluation of model choices	61
7.3	Probabilistic modelling of extreme response coefficients	64
7.3.1	Block duration	64
7.3.2	Uncertainties of dynamic properties	66
7.4	Summary of methods in deriving response coefficients	69
8	Reliability assessment procedure	71
8.1	General assessment procedure	71
8.2	Resistance.	71
8.2.1	Simplified stochastic resistance model.	72
8.2.2	Characteristic value resistance model procedure	72
8.2.3	Full-probabilistic resistance model	73
8.2.4	Conclusion.	74

8.3	Wind loading effect model	74
8.3.1	Air density ρ_{air}	74
8.3.2	Wind speed v_{pot}	75
8.3.3	Roughness factor c_r	75
8.3.4	Response coefficient \hat{c}_M, \hat{c}_Q	75
8.3.5	Dynamic properties uncertainty factor χ_{cd}	75
8.3.6	Model uncertainty factor χ_{model}	75
III	Reliability assessment of the case study	77
9	Description case study	79
9.1	Case study building	79
9.2	Wind speed data	79
9.3	Wind tunnel measurement data	80
10	Description wind speeds	81
10.1	Description of the wind speed data	81
10.2	Distribution fitting of the wind speed data	82
10.2.1	Distribution fitting	82
10.2.2	Level I characteristic and design wind speeds	82
10.2.3	Parameters distribution fits	83
10.3	Sampling uncertainties	83
10.4	Conclusions.	84
11	Description global response coefficients	85
11.1	Description of the response coefficient data	85
11.2	Distribution fitting of the response coefficient data	86
11.2.1	Distribution fitting	86
11.2.2	Cook-Mayne design value	86
11.2.3	Parameters distribution fits	87
11.2.4	Dependence of distribution fit on block duration	87
11.3	Sampling uncertainties	88
11.4	Conclusions.	88
12	Reliability assessment	91
12.1	Input	91
12.1.1	Level of calculation	91
12.1.2	Description of stochastic parameters	91
12.2	Reliability results	91
12.2.1	Simplified stochastic resistance model.	92
12.2.2	Full-probabilistic resistance model	93
12.2.3	Conclusions on the first reliability results	95
12.3	Design values	96
12.3.1	Response coefficients design fractile	96
12.3.2	Derived design values and EN1991-1-4 design values	97
12.4	Sensitivity study stochastic parameters wind loading effect model	97
12.4.1	Influence of the number of stochastic parameters in the reliability analysis	97
12.4.2	Assumptions in dynamic property uncertainty factor χ_{cd}	98
13	Discussion on the reliability results	99
13.1	Wind speeds	99
13.2	Response coefficients	99
13.3	Reliability assessment.	100

Conclusions and recommendations	103
14 Conclusions	105
15 Recommendations	109
Bibliography	111
Appendices	115
A Basics on structural reliability	117
A.1 General	117
A.2 Level III methods	118
A.3 Level II methods	118
A.4 Level I methods	119
A.5 Comparison Level III and Level II methods	119
B Figures to EN1991-1-4	121
C Assessment procedure Meinen (2015)	125
D Numerical procedures	127
D.1 Welch's power spectral density estimation method	127
D.2 Frequency smoothing data	127
D.3 Nonlinear least square curve fitting	128
E Finite element analysis	129
E.1 Time-dependency	129
E.2 Rayleigh damping.	129
E.3 Verification dynamic model.	129
E.4 Time-series of response.	131
E.4.1 Step 2	131
E.4.2 Step 3	132
E.4.3 Timoshenko	133
F Derivation response coefficients	135
F.1 Cross-correlation pressure coefficients on wind- and leeward façade	135
F.2 Autocorrelation base shear coefficients	136
G Input DynaPile	137
G.1 Pile properties	137
G.2 Soil properties	137
H Definition stochastic parameters	139
H.1 Roughness factor	139
H.2 Resistance.	139
H.2.1 Level I resistance procedure	139

List of Figures

1.1	Overview of the structure of the report	4
2.1	Spectrum of horizontal wind after Van der Hoven	7
2.2	Distinction between mean and fluctuating part of the wind speed (Steenbergen et al., 2012)	8
2.3	Davenport’s wind loading chain (Davenport, 1961)	8
2.4	Davenport’s power law profiles of mean wind velocity over different terrain types (Isyumov, 2012)	9
2.5	Davenport’s random vibration approach for the wind-induced response of buildings and structures (Davenport, 1964)	10
2.6	Time histories of: (a) wind force, (b) response of a structure with a high natural frequency and (c) response of a structure with a low natural frequency (Holmes, 2001)	11
2.7	Response spectral density for a structure with significant resonant contributions (Holmes, 2001)	11
2.8	Wind loading model of EN1991-1-4 (Meinen, 2015)	13
3.1	Maximum/minimum force coefficients low-rise building. The two figures on the left represent the time of maximum/minimum coefficients at windward and leeward side, respectively. The right figure displays the time of maximum force on windward and leeward face combined. The dotted lines indicate Eurocode pressure coefficients. (Hansen, 2012). Reproduced by permission of SiteCover.	19
3.2	Power spectral density functions for the longitudinal turbulence component.	23
4.1	Joint probability density function of wind speed \bar{V} and peak loading coefficient \hat{c} Cook and Mayne (1979)	36
4.2	First- and second order joint probability density function of wind speed \bar{V} and peak loading coefficient \hat{c} Cook and Mayne (1980)	36
4.3	Statistical factors in Davenports wind loading chain (Davenport, 1983a)	38
5.1	The three types of generalized extreme value distributions: the PDF and the CDF in the Gumbel domain (Meinen, 2015).	44
5.2	Visualization of the Bootstrap design-point method (Meinen, 2015)	45
6.1	Overview of the focus of this research	51
6.2	Considered building typology	52
7.1	Root coherence	55
7.2	Root coherence of all taps up to a frequency of 0.6 Hz	55
7.3	Tributary areas	56
7.4	Aerodynamic admittance and equivalent moving filter by method of Dyrbye and Hansen (1999) for a pressure tap in the middle of the façade	57
7.5	Aerodynamic admittance and equivalent average moving filter derived by the method of Holmes (1997) for a pressure tap in the middle of the façade	57
7.6	Mechanic scheme case study building	59
7.7	Measured pressure distribution and averaged distribution	59
7.8	Timeseries for the static and simple dynamic model	61
7.9	Autocorrelation base moment coefficients	65
7.10	Shifted t -extremes vs hourly-extremes of static moment coefficients in the Normal domain	65
7.11	Zoom of the upper tail behaviour in the ECDF of the shifted t -extremes vs hourly-extremes of static moment coefficients in the Gumbel domain.	66
7.12	Realizations and means of the structural dynamic properties samples in the two-dimensional sample space	67

7.13	Fitted cumulative distribution functions on the hourly extreme moment coefficients for the different dynamic structural properties	67
8.1	Probability density function of the structural resistance R based on the Level I procedure (Meinen, 2015)	72
8.2	Probability density function of the structural resistance R based on the characteristic value procedure	72
9.1	Case study building	79
10.1	ECDF of yearly extreme wind speeds of 12 different wind directions and independent of wind direction (Meinen, 2015)	81
10.2	ECDF annual maxima of wind speed and fitted Type I and III extreme value distributions	82
10.3	Fitted Type I and III extreme value distributions for yearly extreme wind speeds together with bootstrapped sample fits	84
11.1	Maximum response coefficients for the entire transient analysis results. The Eurocode dynamic response coefficients are also presented.	85
11.2	ECDF and fitted Type I and III distributions on the 20 s extremes of the response coefficients in the Gumbel domain	86
11.3	Fitted distributions of 10 and 20 s extremes versus hourly extremes of static moment coefficients	88
11.4	ECDF and fitted Type I and III distributions on the 20 s extremes of the response coefficients in the Gumbel domain together with the bootstrapped sample fits	88
12.1	α^2 -values and β -values for the simplified resistance model <i>without sampling uncertainties</i>	93
12.2	α^2 -values and β -values for the simplified resistance model <i>including sampling uncertainties</i>	93
12.3	α^2 -values and β -values for the full-probabilistic resistance model for one stochastic resistance parameter <i>without sampling uncertainties</i>	94
12.4	α^2 -values and β -values for the characteristic resistance procedure for steel dominance <i>without sampling uncertainties</i>	94
12.5	α^2 -values and β -values for the full-probabilistic resistance model with two stochastic parameters <i>without sampling uncertainties</i>	94
12.6	α^2 -values and β -values for the full-probabilistic resistance model with three stochastic parameters <i>without sampling uncertainties</i>	95
12.7	α^2 -values and β -values for the full-probabilistic resistance model with three stochastic parameters <i>including sampling uncertainties</i>	95
12.8	ECDF and fitted Type I and III distributions on the 20 s extremes of the response coefficients in the Gumbel domain along with computed and Cook-Mayne design value with accounting for sampling uncertainties	96
12.9	Sensitivity study of reliability results on different stochastic parameters <i>with accounting for sampling uncertainties</i>	98
12.10	β -values for different mean-over-specified of χ_{c_d} <i>with accounting for sampling uncertainties</i>	98
A.1	Two-dimensional combined probability density function with limit state function	117
B.3	Reference height, z_e , depending on h and b , and corresponding velocity pressure profile (Figure 7.4 EN-1991-1-4)	121
B.1	Wind areas in the Netherlands, Dutch National Annex	122
B.4	Reference height, z_s , for general shapes of structures covered by the design procedure to determine the structural factor (Figure 6.1 EN-1991-1-4)	122
B.2	Zonification for vertical walls (Figure 7.5 EN1991-1-4)	123
C.1	Approach of assessment procedure by Meinen et al. (2016)	126
D.1	Hamming window (default in Welch's PSD estimation method)	127
D.2	Frequency averaging of power spectral density of pressures at tap 18 on the windward façade	128
E.1	Spectral density function of the generalized force derived from the wind tunnel measurements.	131

E.2	Mechanical admittance function for the first mode of a SDOF system	131
E.3	Spectral density function of the response modal coordinate of a SDOF system and of the top displacement of the simple beam model in DIANA	132
E.4	Timeseries for the static model, the simple dynamic model and dynamic model of step 2	132
E.5	Timeseries for the static model, the simple dynamic model and dynamic model of step 3	133
E.6	Timeseries for the static model, the dynamic model and dynamic model with Timoshenko beam elements	133
F.1	Contourplot of cross-correlations of one pressure tap with the other taps at the windward face of the case study building	135
F.2	Contourplot of cross-correlations of one pressure tap with the other taps at the leeward face of the case study building	136
F.3	Autocorrelation of the dynamic base shear coefficients	136
F.4	Autocorrelation of the static base shear coefficients	136

List of Tables

2.1	Summary of space-averaging effect in wind loading	12
2.2	Fundamental basic wind velocity in the Dutch National Annex	13
2.3	Pressure coefficients prescribed in Dutch National Annex	14
3.1	Values of the constants in the aerodynamic admittance formula by Dyrbye and Hansen (1999)	26
4.1	Approximate estimates of wind load uncertainty factors (Davenport, 1987)	38
4.2	Approximate estimates of wind load uncertainty factors (Davenport, 1987), (Vanmarcke, 1992)	40
4.3	In put parameters for the direction dependent limit state function $Z(\theta_i)$	41
7.1	Properties FE model of the case study building	62
7.2	Dynamic factors for different modelling steps for the first 15000 time steps (one hour in full-scale)	62
7.3	Properties case study reference building	63
7.4	Maximum/minimum stresses for the first 15000 time steps	63
7.5	Dynamic factors for different wind speeds for the first 15000 time steps	64
7.6	Statistics of dynamic structural parameters according to JCSS (2001)	67
7.7	Coefficient of variation and specified design value of the response coefficients in the Cook frac- tile	68
9.1	Measurement station and measurement data details	80
9.2	Wind tunnel and measurement data details	80
10.1	Probabilistic description of the 64 measured direction independent yearly extreme wind speeds at Schiphol Airport	82
10.2	Moments of the sample data of the yearly extreme wind speeds and of the fitted Type I and III GEV distributions	83
10.3	Model parameters of the fitted Type I and III GEV distributions for the yearly extreme wind speeds	83
10.4	Coefficients of variation for the Level I 'bootstrapped' design points	83
11.1	Probabilistic description of the 20s-extreme response coefficient data	86
11.2	Moments of the sample data of the t -extreme response coefficients and of the fitted Type I and III distributions	87
11.3	Model parameters of the fitted Type I and III distributions of the 20s-extreme response coeffi- cients	87
12.1	Description of stochastic input variables for the reliability assessment of the case study building by limit state function z for a simplified stochastic resistance model	92
12.2	Description of stochastic input variables on the resistance side for the reliability assessment of the case study building by limit state function z for the full-probabilistic resistance model method	92
12.3	Design values for the reliability calculations and EN1991-1-4 design values. (1): Both v_{pot} and \hat{c}_R Type I; (2): v_{pot} Type I and \hat{c}_R Type III; (3): Both v_{pot} and \hat{c}_R Type III	97
E.1	Mode shape first eigenmode	130
E.2	Standard deviation of the base bending moment	131
E.3	Standard deviation of the top displacement	132
G.1	Pile properties	137
H.1	Model parameters of the stochastic description of c_r^2	139
H.2	Input parameters for the EN1991-1-4 wind load model	140

H.3 Model parameters lognormal distribution structural resistance Level I procedure 140

List of symbols

List of Latin symbols

sign	description	unit
A	Area	m^2
A_c	Cross-sectional area concrete core	m^2
A_{ref}	Reference area	m^2
A_{sw}	Shear reinforcement area	m^2
B^2	Background response factor	
C_j	The modal damping ($= 2\zeta_j G_j \omega_j$)	kg/s
Coh_{uu}	Coherence of turbulent component u at two different locations	-
$C_{r;y,z}$	Decay constants	-
C_T	Constant belonging to an appropriate averaging time. According to Lawson (1976) $C_T = C_r$	-
E	Young's modulus	N/m ²
E_{wind}	Wind loading effect at foundation level	-
F_G	Normal force due to self-weight	N
$F_x()$	Cumulative distribution function	-
G_F	Gust load factor	-
G_i	Constant in aerodynamic admittance by Dyrbye and Hansen (1999) that depends on the shape of the response influence function	-
G_j	The generalized mass: $\int_0^L \mu(z) \phi_j^2(z) dz$	kg
$ H ^2$	Mechanical admittance	
$H_j(n)$	The transfer function or mechanical admittance for the j th mode	-
I	Area moment of inertia	m ⁴
I_R	Response influence function	-
I_u	Turbulence intensity	-
Je	Jensen number: non-dimensional parameter describing the relationship between the flow and the building geometry, used in the scaling of similar but different-sized flow situations (wind tunnel)	-
K_j	The modal stiffness ($= G_j \omega_j^2$)	kg/m ²
L_{char}	Characteristic dimension of the area considered	m
L_u^x	Longitudinal turbulence integral length scale	m
$L(z)$	Turbulent length scale in EN1991-1-4: $L(z) = L_t(z/z_t)^\alpha$. With $z_t = 200$ m, $L_t = 300$ m and $\alpha = 0.67 + 0.05 \ln(z_0)$	m
M	Base bending moment	Nm
Q	Base shear force	N
$Q_j(t)$	The generalized force equal to $\int_0^L f(z, t) \phi_j(z) dz$	N
R^2	Resonant response factor	
Re	Reynolds number: dimensionless quantity in fluid mechanics, used in the scaling of similar but different-sized flow situations (wind tunnel)	-
$R_{foundation\ level}$	Shear or moment resistance of the main bearing structure at foundation level	-
R_M	Bending moment resistance	Nm
R_Q	Shear force resistance	N
$S_{\hat{c}_R}$	Factor considering sampling uncertainties of response coefficient modelling	-
St	Strouhal number: dimensionless number describing oscillating flow mechanisms, used in the scaling of similar but different-sized flow situations (wind tunnel)	-

sign	description	unit
S_v	Factor considering sampling uncertainties of basic wind velocity modelling	-
S_{wind}	Wind load	N
$S_x(P, P; n)$	Power spectral density function of data at one location	
$S_{xy}(P, P'; n)$	Cross-power spectral density function of data at two different locations	
$T(z)$	Characteristic time of memory: measurement of time for which components can still be considered correlated	s
$U(t)$	Instantaneous wind speed	m/s
U_m	Mean longitudinal wind velocity	m/s
U_z	Mean longitudinal wind velocity at structures height	m/s
\bar{V}	Annual-maximum hourly-mean wind speed	m/s
\hat{X}	Peak load	N
b_c	Width concrete core	m
\hat{c}	Peak loading coefficient (both minimum and maximum)	-
$\hat{c}_{R,t}$	Peak response coefficient: t minute extreme	-
c_a	Aerodynamic shape coefficient (force or pressure)	-
c_D	Drag coefficient: total longitudinal force coefficient, both windward and leeward combined	-
c_d	Dynamic response factor	-
c_e	Exposure coefficient (terrain influences)	-
c_f	Force or load effect coefficient	-
c_g	Gust factor	-
c_p	Pressure coefficient	-
c_r	Terrain roughness factor	-
c_{str}	Structural response factor including gust factor and dynamic response	-
f_c	Compressive strength concrete	N/m ²
f_L	Non-dimensional frequency: $nL(z_s)/u_m$	-
f_x0	Probability density function	-
f_y	Yield strength reinforcement steel	N/m ²
g	Gust factor	
h	Height	m
k_r	Terrain factor depending on roughness length z_0	-
l	Length	m
n	Frequency	Hz
n_j	Natural frequency	Hz
p	Pressure	N/m ²
p	Distributed load	N/m
q	Wind pressure (open field)	N/m ²
$r_{y,z}$	Horizontal or vertical distance between two points on the façade	m
s	Shear reinforcement spacing	m
s_{ln}	Sample standard deviation of the data X after a natural log transformation	-
t	Thickness concrete core	m
u	Fluctuating component of the wind velocity in the direction of U_m at time t	m/s
v_{pot}	Basic wind velocity: t minute mean wind speeds at $z = 10$ m and for terrain roughness $z_{0,ref}$	m/s
$v_{ref,h}$	Wind velocity at reference height	m/s
w	Wind load per unit area	N/m ²
x	Dynamic response of the structure	
x_u	Length concrete compression zone	m
z_0	Roughness length in full scale	m
$z_{0,II}$	Reference roughness length (terrain category II in EN1991-1-4): 0.05 m	m

List of Greek symbols

sign	description	unit
α	Shape parameter of the wind profile	-
γ_m	Material factor	-
δ	Logarithmic decrement of damping	-
ζ_j	The damping as a fraction of the critical damping	-
θ	Strut angle	o
θ_i	Incident wind direction	o
$\mu(z)$	The mass per unit length along the length L of the structure	kg/m
ν	Poisson's ratio	-
ρ	Mass density	kg/m ³
ρ_{air}	Air density	kg/m ³
ρ_s	Reinforcement ratio	-
ρ_u^T	Autocorrelation of the longitudinal turbulent component	-
ρ_u	Cross-correlation of the instantaneous longitudinal turbulent component at two different locations	-
σ_{max}	Stress in the outer fibre	N/m ²
σ_u	Standard deviation of wind velocity: $I_u(z)u_m(z)$	m/s
τ	Averaging time	s
ϕ_i	Non dimensional parameter $C_r n l_i / U$	-
ϕ_j	Mode shape	-
$ \chi ^2$	Aerodynamic admittance	-
χ_{cd}	Dynamic properties uncertainty factor	-
χ_{model}	Model uncertainty factor	-
χ_R	Resistance uncertainty factor	-
ψ_p	Normalized co-spectrum of wind pressures at two different locations	-
ψ_T	Moving average filter	-
ψ_u	Normalized co-spectrum of the turbulent component u	-
ω_j	The natural undamped circular frequency = $2\pi n_j$	rad/s

List of abbreviations

abbreviation	description
ABL	Atmospheric boundary layer
ECDF	Empirical cumulative distribution function
GEV	Generalized extreme value



Introduction

1.1. Problem statement

Structures are designed to withstand multiple types of loads and load combinations. Due to uncertainties in the loads and the resistance of the structure, safety can never be guaranteed completely. Instead structures are considered safe, when they comply with minimum reliability requirements. In the European Union these requirements are set out in the Eurocodes (EN1990). They are expressed by a minimum reliability index β which is related to a maximum failure probability. To prevent the need to perform a complete reliability analysis for every individual structure, in the Eurocode, partial factors have been determined. In a previous graduation work (Meinen, 2015) it has been investigated whether the current partial factor ($\gamma_s = 1.5$) for wind loads is able to guarantee the minimum reliability requirements of wind-loaded façade elements for standard design situations. However, the behaviour of the wind on the entire façade and supporting structures are yet unknown. Thereby can façade elements be considered static, so no resonant response of the element is to be expected.

The upscaling of façade element (local) loading to global structural response in the Eurocode framework involves several extra factors than evaluated in the work of Meinen (2015). These factors include c_s and c_d , respectively the size and dynamic factor. The size factor c_s , as defined in EN1991-1-4 (Eurocode for wind loading), takes into account the reduction effect on the wind action due to the non-simultaneity of occurrence of the peak wind pressures on the surface. The dynamic factor c_d , takes into account the amplification effect from vibrations in resonance with the structure due to the turbulent character of the wind. The global response of buildings to wind loading as well as uncertainties accompanying this wind load have been the subject of extensive research over the last decades, but few reference has been made to the reliability of structures designed within the Eurocode framework by linking both aspects. Current research will try to provide this link and investigate the reliability of dynamically sensitive structures designed within the Eurocode framework considering global wind action effects.

1.2. Aim of the research

The main research question that is therefore addressed in this research is:

How could the reliability of the main bearing structure of a dynamically sensitive building designed within the Eurocode framework be assessed in a full-probabilistic way for global response through coupling of the uncertainties in wind climate, global dynamic response of the structure and resistance?

In order to answer this question several sub-questions are formulated:

- *What are the factors that should be incorporated in a stochastic wind load model based on literature?*
- *How can these factors be incorporated in a full-probabilistic assessment procedure?*
- *How can global response at foundation level be evaluated and included directly in this model?*

- *How can the uncertainties on the resistance side of the reliability analysis be incorporated?*
- *How does the reliability of current designed buildings by EN1991-1-4 relate to the requirements in EN1990, which are expressed by a target reliability?*

The objective of this research is therefore to give insight in the reliability based assessment of structures subjected to wind loading within the Eurocode framework,

by developing a probabilistic assessment procedure for global response of the main bearing structure at foundation level,

including dynamic response,

based on literature and numerical methods and,

by giving a first indication on the reliability for global response of the main bearing structure at foundation level,

by means of a case study approach,

for common structural properties,

with the aid of a finite element analysis.

First this research should provide a full-probabilistic assessment procedure that links both the uncertainties in wind climate, in the global and dynamic response of buildings subjected to this wind loading and in the resistance. This will also give insight on the research that has already been performed and how this can be used for a full-probabilistic assessment of wind-loaded buildings for global response. In addition, this research should provide a more realistic approach on the dynamic response of buildings to wind loading and the global effect of this loading by using a finite element analysis.

1.3. General scope

- The reliability of the structure in ultimate limit state (ULS) will be the subject of this research. Therefore a reference period of 50 years for wind loading will be considered. For the resistance in ULS internal failure of the structure or structural members will be considered.
- Wind loading is considered to be the dominant loading of the building. Load combinations are not taken into account.
- Other responses to wind loading except for the alongwind buffeting response will not be the subject of this research (this will be further discussed in chapter 6).
- Subject of this research are dynamically sensitive buildings. Structures are generally classified as dynamically sensitive when their fundamental frequency is $n_0 < 1$ Hz. This is usually the case for high- (and sometimes medium-) rise and slender buildings. Therefore in this research slender high-rise structures are considered.
- The assessment procedure is derived for only one structural system, which is considered to be of common use in Dutch high-rise buildings, namely a concrete core structure.

1.4. Outline

For the purpose of this report the research was divided into three parts; Part I summarizes the literature study that was needed for overall understanding on the topic and for background knowledge for the development of the assessment procedure; Part II describes the derivation of the assessment procedure and presents the final procedure; Part III shows an application of the assessment procedure by means of a case study. In figure 1.1 on page 4 a summary of the structure described next, is given.

Part I: Literature review

In **Chapter 2** the basics of wind engineering are explained by means of the wind loading model mostly adopted in literature. Also the wind loading model according to the Eurocode is presented here. In **Chapter 3** the approaches to global wind loading and dynamic response of a structure are explained in more detail. Several assumptions that are the basis of these approaches are also described. In **Chapter 4** first the uncertainties in wind loading on dynamically sensitive buildings are described. Next, the most important probabilistic methods to wind loading are presented and evaluated. Also the assessment procedure proposed by Meinen (2015) which gave reason for current research is explained here. Description of the stochastic wind load is inherent to the modelling of extremes. Therefore, in **Chapter 5** some basic methods for this modelling are explained.

Part II: Method development

The objective of this research is to contribute to the reliability based assessment of dynamically sensitive structures subjected to wind loading, considering global response of the main bearing structure. Therefore in **Chapter 6** the general approach of this research for the development of the full-probabilistic assessment procedure including the stochastic resistance and wind load model is presented. Furthermore the applicability of the assessment procedure is described. In **Chapter 7** the methods which are used for the determination of the global response of the structure are derived and explained. Some of these methods are explained and presented on the basis of a case study approach. However, the methods described are generally applicable to other buildings of similar typology. In **Chapter 8** the final assessment procedure which is able to determine the structural reliability of the main bearing structure at foundation level of dynamically sensitive buildings is presented and explained. Both stochastic description of the resistance as the wind load is given.

Part III: Reliability assessment of a case study

In order to obtain a first indication on the reliability for global response of the main bearing structure at foundation level, the previously derived assessment procedure is applied to a case study, using both location-specific wind speed measurements as wind tunnel pressure measurements. For the case study a high-rise reference building with rectangular plan (30x30 m) and a height of 120 m is considered. The reference structure is located in the Netherlands at Schiphol Airport. A more detailed description of the case study can be found in **Chapter 9**. In **Chapters 10 and 11** the stochastic description of the wind velocity and global response coefficients are presented, respectively. In **Chapter 12** the results of the reliability assessment are given and evaluated. In **Chapter 13** a discussion on the main findings in the reliability based assessment of the case study described in previous chapters is presented.

In **Chapter 14** and **Chapter 15** the main conclusions of the research and recommendations for further research are given.

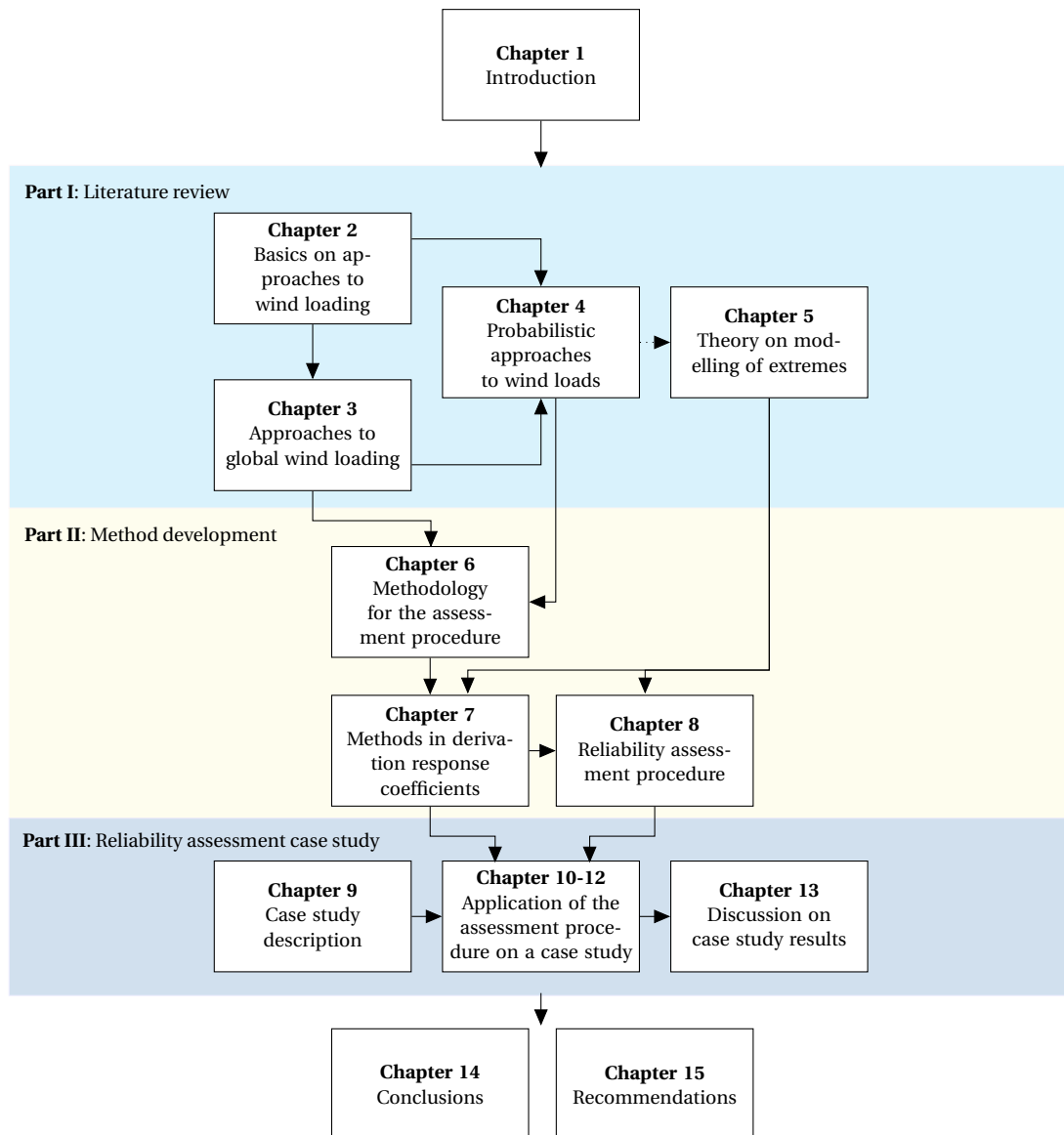


Figure 1.1: Overview of the structure of the report

I

Literature review

2

Basics on approaches to wind loading

In this chapter the basics on wind engineering are presented. These basics form the ground of the current approaches to wind loading, which are also followed during this research. In § 2.1 the basic characteristics of wind are given. Next, in § 2.2 the basics of wind engineering are presented using the wind loading chain proposed by Davenport (1961). In § 2.3 the approach on wind loading prescribed by the Eurocode (EN1991-1-4) is given.

2.1. Basic description of wind

Wind speeds near the earth's surface have a fluctuating nature. This fluctuating nature can be subdivided in two types of fluctuations. This is fluctuation of the mean wind speed and a more rapid fluctuation, originating from the turbulent nature of wind. This subdivision can be seen clearly when looking at the autospectrum of the horizontal wind in Figure 2.1. The autospectrum shows how the variance is distributed over the wind frequencies.

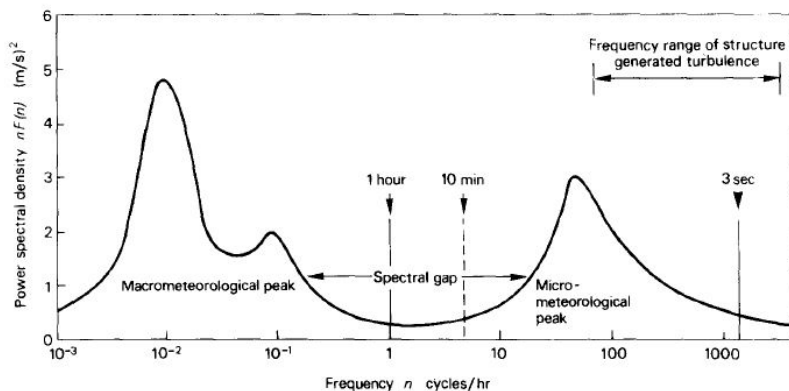


Figure 2.1: Spectrum of horizontal wind after Van der Hoven

Two clear peaks can be distinguished. The first, macrometeorological, peak belongs to large scale weather systems of typically 1 to 4 days. The second, micrometeorological, peak around the frequencies corresponding to periods of seconds to about 5 minutes, corresponds to turbulence. The amount of variance in periods between 10 minutes to 1 hour is very low and this is referred to as the spectral gap. Mean wind velocities belonging to 1 hour or 10 minute periods show not much difference, due to this spectral gap. Therefore these periods are usually taken as an averaging time to describe the mean wind speed. This mean and fluctuating part of the wind speed is visualised in figure 2.2 on the following page.

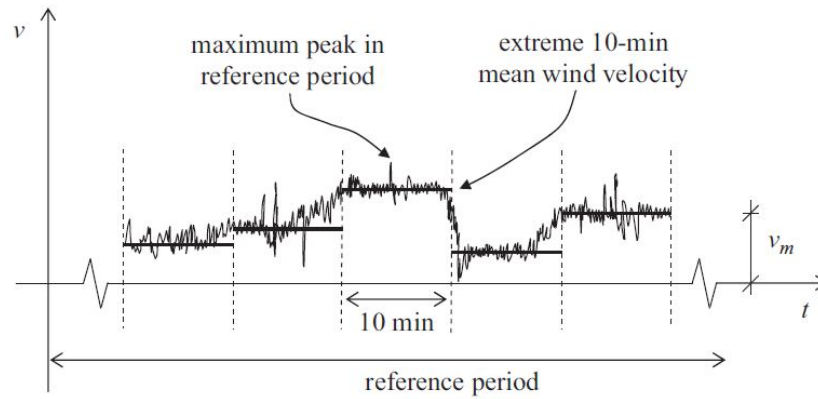


Figure 2.2: Distinction between mean and fluctuating part of the wind speed (Steenbergen et al., 2012)

2.2. Davenport's wind loading chain

Davenport was the first to describe the wind load effect on a structure as the combined effects of the wind climate, terrain characteristics, the wind-structure interaction, the structural properties and the criteria to assess the acceptability of certain loads and load effects. This is visualized in figure 2.3. The parameters in the figure are the ones used to describe the effects of the different chain links by the Eurocode. The Eurocode has used Davenport's wind loading chain as a clear way to structure their wind loading model, to create a framework that is straightforward in use for engineers.



Figure 2.3: Davenport's wind loading chain (Davenport, 1961)

Meinen (2015) considered the first three and the last of the five links in the assessment procedure for wind loaded façade elements, but the fourth link was considered outside the scope of the research as only local loading and static response were considered. When considering the response of a structure to global wind loading this fourth link is of importance. In this section the links are described briefly. In the next chapter a more detailed description of the fourth link describing global structural response is given.

2.2.1. Wind climate

The momentary distribution of the wind speed depends on the return period considered. The wind climate in Davenport's chain is described by a mean wind velocity for a certain return period. The wind climate depends on several natural forces and is a result of the differences in earth solar heating. All natural forces combined produce certain weather systems. There are large scale weather systems of several hundreds of kilometers and small scale weather systems, which result in more local wind climate. Weather systems of this last category are for instance thunderstorms and tornadoes. The characteristics of the wind climate change during seasons and they can be dependent on direction, as certain dominant wind directions can be observed.

2.2.2. Influence of terrain

The earth's surface exerts a frictional force upon the wind, which creates an atmospheric boundary layer (ABL) with a mean wind velocity profile that increases with height. A visualization of this profile can be seen in figure 2.4 on the facing page.

The terrain influences the characteristics of the wind velocity in this ABL, which results in the turbulent character of the wind velocities in this boundary layer. This turbulent character makes the determination of the design wind load especially complex, while exactly the wind characteristics in this boundary layer are of interest for the design of buildings. Above the ABL the wind flows with an approximately constant speed.

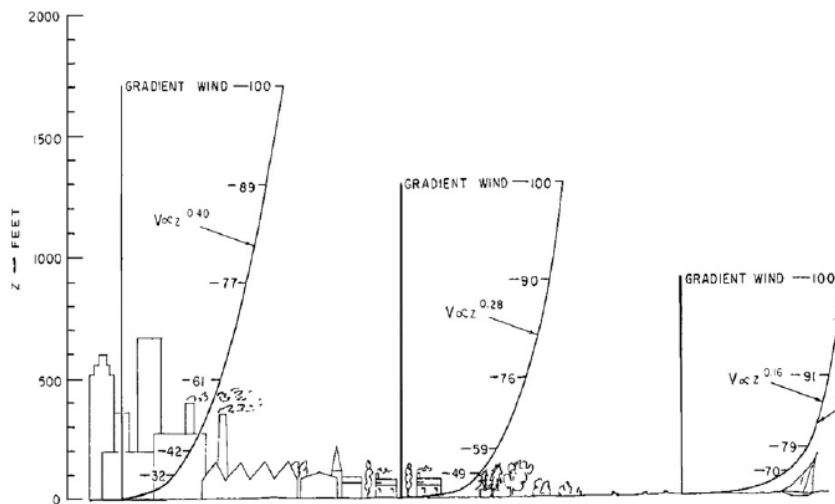


Figure 2.4: Davenport's power law profiles of mean wind velocity over different terrain types (Isyumov, 2012)

Several factors that influence the wind characteristics within the ABL are:

- Atmospheric instabilities
- The roughness of the upwind terrain
- The terrain orography
- The effect of neighboring structures

Like in the research by Meinen (2015) only the influence by the roughness of the upwind terrain will be considered. The other three types of influences are out of scope for this project.

Due to the turbulent character of the wind, the wind flow in the ABL can only be described by a vector notation. Therefore, for general purposes, a Cartesian coordinate system is applied, with the x-axis in the direction of the mean wind velocity. This is called the longitudinal direction and both a mean component (mean wind speed) and a turbulent component can be distinguished, U_m and u respectively. For the lateral and vertical direction only turbulent components are defined. For the purpose of this research only the longitudinal direction is considered and the lateral and vertical turbulent wind component are not taken into account. In code approaches only the mean component of the wind speed in longitudinal direction is defined and the turbulent components are tackled in a different way. Therefore, for code purposes, the wind velocity is presented by symbol v .

2.2.3. Wind-structure interaction - Aerodynamic coefficients

The aerodynamic coefficients are expressed in terms of force or pressure coefficients. They are defined as the ratio between the local mean or peak pressure measured at the façade and the global mean wind pressure q in front of the façade. They vary for every location on the building's façade and depend on the type of flow around the building.

Pressure coefficients are generally not determined for every point on the façade, but they are assumed to have a constant value over a certain area A_{ref} . Peak pressures are not found simultaneously at all locations on the building. Therefore the pressure coefficient contains a space-averaging effect for considered A_{ref} (e.g. 1 m^2 or 10 m^2). Where at one point on a larger façade element a large pressure is present, at other locations a lower (absolute) pressure will be found. This lack of full correlation between pressures at different locations on the building's façade results in a lower pressure coefficient for a larger A_{ref} .

Pressure coefficients also depend on the averaging time considered. The load duration is very important in the field of wind loading, as the largest peaks have very short durations. Therefore the pressure coefficients for larger duration will be smaller than the coefficients for short duration peaks.

2.2.4. Global structural response

Davenport turned to structural dynamics and random vibration theory to describe the global wind-induced loads and the structural response, which is summarized in figure 2.5.

The turbulent character of the wind is described by a variance spectrum. This wind spectrum describes how the variance of the stochastic process is distributed over the frequencies. The aerodynamic admittance relates the wind spectrum to the actual pressures present on the façade of the building. The dynamic response of the structure is introduced by a mechanical admittance function, which describes the sensitivity of the building to fluctuations of different frequencies. Multiplying the wind spectrum by both the aerodynamic and mechanical admittance results in a response spectrum that describes the response in the frequency domain.

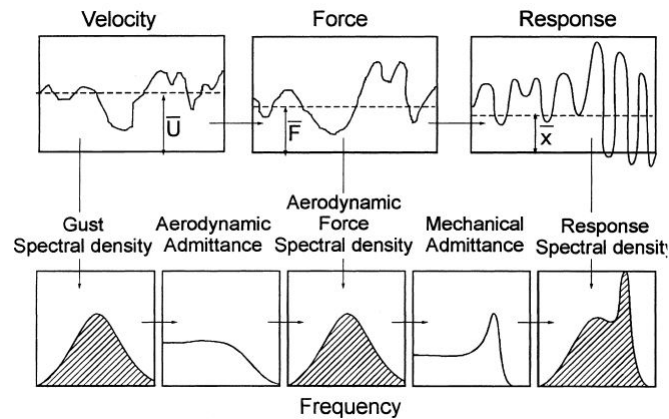


Figure 2.5: Davenport's random vibration approach for the wind-induced response of buildings and structures (Davenport, 1964)

Analogous to the approach to describe the local wind velocities, also the response can be divided in mean fluctuating response and a fast fluctuating response (resonance). The contribution of this resonant response to the total dynamic response of a structure depends on the natural frequency and damping of a structure. When structures or parts of structures have low natural frequencies and low damping the fluctuating wind velocities may cause significant resonant vibrations of the structure. This becomes more and more significant in taller and more slender structures. The effect of the natural frequency of a structure on the response has been visualised by Holmes (2001) in figure 2.6 on the facing page.

In the last step of the spectral approach used by Davenport the response spectrum is formed. In such a spectrum the existence of a mean (background) and a resonance response can be clearly distinguished. A more detailed response spectrum for a structure which is sensitive to resonant contributions can be found in figure 2.7 on the next page. The resonant peaks are located at the natural frequencies of the structure. For most structures only the response in the first natural frequency, or fundamental frequency, is of importance and the resonant response is just a small fraction of the total dynamic response.

Central to this spectral approach lies the linearization of the relationship between the turbulent component of the wind speed and the dynamic wind load.

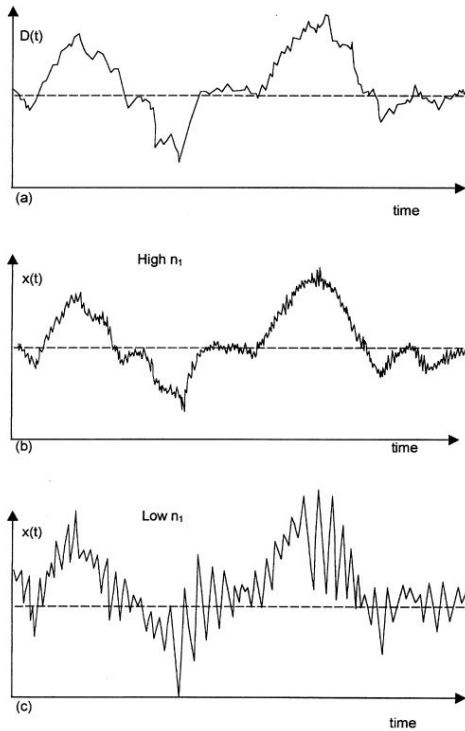


Figure 2.6: Time histories of: (a) wind force, (b) response of a structure with a high natural frequency and (c) response of a structure with a low natural frequency (Holmes, 2001)

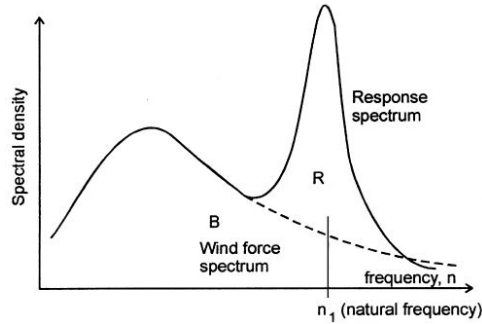


Figure 2.7: Response spectral density for a structure with significant resonant contributions (Holmes, 2001)

$$q_{rep}(t) = 0.5\rho(U(t))^2 = 0.5\rho(U_m + u(t))^2 \approx 0.5\rho U_m^2(1 + 2u(t)/U_m) \quad (2.1)$$

q = Wind pressure

ρ_{air} = Air density

$U(t)$ = Instantaneous wind speed

U_m = Mean wind velocity

u = Fluctuating component of the wind velocity in the direction of U_m at time t

It is also assumed that the wind loading is quasi-static, which means that the aerodynamic data for time averaged wind loads can also be used for the dynamic loading. This resulted in Davenport's gust factor approach. He proposed that the peak value of the wind load can be related to the time averaged mean value. This approach is applicable to wind effects where the mean value of the wind load is significant, which is true for the buffeting dynamic alongwind or drag forces. It also assumed that the resonant vibrations of the structure are in the fundamental mode of vibration having a linear mode shape.

The gust factor approach of Davenport for global wind loading includes a certain size and dynamic factor, respectively c_s and c_d . The size factor takes into account the non-simultaneity of occurrence of the peak wind pressure over the entire surface of the building. The used space-averaging effect in global wind loading is summarised in table 2.1. The dynamic factor is only included when considering global wind loading, because it is assumed that the fundamental frequency of vibration for a façade element is large enough for the element to be considered static ($n_0 > 5$ Hz).

A more elaborate discussion on this dynamic approach to wind loading can be found in §3.3.

Table 2.1: Summary of space-averaging effect in wind loading

A_{ref} [m ²]	Coefficient [-]
1	$c_{pe,1}$
10	$c_{pe,10}$
N	$c_s \cdot c_{pe,10}$

2.3. Wind loading according to the Eurocode

This section provides the procedure as followed by the EN1991-1-4 wind loading model. When establishing the Eurocode on wind loading, Davenport's wind loading chain has been used as a guidance to structure the document. This was decided in order to make the presentation as user friendly as possible. The characteristic global wind load as specified in EN1991-1-4 is given by:

$$F_w = c_s c_d \cdot \sum_{surfaces} w_e \cdot A_{ref} \quad (2.2)$$

$$F_w = c_s c_d \cdot \sum_{surfaces} q_b \cdot c_e(z) \cdot c_{pe} \cdot A_{ref}$$

In this formula, $c_s c_d$ accounts for the structural effects. The wind climate is represented in the basic velocity pressure q_b , the terrain effects by the exposure factor $c_e(z)$ and the wind-structure interaction by the mean pressure coefficients c_{pe} .

Next all individual parameters of EN1991-1-4 for global wind loading will be explained. The relation of these factors to the overall wind loading model in the Eurocode can be found in figure 2.8 on the facing page.

2.3.1. Wind climate

Air density ρ_{air}

The air density depends on altitude, temperature and barometric pressure expected in the region during storm conditions. A recommended value of $\rho_{air} = 1.25 \text{ kg/m}^3$ is also adopted in the Dutch Annex.

Basic wind velocity v_b

The basic wind velocity is a function of wind direction and season at a height of 10 m above ground with terrain category II ($z_{0,II} = 0.05 \text{ m}$).

- **Fundamental basic wind velocity** $v_{b,0}$ is the characteristic 10 minutes mean wind velocity, irrespective of wind direction and time of year, at 10 m above ground level in open country terrain (terrain category II). The characteristic value has a reference period of 50 years. If the design life of the structure is less or more than those 50 years, the characteristic value should be determined accordingly through c_{prob} (reference is made to EN1991-1-4 4.2(2)P). The values for the fundamental basic wind velocity are given in the National Annex of each country. In the Dutch National Annex three wind areas are distinguished. These wind areas can be found in appendix B. Accompanying wind velocities are given in table 2.2 on the facing page.
- **Directional factor** c_{dir} accounts for wind directionality. The directional factor is defined as the ratio between the characteristic wind velocity within a certain direction and the characteristic wind velocity irrespective of wind direction. It is recommended to take a value $c_{dir} = 1.0$ and this value is considered normative for Dutch design purposes. This is a conservative choice.
- **Seasonal factor** c_{season} depends on the season where the structure is designed for. This is particularly important for temporary structures or structures in the construction phase. $c_{season} = 1.0$ is recommended and this value is considered normative for Dutch design purposes.

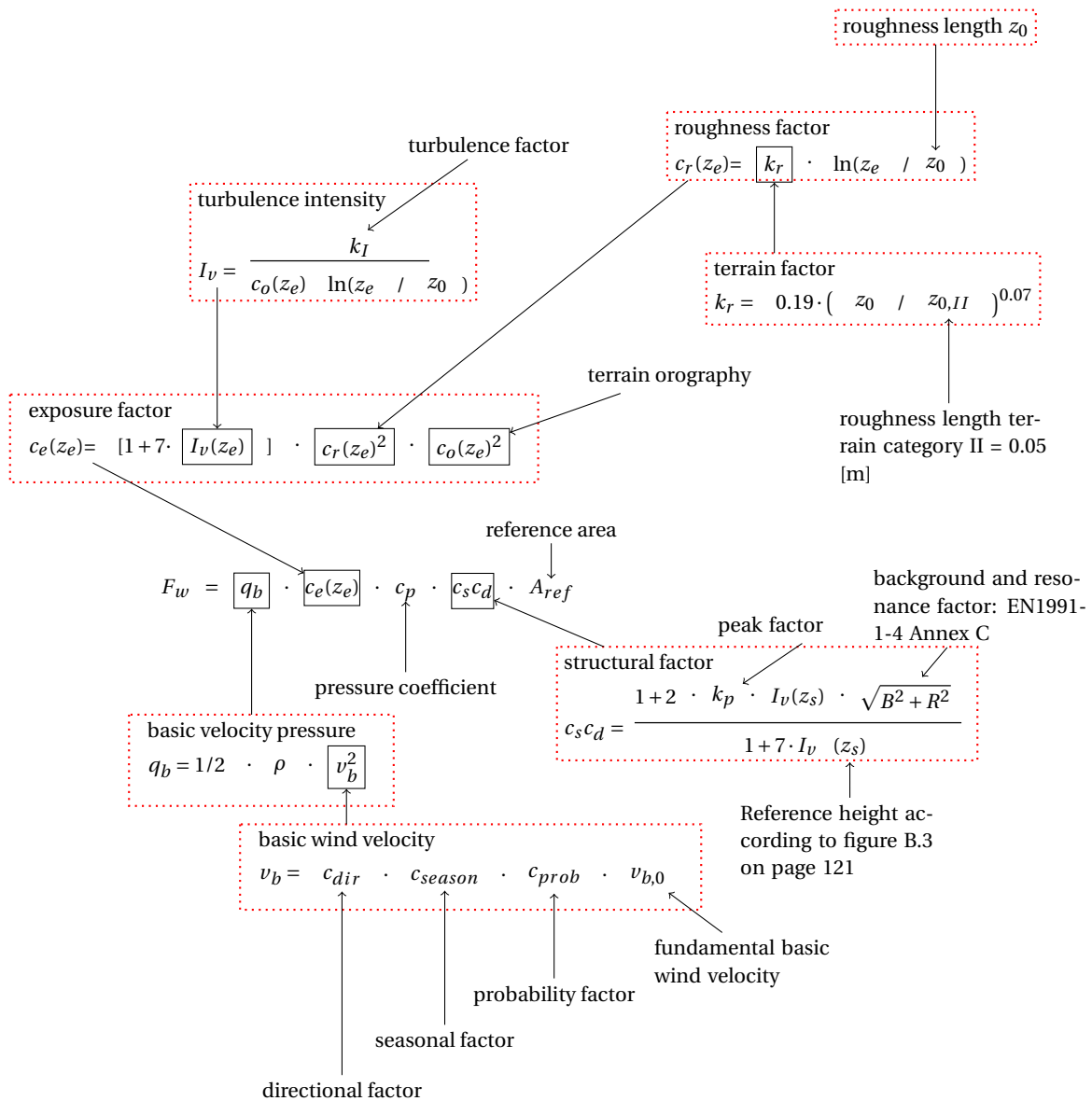


Figure 2.8: Wind loading model of EN1991-1-4 (Meinen, 2015)

Table 2.2: Fundamental basic wind velocity in the Dutch National Annex

Wind area	I	II	III
$v_{b,0}$ [m/s]	29.5	27.0	24.5

2.3.2. Influence of terrain

Roughness factor $c_r(z)$

The roughness factor accounts for the variability of the mean wind speed due to height above ground and the ground roughness upstream of the structure. Where the basic wind velocity belongs to a height of 10 m above ground, the roughness factor corrects for the logarithmic profile of the mean wind speed with height z . Thereby the basic wind velocity is defined for terrain category II with roughness length $z_{0,II} = 0.05$ m, so the roughness factor also corrects for different terrain categories.

- **Roughness length** z_0 is used to characterize the terrain category roughness. In the Dutch Annex three terrain categories are distinguished. Characterising a terrain usually happens on a visual basis, by a procedure also presented in the National Annex. A lower roughness length always provides a conservative result as seen from figure 2.4 on page 9.

Orography factor $c_o(z)$

Terrain orography, like hills and cliffs, can increase the mean wind velocity considerably. Therefore when relevant this effect has to be taken into account by the orography factor $c_o(z)$. This effect can be considered negligible when the slope of the upwind terrain is less than 3° . For the purpose of this research the terrain orography is considered out of scope and the orography factor is set to $c_o(z) = 1.0$.

Gust amplification factor $[1 + 7I_v(z)]$

The turbulent character of the wind velocities is caused by the influences of the terrain on the undisturbed wind flow. This turbulent character causes short duration peak loads on the structure which Davenport addressed by multiplying the mean wind pressure for a characteristic wind velocity by an amplification factor. This is called his gust factor approach. This method is further explained and derivations are presented in §3.3. This approach is also followed in EN1991-1-4 by amplifying the basic velocity pressure by a gust (or turbulence) amplification factor $[1 + 7I_v(z)]$. Where $I_v(z)$ is the turbulence intensity, defined by:

$$I_v(z) = \frac{\sigma_v}{v_m(z)} \quad (2.3)$$

Here $v_m(z)$ is the basic wind velocity corrected for terrain roughness, height z and terrain orography and σ_v is the standard deviation of the wind velocity.

Other corrections

The basic wind velocity should also be corrected for large neighbouring structures and closely spaced structures when relevant. These effects are considered out of scope of this research and these corrections are therefore not applied.

2.3.3. Wind-structure interaction**Pressure coefficients** c_p

Wind-structure interactions are represented by pseudo-steady pressure coefficients. These coefficients purely indicate the relationship between the undisturbed dynamic pressure in front of the building due to the mean wind velocity v_m and the pressure that is present on the façade. Turbulence effects are taken into account by the gust amplification factor. EN1991-1-4 provides pressure coefficients only for orthogonal wind direction ($0^\circ, 90^\circ, 180^\circ$ and 270°). These values represent the most unfavourable values obtained within a range of wind direction $\theta_i = \pm 45^\circ$ either side of the relevant orthogonal direction.

For overall wind loading the pressure coefficients correspond to a reference area of $A_{ref} = 10 \text{ m}^2$. These pressure coefficients are given in table 2.3. For intermediate height-over-width ratios (aspect ratios) h/d the values should be interpolated. Different coefficients are prescribed for different locations on the building. This zonification can be found in figure B.2 on page 123 in appendix B. For windward and leeward faces of the building both zone D and E are of relevance.

Table 2.3: Pressure coefficients prescribed in Dutch National Annex

Zone	A	B	C	D	E
h/d	$c_{pe,10}$	$c_{pe,10}$	$c_{pe,10}$	$c_{pe,10}$	$c_{pe,10}$
5	-1.2	-0.8	-0.5	+0.8	-0.7
1	-1.2	-0.8	-0.5	+0.8	-0.5

2.3.4. Structural effects**Structural factor** $c_s c_d$

The EN1991-1-4 wind loading model prescribes a structural factor $c_s c_d$ of non-unity value for general buildings with a height more than 15 m which is the starting point of this research. A structural factor of non-unity value should also be applied to façade and roof elements with a natural frequency below 5 Hz and for framed buildings with structural walls and chimneys with height and aspect ratio above a certain value.

The structural factor takes into account the non-simultaneous occurrence of peak pressures on the façade c_s together with the response of the structure due to turbulence c_d .

- **Peak factor** k_p is defined as the ratio of the maximum value of the fluctuating part of the response to its standard deviation.
- **Background response factor** B^2 allows for the lack of full correlation of the pressures on the buildings façade.
- **Resonance response factor** R^2 allows for turbulence in resonance with the vibration mode. Only to be used for structures where only the alongwind vibration (buffeting) at the fundamental frequency is of significance and the mode shape has a constant sign.
- **Reference height** z_s for determining the structural factor. This reference height is determined in figure B.4 on page 122 in appendix B. The structural factor should only be derived by the standard descriptions in EN1991-1-4 for types of structures that correspond to the general shapes defined in this figure. For slender high-rise structures $z_s = 0.6h$.

This method is analogous to the dynamic approach proposed by Davenport as described in § 3.3. In this section the theoretical definition of the background B and resonance response factor R are given. In EN1991-1-4 two different methods to derive this factor are given, in Annex B and C respectively. In the Dutch National Annex the method of Annex C is prescribed to be normative. The method in Annex B is based on empirical studies by Solari (1982, 1988, 1993a,b), while the method of Annex C is a more theoretical approach that originates from Dyrbye and Hansen (1999). Both methods are based on different simplifications. In Steenbergen et al. (2012) both methods were compared to the theoretically correct values and it was concluded that there are substantial differences.

The most noticeable difference between both methods lies in the fact that the mode shape in the method of Annex B is taken outside of the integral while in the method of Annex C this mode shape is evaluated inside of the integral, which is consistent with the theoretical approach. The differences between the methods in Annex B and C for the determination of $c_s c_d$ do not exceed 5%. More detailed information on both methods is given in chapter 3 in § 3.4.

In EN1991-1-4 the following is stated: 'When the wind load on buildings is determined by application of the pressure coefficients c_{pe} on windward and leeward side (zones D and E) of the building simultaneously, the lack of correlation of wind pressures between the windward and leeward side may have to be taken into account'. In the Dutch National Annex a reduction factor of 0.85 is prescribed to account for this lack of correlation. Furthermore, the Dutch National Annex also prescribes a minimum value for the structural factor. When for $c_s c_d$ a value smaller than 0.85 is found, $c_s c_d$ must be set equal to 0.85.

3

Approaches to global wind loading

For the determination of the structural response in the form of e.g. a bending moment an appropriate pressure distribution needs to be found that can reproduce the extreme structural load effect. In this chapter several aspects of global wind loading are discussed and both theoretical and empirical methods are presented. First, in § 3.1 the correlation of wind pressures and the approaches to incorporate this correlation are described. Then in § 3.2 the approach on dynamic response of buildings is discussed. Davenport's approach to global wind loading is presented in more detail in § 3.3, as this method is the basis for the current way of practice to include both dynamic response and influence of local loads on the global response. In § 3.4 some other approaches based on Davenport's are described, like the methods used in the Eurocode. Last, several assumptions in these approaches are highlighted and discussed in § 3.5.

3.1. Correlation of wind pressures

The instantaneous pressures on a structures face are correlated in time and space, but extreme pressures are not found simultaneously at every location on a structures façade. In this section time and spatial correlation between pressures on a single face and between pressures on the windward and leeward faces of a structure are discussed. The definitions used in this section are based on Dyrbye and Hansen (1999). Also several approaches in wind engineering to take into account the correlation of wind pressures are explained; the aerodynamic admittance and moving average filter.

3.1.1. Correlation

Time correlation

Correlation of turbulent wind components in time can be described by the autocorrelation function $\rho_u^T(z, \tau)$. This function provides a measurement of how much the turbulent component at time t , $u(x, y, z, t)$, tells about the turbulent component at time $t + \tau$, $u(x, y, z, t + \tau)$. A good approximation of the autocorrelation function is given by:

$$\rho_u^T(z, \tau) = \exp(-\tau / T(z)) \quad (3.1)$$

ρ_u^T = Autocorrelation of the longitudinal turbulent component

τ = Time lag

$T(z)$ = Characteristic time of memory: measurement of time for which components can still be considered correlated

Spatial correlation of pressures on a single face

As a measure of the statistical dependence between the turbulent components of the wind speed at two points the coherence can be used. There is such dependence due to the size of the vortices, or gusts, of the turbulent wind. The turbulence integral length scale is a measure of this size of the vortices or gusts in a certain direction. For the longitudinal component of turbulence this integral length scale is defined as the

integral of the cross-correlation function between the simultaneously measured turbulent component u of two separate points separated with a longitudinal distance r_x .

$$L_u^x(z) = \int_0^\infty \rho_u(z, r_x) dr_x \quad (3.2)$$

L_u^x = Longitudinal turbulence integral length scale

ρ_u = Cross-correlation of the instantaneous longitudinal turbulent component at two separate locations

The coherence is a variable to describe the correlation of wind pressures or wind velocities at two different locations. To compute the coherence, use is made of spectral analysis. It is defined by:

$$Coh_{uu}(P, P'; n) = \frac{|S_{uu}(P, P'; n)|^2}{S_u(P, P; n)S_u(P', P'; n)} \quad (3.3)$$

Where:

Coh_{uu} = Coherence of turbulent component u at two different locations

$S_x(P, P; n)$ = Power spectral density function of data at one location

$S_{xy}(P, P'; n)$ = Cross-power spectral density function of data at two different locations

Evaluating the coherence leads to a normalized co-spectrum and a phase spectrum. Davenport proposed an exponential expression on an empirical basis to express the decay in correlation of the turbulent component u for both horizontal and vertical direction for the normalized co-spectrum and a zero phase spectrum. Several remarks on the shortcomings of this expression are made by Dyrbye and Hansen (1999). One of these shortcomings involves the fact that this expression approaches unity for small frequencies, while for larger separations a lack of correlation in the wind structure is found even for low frequencies. The root-coherence or normalized co-spectrum expression proposed by Davenport is given by:

$$\sqrt{Coh_{uu}(P, P'; n)} = \psi_u(r_y, r_z, n) = \exp\left(-\frac{n}{U} \sqrt{(C_{r,y}r_y)^2 + (C_{r,z}r_z)^2}\right) \quad (3.4)$$

ψ_u = Normalized co-spectrum of the turbulent component u

$r_{y,z}$ = Horizontal or vertical distance between two point on the façade

C_r = Decay constant

A typical value for $C_{r,y}$ and $C_{r,z}$ is 11.5 as used in the Eurocode. This value is based on full-scale measurements by Solari (1993a,b). This expression can also be applied to pressures on the façade, but it might be necessary to adopt different values for the decay constants. In the Eurocode the values proposed by Solari are also used for the correlation of pressures acting on a façade. However, these values are derived for the wind flow in front of the building instead of the pressure on the buildings façade. Therefore, the fact that pressures on the façade have a higher correlation compared to the correlation in the wind flow is not incorporated in this value. For surface pressures on a building a decay constant C_r of 4.5 is proposed from full-scale measurements by Newberry et al. (1967). This value was also proposed by Cook (1985). In chapter 7 in § 7.1 the decay constant for the case study wind tunnel measurements is derived.

Spatial correlation of windward and leeward pressures

Similar to a lack of correlation between pressures at different locations on a single face, there is also a no full correlation between pressures at the windward and leeward face of a building. The Dutch Annex of the Eurocode takes into account this lack of correlation by using a reduction factor of 0.85 for global structural response. Previous research provides proof that even lower reduction factors could be used. One such research was performed on a building model of the standard CAARC building (30 × 45 × 180) (Pastorino et al. (Hansen)). It was shown that a low correlation between pressures at the wind- and leeward face was present.

Also by Geurts (1997) it was found from full-scale measurements that the correlation between pressures at the wind- and leeward face of the mid-rise building considered, yield lower values than were calculated using

relevant expressions from literature. In Hansen (2012), it was concluded from measurements in a wind tunnel on a low-rise building that lower correlation and peak pressures were found than were provided by the Eurocode. This can be seen in figure 3.1, where the maximum/minimum force coefficients are compared to the value designed for using EN1991-1-4. The maximum or minimum coefficients for the entire test duration are found to be lower than the values proposed in EN1991-1-4.

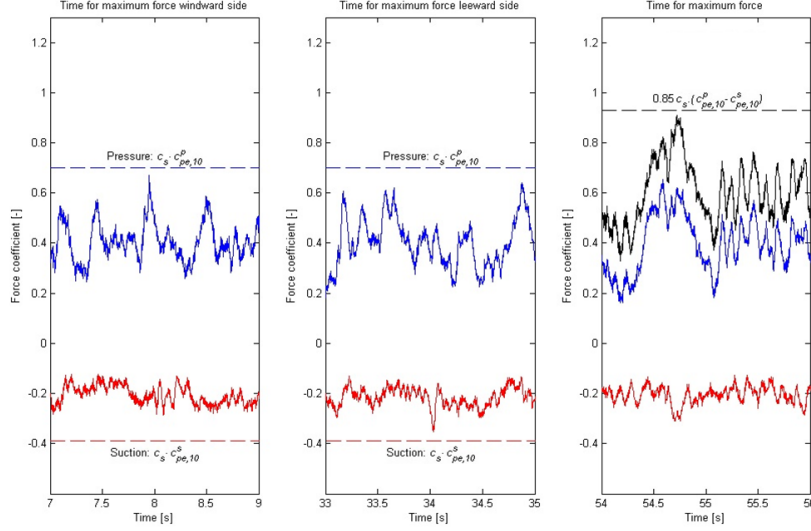


Figure 3.1: Maximum/minimum force coefficients low-rise building. The two figures on the left represent the time of maximum/minimum coefficients at windward and leeward side, respectively. The right figure displays the time of maximum force on windward and leeward face combined. The dotted lines indicate Eurocode pressure coefficients. (Hansen, 2012). Reproduced by permission of SiteCover.

A similar analysis on the case-study wind tunnel measurements has been performed to investigate the effect on a high-rise building. In chapter 11 the results can be found.

3.1.2. Low-pass filters

The effect of pressure fluctuations on the structure depends on the size of the structural element considered. Faster fluctuations are smaller size gusts which have a small effect on a larger element, while larger size gusts cause slower fluctuations, but higher correlated pressures and a larger effect on the element. Therefore for global loading the faster (higher frequency) fluctuations should be filtered out. Low-pass filters provide such filtering as they only pass signals with a frequency below a certain cut-off frequency.

The aerodynamic admittance as described in § 2.2 provides such filtering, but there are different low-pass filters used in wind engineering. A moving average filter is one such filter. This type of low-pass filter especially provides benefits when using pressure measurements, both full scale and wind tunnel measurements. Next, several formulations of the aerodynamic admittance are given and the approach by a moving average filter is presented.

Aerodynamic admittance

The aerodynamic admittance function $\chi_u^2(n)$ takes into account the lack of full correlation between pressures at different locations on the considered element. This is a new definition of the aerodynamic admittance from the definition in § 2.2.4 where the aerodynamic admittance, χ_a , accounted for the total relation between the wind velocity and the pressure measured at the buildings façade. χ_a is related to χ_u by $\chi_a = \rho U_m c_p A \chi_u$. For rectangular areas the aerodynamic admittance is defined by:

$$\chi_u^2(\phi_1, \phi_2) = \frac{\frac{1}{l_1 l_2} \int_0^{l_1} \int_0^{l_2} k(r_1, r_2) \psi_p(r_1, r_2, n, U) dr_1 dr_2}{\left(\frac{1}{l_1 l_2} \int_0^{l_1} \int_0^{l_2} |I_R(z_1, z_2)| dz_2 dz_1 \right)^2} \quad (3.5)$$

With $k(r_1, r_2)$ being the normalized co-influence function:

$$k(r_1, r_2) = \frac{2}{l_1 l_2} \int_0^{l_1 - r_1} \int_0^{l_2 - r_2} I(z_1, z_2, r_1, r_2) dz_1 dz_2$$

Where:

- ϕ_i = Non-dimensional parameter $C_r n l_i / U_z$
- C_r = Decay constant
- n = Frequency
- U_z = Mean longitudinal wind velocity at structures height
- ψ_p = Normalized co-spectrum of wind pressures at two different locations
- I_R = Response influence function
- l_1, l_2 = Dimensions of the rectangular element

Estimation formula by Dyrbye and Hansen

Dyrbye and Hansen (1999) give an estimation formula for the aerodynamic admittance which is also adopted in EN1991-1-4 Annex C. This formula is given in equation (3.30) on page 26.

Aerodynamic admittance from pressure measurements

The aerodynamic admittance can also be computed from pressure measurements in a wind tunnel test. In such a wind tunnel test, pressure taps are spread along the façade of the building model. During the test pressures are measured at all taps individually and these time series are stored. The procedure to compute the empirical aerodynamic admittance is given in equation 3.6 for each pressure tap t .

$$|\chi_u(\phi_1, \phi_2)|_t^2 = \frac{S_{p,t}}{\rho_{air}^2 U^2 c_{pm,t}^2 S_{u,t}} \quad (3.6)$$

Where $S_{p,t}$ is the power spectral density of the pressure, c_{pm} the mean pressure coefficient and $S_{u,t}$ the measured wind speed spectrum at tap height or a proposed wind velocity spectrum, e.g. the spectrum specified in EN1991-1-4 given in § 3.3.

Moving average filter by Lawson

Another form of low-pass filter is the moving average filter. The equivalent static gust concept in codes corresponds to a moving average filter of the form by Lawson (1976):

$$\psi_T^2(n, \tau) = \left(\frac{\sin(\pi n \tau)}{\pi n \tau} \right)^2 \quad (3.7)$$

Where:

- ψ_T = Moving average filter
- τ = Averaging time.

Where the averaging time is defined as:

$$\tau = C_T L_{char} / U_z \quad (3.8)$$

With:

- C_T = Constant belonging to an appropriate averaging time. According to Lawson (1976) $C_T = C_r$
- L_{char} = Characteristic dimension of the area considered
- U_z = Mean longitudinal wind velocity at structures height

The characteristic dimension can be the diagonal of the rectangular area or the largest dimension, either height or width. According to Lawson (1976) $C_T = C_r = 4.5$. From Dyrbye and Hansen (1999) it is concluded that setting $C_T = C_r$ will underestimate the response based on the theoretical description of the aerodynamic admittance in equation (3.30) on page 26. This is further explained and derived for the pressure measurements in chapter 7.

3.2. Dynamic response of a structure

Due to the turbulent character of the wind a structure experiences a fluctuating response. Besides a background fluctuating response to which all structures are subjected, structures may experience a resonant vibratory response, provided that their fundamental frequency and damping are low enough to be in range of the dominant wind frequencies. In this section, the essential parameters that determine the dynamic behaviour of buildings are described and models to calculate the response are given.

3.2.1. Cantilever beam model

For the sake of simplicity a building is often schematized by a cantilever beam. The dynamic behaviour of this beam is then represented by a SDOF system for every individual mode of vibration. Due to this simplification torsional vibrations of the building are not included. This same simplification is found in EN1991-1-4. For the purpose of this research only alongwind buffeting response is considered, so torsion is not included in the results.

Separate equations of motion can be written for the a time-varying modal coordinate $a_j(t)$, for each mode j of the structure.

$$G_j a_j + C_j \dot{a}_j + K_j a_j = Q_j(t) \quad (3.9)$$

Where:

- G_j = The generalized mass: $\int_0^L \mu(z) \phi_j^2(z) dz$
- $\mu(z)$ = The mass per unit length along the length L of the structure
- ϕ_j = Mode shape
- C_j = The modal damping ($= 2\zeta_j G_j \omega_j$)
- K_j = The modal stiffness ($= G_j \omega_j^2$)
- ζ_j = The damping as a fraction of the critical damping
- ω_j = The natural undamped circular frequency $= 2\pi n_j$
- $Q_j(t)$ = The generalized force equal to $\int_0^L f(z, t) \phi_j(z) dz$

The response of a SDOF system to a random load in the frequency domain is described by the spectral density of the modal coordinate. This spectral density is then given by:

$$S_{a_j}(n) = |H_j(n)|^2 S_{Q_j}(n) \quad (3.10)$$

With:

- S_{a_j} = Power spectral density of the modal coordinate
- $H_j(n)$ = The transfer function or mechanical admittance for the j th mode
- S_{Q_j} = Power spectral density of the generalized force

And the transfer function is given by:

$$|H_j(n)|^2 = \frac{1}{K_j^2 \left(\left[1 - \left(\frac{n}{n_j} \right)^2 \right]^2 + 4\zeta_j^2 \left(\frac{n}{n_j} \right)^2 \right)} \quad (3.11)$$

With:

- n_j = Natural frequency

3.2.2. White noise approach

In practice the response of a single degree of freedom system is often determined using the white noise approach as the spectrum of the response is fully determined by the peak at the natural frequency. Therefore the loading spectrum is assumed constant with frequency with intensity $S_{Qj}(n_j)$. Using both white noise approach and the cantilever beam model, the variance of the modal coordinate can be given by:

$$\sigma_{aj}^2 = \int S_{aj}(n) dn = \frac{\pi n_j}{4\zeta_j G_j^2} S_{Qj}(n_j) \quad (3.12)$$

3.3. Davenports approach to dynamic global wind loading

In this section the spectral approach used by Davenport will be explained in more detail. It is based on the description given by Solari and Tubino (2007) and by Steenbergen et al. (2012).

As discussed previously the instantaneous wind velocity at a certain location can be expressed as a summation of the mean wind speed at height z of that location and a longitudinal turbulent zero-mean component. Traditionally, when analyzing the alongwind buffeting response, the lateral and vertical components of the turbulence are not considered.

3.3.1. Single degree of freedom system

Global wind loading

The instantaneous pressure at point P can be described in a similar way as the wind velocity, by a mean and turbulent component. Using the strip and quasi-steady theory (Davenport, 1961) and assuming little turbulence with respect to the mean wind velocity, the mean and turbulent component of the instantaneous pressure can be described in terms of wind velocity by:

$$\bar{p}(z) = \frac{1}{2} \rho_{air} U_m^2(z) c_{pm}(P) \quad p'(z, t) = \rho_{air} U_m(z) u(P; t) c_{pm}(P) \quad (3.13)$$

p = Pressure

ρ_{air} = Air density

U_m = Mean longitudinal wind velocity

u = Fluctuating component of the wind velocity in the direction of U_m at time t

c_{pm} = Mean pressure coefficient

The resultant force can also be described in terms of a mean and turbulent component.

$$\bar{F} = \int \bar{p} dA \quad F'(t) = \int p'(t) dA \quad (3.14)$$

This can be simplified when it is assumed that the pressure coefficient is constant over an area A and when this area is small enough that the description of the wind velocity can be considered constant over A .

$$\bar{F} = \frac{1}{2} \rho_{air} U_m^2(z) c_{pm} A \quad S_F(n) = \rho_{air}^2 U_m^2(z) S_u(n) |\chi_u|^2(n) c_{pm}^2 A^2 \quad (3.15)$$

F = Overall force on a certain area

A = Area

S_F = Power spectrum or variance spectrum of the force

S_u = Power spectrum of turbulent wind component at a certain location

$|\chi|^2$ = Aerodynamic admittance

The aerodynamic admittance function, $|\chi_u|^2(n)$, corrects for the lack of full correlation between the turbulent pressure components at area A .

For the wind variance spectrum, S_u several empirically based expressions exist. Davenport (1967) suggested:

$$S_u(n) = S_N \frac{\sigma_u^2}{n} = \frac{2}{3} \frac{f_L^2}{(1 + f_L^2)^{\frac{4}{3}}} \frac{\sigma_u^2}{n} \quad (3.16)$$

With:

f_L = Non-dimensional frequency: $nL(z_s)/u_m$

$L(z_s)$ = Turbulence length scale: determined by the average size of a wind gust at the reference height z_s

U_m = Mean longitudinal wind velocity

σ_u = Standard deviation of wind velocity: $I_u(z)u_m(z)$

I_u = Turbulence intensity

In EN1991-1-4 use is made of the expression:

$$S_u(n) = S_N \frac{\sigma_u^2}{n} = \frac{6.8f_L}{(1 + 10.2f_L)^{\frac{5}{3}}} \frac{\sigma_u^2}{n} \quad (3.17)$$

In figure 3.2 both expressions for the spectral density S_N are shown, illustrating the differences between the two spectra. Especially in the lower frequency range these spectra show considerable differences.

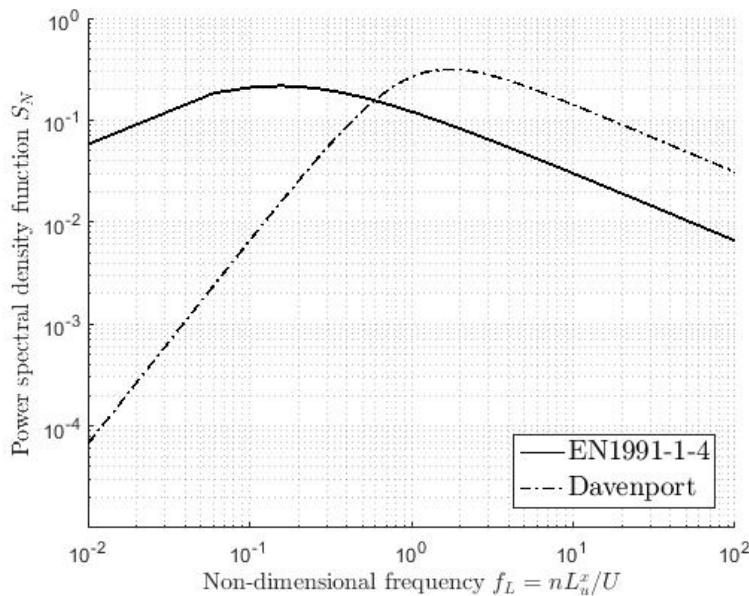


Figure 3.2: Power spectral density functions for the longitudinal turbulence component.

Using the gust factor approach as has been suggested by Davenport (1961) the mean value of the maximum resultant force is given by:

$$\bar{F}_{max} = \bar{F} + g\sigma_F = G_F \bar{F} \quad \text{where} \quad G_F = 1 + g \frac{\sigma_F}{\bar{F}} = 1 + 2gI_u B^2 \quad (3.18)$$

G_F = Gust load factor

g = Gust factor

I_u = Turbulence intensity

B^2 = Background response factor

B is a non-dimensional quantity provided by the relationship:

$$B^2 = \frac{1}{2I_u} \frac{\sigma_F}{\bar{F}} \quad \text{with} \quad \sigma_F^2 = \int_0^\infty S_F dn \quad (3.19)$$

Response including resonant behaviour

The dynamic response $x(n)$ of a structure (e.g. the displacement at the top) can also be divided in a mean and fluctuating part:

$$\bar{x} = f(\bar{F}) \quad S_x(n) = |H(n)|^2 S_F(n) \quad (3.20)$$

- x = Dynamic response of the structure
- S_x = Power spectrum of the dynamic response
- $|H|^2$ = Mechanical admittance

The root mean square of the modal load also accounting for the resonant part is given by:

$$\sigma_F^2 = \sigma_{B,F}^2 + \sigma_{R,F}^2 \quad \text{which can be written as} \quad \sigma_F^2 = \rho_{air}^2 U_m^2(z) c_{pm}^2(z) A^2 \sigma_u^2 [B^2 + R^2] \quad (3.21)$$

R^2 = Resonant response factor

Where the resonance response factor is defined as (using white noise approach):

$$R^2 = \frac{\pi^2}{2\delta\sigma_u^2} n_j S_u(n_j) |\chi_u(n_j)|^2 \quad (3.22)$$

- δ = Logarithmic decrement of damping
- n_j = Natural frequency

The mean value of the maximum alongwind response can be written as the multiplication of the gust response factor G_x and the mean response \bar{x} . Where the gust response factor (GRF) is given by:

$$G_x = 1 + g_x \frac{\sigma_x}{\bar{x}} = 1 + 2g_x I_u \sqrt{B^2 + R^2} \quad (3.23)$$

The equivalent static pressure is the pressure applied to area A that produces the mean value of the maximum alongwind response:

$$p_{es} = G_x \bar{p} \quad \text{alternatively:} \quad p_{es} = c_s c_d \bar{p}_{max} \quad (3.24)$$

Where c_s, c_d are the size and dynamic factor respectively as defined in EN1991-1-4 and \bar{p}_{max} is defined as:

$$\bar{p}_{max} = G_p(z) \bar{p} = \{1 + 2g_p(z) I_u(z)\} \bar{p} \quad (3.25)$$

3.3.2. Cantilever beam model

When applying this procedure to buildings, the cantilever beam model can be applied. This approach to global wind loading is then applied to modal analysis of the structure. In Steenbergen et al. (2012) it can be seen that this introduces the vibration mode Φ into the definitions of the aerodynamic admittance $|\chi_u|^2$, the background B and resonance response factor R . The rest of the procedure is equivalent to the procedure described above.

3.4. Other approaches to dynamic global wind loading

Other approaches to global wind loading including dynamic response are merely based on the approach proposed by Davenport (1961). However, different assumptions and simplifications are made. In this section some of these approaches are discussed with a focus on the approaches used in EN1991-1-4. In §3.4.3 an alternative approach on the gust response factor is described.

3.4.1. EN1991-1-4 Annex B

In EN1991-1-4 two different approaches exist on deriving the structural factor $c_s c_d$. The method in Annex B is merely based on the work of Solari (1982, 1988, 1993a,b). According to the method in Annex B the background response factor is given by:

$$B^2 = \frac{1}{1 + 0.9 \left(b + \frac{h}{L(z_s)} \right)^{0.63}} \quad (3.26)$$

$L(z)$ = Turbulent length scale in EN1991-1-4: $L(z) = L_t (z/z_t)^\alpha$. With $z_t = 200$ m, $L_t = 300$ m and $\alpha = 0.67 + 0.05 \ln(z_0)$

z_s = Reference height, see appendix B

b, h = Width and height of the structure

The resonance response factor is defined as:

$$R^2 = \frac{\pi^2}{2\delta} S_L(z_s, n_{1,x}) R_h(\eta_h) R_b(\eta_b) \quad (3.27)$$

Where:

δ = Logarithmic decrement of damping

S_L = non-dimensional power spectral density function used in EN1991-1-4: $= S_u n / \sigma_u^2$

$R_h = \frac{1}{\eta_h} - \frac{1}{2\eta_h^2} (1 - e^{-2\eta_h})$; $R_h = 1$ for $\eta_h = 0$

$R_b = \frac{1}{\eta_b} - \frac{1}{2\eta_b^2} (1 - e^{-2\eta_b})$; $R_b = 1$ for $\eta_b = 0$

$\eta_h = \frac{4.6h}{L(z_s)} f_L(z_s, n_{1,x})$

$\eta_b = \frac{4.6b}{L(z_s)} f_L(z_s, n_{1,x})$

f_L = Non-dimensional frequency: $nL(z)/v_m(z)$

v_m = Mean wind velocity

$n_{1,x}$ = Fundamental frequency according to approximations in Annex F to EN1991-1-4. For multi-story buildings estimation formula $n_1 = 46/h$ is provided.

In Steenbergen et al. (2012) it is noted that in both relations for B^2 and R^2 the vibration mode is taken outside the integral when deriving these equations.

3.4.2. EN1991-1-4 Annex C

The method in Annex C originates from Dyrbye and Hansen (1999) and is prescribed normative in the Dutch National Annex. It is valid for response-influence functions that have a constant sign.

The background response factor is given by:

$$B^2 = \frac{1}{1 + \frac{2}{3} \sqrt{\left(\frac{b}{L(z_s)} \right)^2 + \left(\frac{h}{L(z_s)} \right)^2 + \left(\frac{b}{L(z_s)} \frac{b}{L(z_s)} \right)^2}} \quad (3.28)$$

The resonance response factor is defined as:

$$R^2 = \frac{\pi^2}{2\delta} S_L(z_s, n_{1,x}) K_s(n_{1,x}) \quad (3.29)$$

Where K_s is the aerodynamic admittance estimation formula by Dyrbye and Hansen (1999):

$$K_s(n) = \frac{1}{1 + \sqrt{(G_y\phi_y)^2 + (G_z\phi_z)^2 + \left(\frac{2}{\pi}G_y\phi_yG_z\phi_z\right)^2}} \quad (3.30)$$

Where:

$$\begin{aligned} G_i &= \text{Constant in aerodynamic admittance by Dyrbye and Hansen (1999) that depends on the shape of} \\ &\quad \text{the response influence function, defined in table 3.1} \\ \phi_y &= \frac{C_{r,y}bn}{v_m(z_s)} \\ \phi_z &= \frac{C_{r,z}hn}{v_m(z_s)} \\ C_{r;y,z} &= \text{Decay constants} \end{aligned}$$

Table 3.1: Values of the constants in the aerodynamic admittance formula by Dyrbye and Hansen (1999)

Mode shape	Uniform	Linear	Parabolic	Sinusoidal
G_i	$\frac{1}{2}$	$\frac{3}{8}$	$\frac{5}{18}$	$4/\pi^2$

Important constants in the aerodynamic admittance function by Dyrbye and Hansen (1999) are the decay constants $C_{r;y,z}$. In EN1991-1-4 the decay constants for both the horizontal as vertical decay are set to be equal to 11.5. This value is based on full-scale measurements by Solari (1993a,b). However, the fact that pressures on the façade have a higher correlation compared to the correlation in the wind flow is not incorporated in this value. From different full-scale measurement studies values of the order 5 are found. Generally a value of 4.5 is adopted to express the decay of correlation of wind pressures on a façade. This value is based on measurements by Newberry et al. (1967). In § 7.1.1 an evaluation of the decay constant for the wind tunnel measurements of the case study is given.

In Steenbergen et al. (2012) it was noted that the procedure in Annex C is more consistent with the theoretical expressions, as the vibration mode is evaluated inside the integral when computing R^2 . The background factor B^2 is still independent of the mode shape, however it was found that the influence of the background factor on the mode shape is relatively small compared to R^2 .

3.4.3. Alternative gust response factor

In the original gust response factor (GRF) approach that is used in most codes, the peak response is defined by a GRF that is based on the top displacement of a single degree of freedom system. Original approaches can overestimate the response in case of base bending moment or shear force considerably.

In Zhou and Kareem (2001) a new method is proposed to derive a GRF based on the base bending moment. This way a more realistic definition of the loading is given also for nonlinear mode shapes (and non-uniform mass distributions). From some numerical examples it was concluded that the displacement based GRF method slightly overestimates 'true' loading and associated responses at the base of the structure.

3.5. Assumptions in global approaches

Assumptions are made in the approaches on global wind loading. These assumptions have been subject of research in the past. Several assumptions and discussions from previous research are therefore presented here.

The first assumption is the one of quasi-steady theory. This quasi-steady theory assumes that the instantaneous pressure is proportional to instantaneous velocity pressure of oncoming flow. In case of this theory, as used in the codes, the peak factor for pressures g_p equals the peak factor for the oncoming wind velocity g_u . Geurts (1997) investigated the applicability of the calculation methods for wind loading on buildings, especially the turbulence, size and dynamic effect, using experimental data of full-scale measurements in Eindhoven. Geurts (1997) found that for wind loading on buildings as a whole only a small error is introduced from the assumption of quasi-steady theory, as negative effects on the windward face and positive

effects on the leeward face balance each other. Kawai (1983) proposed a correction for the windward face, using the pressure/velocity admittance.

From his investigation to the effect of turbulence intensity on the negligibility of the non linear quadratic term ($u(t)^2$) in codes, Kawai (1983) concludes that this has a large effect for low rise buildings in built-up terrain, because of a turbulence intensity $I_u > 0.20$. For dynamic sensitive (high-rise) buildings this underestimation is not relevant and the non linear quadratic term can be ignored.

In Geurts (1997) the factors in the previous Dutch code C_{dim} and ϕ_1 , in the Eurocode c_s and c_d respectively, are compared to the experimental results from full scale measurements using the force spectra from the procedure in the code and from a modified procedure using the experimental data in Eindhoven. Also the effect of wind spectrum is under consideration. A new wind velocity spectrum is proposed than the spectrum by Davenport. He concludes that the choice of expression for the wind spectrum can effect the response of the structure considerably. An accurate description of the wind spectrum is therefore very important.

In the approach by Davenport it is also assumed that the lateral and vertical coherence of the pressures on the windward and leeward façade are equal to the coherence of the wind velocity fluctuations upstream of the structure. However, Geurts (1997) amongst others found that the coherence of the pressures is higher than the coherence of wind velocity.

Last, in Davenport's approach full correlation is assumed between pressures on the wind- and leeward side of the building as the coherence is set to be 1. This assumption leads to an overestimation of the response as these pressures are not fully correlated (full correlation of the absolute values of the pressures on wind and leeward face is meant). In the Dutch Annex to EN1991-1-4 therefore the resulting force may be multiplied by an additional reduction factor to account for this lack of correlation.

Dynamic response of the structure is evaluated by modelling the building by simple beam model and deriving dynamic amplification on the top displacement of the building. This leads to a resonance or dynamic amplification factor. Using a simple beam model is usually considered to be accurate for modelling the response of a building. However, simplifications with respect to incorporating the mode shape and deriving global response at foundation level by a method based on top displacement, can have considerable effect as was shown by Steenbergen et al. (2012) and Zhou and Kareem (2001).

In current research it is ought to provide a method to combine the true correlation effects of wind pressures in time and space and the dynamic amplification of the response considered in a more realistic manner. Thereby this method incorporates both effects directly in the wind load model in contrast to the use of correcting factors in conventional approaches.

4

Probabilistic approaches to wind loading

In this chapter the parameters affecting the uncertainty of the wind load are discussed. Different methods for approaching these uncertainties will be presented. In § 4.1 a general overview to uncertainties in wind loading addressed in literature is given. In § 4.2 an introduction to the historic development of considering these wind load uncertainties is given. In § 4.3 the method described by Cook (1985) is presented. Where in § 4.4 the method proposed by Davenport (1983a,b) and in § 4.5 the method prescribed in the Probabilistic Model Code for wind loading JCSS (2001) is explained. § 4.6 describes the assessment procedure proposed by Meinen (2015) for wind loaded façade elements. Last, in ?? a discussion on to what extent the presented methods can be used for current research is given.

4.1. Uncertainties in the wind loading model

The general wind load effect is dependent on several parameters that contain uncertainties which are named and grouped in equation (4.1). The first group relates to the meteorological uncertainties, the second to the structure-fluid interaction and the third to the structural properties.

$$W = W [(\bar{q}, I_u, S_u(n), \alpha, \rho_{air}); c_f(shape, \bar{q}, I_u, Re, St, Je, C_{r,y}, C_{r,z}); (n_j, \zeta_j, \phi_j)] \quad (4.1)$$

- q = Wind pressure (open field)
- I_u = Turbulence intensity
- S_u = Power spectral density of the longitudinal turbulent wind component u
- α = Shape parameter of the wind profile
- ρ_{air} = Air density
- c_f = Force or load effect coefficient
- Re = Reynolds number: dimensionless quantity in fluid mechanics, used in the scaling of similar but different-sized flow situations (wind tunnel)
- St = Strouhal number: dimensionless number describing oscillating flow mechanisms, used in the scaling of similar but different-sized flow situations (wind tunnel)
- Je = Jensen number: non-dimensional parameter describing the relationship between the flow and the building geometry, used in the scaling of similar but different-sized flow situations (wind tunnel)
- $C_{r,y,z}$ = Decay constants
- n_j = Natural frequency
- ζ_j = The damping as a fraction of the critical damping
- ϕ_j = Mode shape

In this section all uncertainties that arise in wind loading and the wind loading effect on the main bearing structure are discussed. Therefore in § 4.1.2 a summary is given of the uncertainties described by Meinen (2015) for wind loading on static façade elements. For the elaborate description of these uncertainties, reference is made to this document. In § 4.1.1 the typecasting of uncertainties consistent with the typecasting used in Meinen (2015) is described. The uncertainties accompanying the dynamic and global effects of wind loading will be discussed in § 4.1.3 in more detail.

4.1.1. Uncertainty typecasting

Several types of uncertainties can be specified which all have different origin. Davenport (1983b) specified three of them in the field of wind engineering: intrinsic, knowledge and codification uncertainties.

Intrinsic uncertainties follow from the random nature of the wind loading problem. Wind climate and turbulence are two of this type of uncertainties. They can not be described in any other way than in statistical terms.

Knowledge uncertainties are due to the lack of knowledge of how to model the wind loading process. They tend to decrease with time as more research on the subject is performed. In Meinen (2015) this type of uncertainties is divided into 4 subtypes; measurement, statistical, sampling and model uncertainties.

Measurement uncertainties are uncertainties due to the errors in observation, sampling or representativity in the measurements.

Statistical uncertainties arise from the statistical methods chosen to derive the stochastic approximation of the random variable considered. These statistical methods are used to derive the distribution parameters of the random variables and the choice of statistical method can greatly affect the shape of the fitted distribution. In the wind loading model, the modelling of extremes greatly depends on the statistical method and its quality.

Sampling uncertainties are uncertainties due to the estimation of distribution parameters from a limited amount of samples or realizations. A different set of sample data realized from the same 'true' random variable distribution function will result in different estimated parameters. As wind speed measurements and wind tunnel measurements are always limited in size due to economic and time reasons, this type of uncertainties can be quite influential in wind engineering.

Model uncertainties are related to the model used to describe the wind loading. Calculation models are of a predictive nature and 'man-made' and are therefore not the true representation of the wind loading. They can be inexact and incomplete which gives rise to uncertainties.

Codification uncertainties arise from the simplifications made in the standards to make the engineering easily controlled.

4.1.2. Summary static local wind loading uncertainties

In this section the uncertainties relating to the wind loading as described by Meinen (2015) for static and local wind loading are summarized and evaluated. For a detailed description reference is made to the thesis report (Meinen, 2015).

Air density

In Kasperski (2009) the uncertainties with respect to the air density are evaluated. It was found that the scatter of the air density, which depends on air temperature, barometric pressure and relative humidity, reduces with increasing wind speeds (measurements in Düsseldorf). For wind speeds in storm conditions, with a threshold value of $v = 14$ m/s, the scatter is very small. For this research it is found that wind speeds under storm conditions exceed this threshold value as well. Therefore it can be assumed that the uncertainties in the air density have a relatively small effect on the reliability of the structure. In EN1991-1-4 a conservative value of $\rho_{air} = 1.25$ kg/m³ is adopted.

Wind velocity

As stated before the uncertainties in wind speeds is of **intrinsic nature**. The fundamental basic wind velocity v_{b0} can only be described in a statistical way. Intrinsic uncertainties in the wind velocity are generally taken into account in wind engineering also for not full probabilistic procedures. The coefficient of variation for the dynamic pressure ($\propto v^2$) in the Probabilistic Model Code (JCSS, 2001), $V_Q = 0.2-0.3$, also suggests substantial influence of the intrinsic uncertainties in the wind speed on the reliability of the structure.

A long history of research has shown that both **statistical and sampling uncertainties** play a significant role in the description of the extreme wind speeds. This results from the need of modelling extreme wind speed as a stochastic random variable, which is mostly achieved by taking measurements from meteorological stations. From these, for CC2, 50-yearly extreme 10 minute averaged wind speeds have to be modelled, which leads to uncertainties due to the statistical method chosen for this modelling and sampling uncertainties due to the limited amount of measurement data. From Meinen (2015) and Rojani and Wen (1980) it was found that the choice of model distribution type and the sampling uncertainties generally have more influence on the extreme wind load modelling than the choice of parameter estimation technique.

Several types of **measurement uncertainties** in the wind velocity measurements obtained from meteorological stations are considered in Meinen (2015) e.g. systematic sampling errors, observation errors, uncertainties in the exposure correction, uncertainties due to small-scale weather systems and uncertainties due to climate change. The first can be caused by both limitations of the equipment or biased human observations. Observation errors are due to the fact that momentary wind speed measurements correspond to specific meteorological conditions at that moment of time. These conditions tend to change with time which causes differences between several measurements. In the Netherlands several corrections, validations and verifications on the raw measurement data are performed, so both types of errors are minimized. The other three types of measurement uncertainties are considered negligible in Dutch wind design as only small errors or small influence on the extreme wind speed modelling is found in multiple research.

Last, also **codification uncertainties** are considered, due to limited acknowledgement of wind directionality and seasonality and uncertainties in the derivation of the fundamental basic wind velocity v_{b0} from measurement data. Significant advantages are found when accounting for wind-directionality both for cladding loads as global structural response. Little literature is yet found on the advantages of accounting for wind seasonality. For the purpose of this research wind directionality is not taken into account and only the worst case scenario is considered, similar to the Dutch National Annex of EN1991-1-4. The latter type of codification uncertainties is of importance as the fundamental basic wind velocity as specified in the EN1991-1-4 wind loading model corresponds to the 10 minute averaged wind velocity at a height of 10 m, terrain roughness $z_0 = 0.05$ and a rate of occurrence of 1/50 per year. Measurements obtained by the KNMI, however, are provided as hourly mean wind speeds for terrain roughness $z_0 = 0.03$. Correction models exist, but uncertainties in these differences remain. Influences of these uncertainties is reduced when adapting the EN1991-1-4 wind loading model to correspond to the wind velocity measurements. This latter approach is also adopted for the purpose of this research.

Terrain effects

The approach proposed in EN1991-1-4 to account for terrain effects gives rise to multiple **codification uncertainties**. Most importantly only a limited amount of roughness classes are defined, based on a method proposed by Wieringa (1992). This method was proposed as in most cases no accurate measurements of the roughness length z_0 are available. By this method it should be possible to determine the terrain roughness by a visual approach. Wieringa (1992) concludes that at least six or seven classes are needed to provide a 10% accuracy in wind speed estimation at the height of 10 m over the full range of natural observed terrain types.

In EN1991-1-4 only five different roughness classes are defined and in the Dutch National Annex this is even reduced to three classes. This gives rise to the idea that the obtained wind speeds are subject to errors that are possibly larger than 10% at the height of 10 m. In the Dutch National Annex an excluding principle in the determination of the roughness class results in conservative estimations. Generally, a lower roughness length is selected which results in higher wind speeds and therefore conservative wind loads.

Two more conservatisms are introduced through a maximum roughness length and a minimum height. First, even though higher roughness lengths could be the case these are not addressed in EN1991-1-4. Like stated before, a lower roughness length results in conservative values for the wind loads. Second, wind speeds are only derived above a minimum height z_{min} . For structures below this minimum height the wind speed with height z_{min} is used.

Due to possible changes in terrain roughness (usually a higher roughness and therefore lower wind speeds with time) this parameter is subject to **knowledge uncertainties**. However, the influence of these changes

is difficult to quantify, as they situation dependent. Therefore this type of uncertainties is not taken into account explicitly in the assessment procedure.

Also the roughness factor c_r defined in EN1991-1-4 itself is subject to **knowledge uncertainties** as there is a lack of validated experiments on the validity of the used formula for c_r for all situations covered in EN1991-1-4. The Probabilistic Model Code (JCSS, 2001) gives a first estimation of the uncertainties introduced by a coefficient of variation $COV_{c_r} = 0.1 - 0.2$. In Meinen (2015) it is assumed that 'the uncertainties inherent to the (determination of) the terrain roughness z_0 (which have been addressed in the previous paragraphs) are incorporated in this value'. A mean-to-specified value is proposed as $\mu_{c_r} / (c_r)_s = 0.8$ which implies that code specified values for the roughness factor are conservative estimates. The considerable high value of the coefficient of variation results in the fact that these uncertainties will be taken into account in the full probabilistic assessment procedure.

Last, the **codification uncertainties in the gust amplification factor** $[1 + 7I_v]$ are considered. When quasi-static pressure/force coefficients are used which only include the wind-structure interaction effect with averaging time T , the short-term fluctuations are introduced by this gust amplification factor. The Probabilistic Model Code (JCSS, 2001) provides a first estimation on the coefficient of variation of this gust factor: $COV_G = 0.1 - 0.15$.

4.1.3. Global dynamic wind load uncertainties

Load effect coefficients

Intrinsic uncertainties

The turbulent character of the wind which causes short term fluctuations of the load and therefore also of the load effect, like bending moment and shear. These short term fluctuations in the response have an unpredictable nature and are therefore subject to **intrinsic uncertainties**. The uncertainties in load coefficients are generally the first to be acknowledged after the uncertainties in wind velocity. However, most methods focus only on local pressure coefficients where the combined effect of these pressures on the façade are taken into account in a different way like the introduction of a structural factor (e.g. Davenport (1967) and in EN1991-1-4).

The Probabilistic Model Code does JCSS (2001) does include an indication on the intrinsic uncertainties in the force coefficients. These force coefficients multiplied by the wind velocity pressure q give the overall force on a structure. This overall force is the external force on the structure. Load effect is not incorporated as no influence function is applied. However the approximated uncertainties of these force coefficients do give a good estimation on the intrinsic uncertainties of the peak load effect coefficients.

The peak force coefficients are derived by multiplying the gust factor with the pseudo-steady force coefficients (averaged over a certain time t). In JCSS (2001) first estimates of the coefficients of variation for the gust factor and force coefficients are $COV_G = 0.1 - 0.15$ and $COV_{c_f} = 0.1 - 0.15$. The coefficient of variation for the force coefficients is slightly lower than the proposed value for the pressure coefficients. This is to be expected as the fast unpredictable fluctuations in the local pressure slightly even out over the entire façade. The combined coefficient of variation is therefore estimated by:

$$COV_{\hat{c}_f} \approx \sqrt{COV_G^2 + COV_{c_f}^2} \approx 0.14 - 0.21$$

This value for the coefficient of variation indicates that the intrinsic uncertainties in the load effect coefficients are significant and should be taken into account in the full probabilistic assessment procedure.

Statistical and sampling uncertainties

Similar to the wind velocity also peak load effect coefficients are subject to **statistical and sampling uncertainties**. Due to the intrinsic uncertainties in the coefficients, there is the need of modelling them by a stochastic random variable in the description of the stochastic wind load. Usually boundary layer wind tunnel measurements are used, but full-scale measurements are also a possibility. In a boundary layer wind tunnel two measurement approaches for the load effect coefficients are available; integration of pressures over the façade multiplied by their influence function or high frequency base balance technique (HFBB). This last

technique implies direct measurement of the load effects at the base of a static model.

For cost and time saving purposes the measurement length is minimized and therefore a limited amount of sample data is available. The effects of this limited amount of data can be reduced by different peak analysis techniques, but still both statistical and sampling uncertainties are introduced. Similar to the approach on wind velocity, for the purpose of this research both choice of distribution type and sampling uncertainties are addressed as wind tunnel measurements are used.

Modelling uncertainties

Similar to the description by Meinen (2015) the wind tunnel measurements introduce several **modelling uncertainties**. A summary of these uncertainties described by Meinen (2015) is given.

Wind tunnel measurements introduce *scaling uncertainties* which are a result of the scaling between full-scale and model-scale in the wind tunnel. To obtain a similar flow around the model as is found in the full-scale situation, the non-dimensional parameters describing this flow (e.g. Reynolds Re , Strouhal St and Jensen Je number) must obtain equal values in the scaled situation as in the full-scale situation. However it is physically impossible to full-fill all these requirements at the same time. As a result, no wind tunnel scaled model will give a true representation of the required full-scale conditions. Therefore a compromise between desired scale factors and resulting accuracy is always necessary (Cook, 1990). E.g. it was found that while wrong representation of the Jensen number Je strongly influences the pressure measurements at façade level, the Reynolds number Re has negligible influences for most design purposes.

Uncertainties in the *measure of detailing* of the scaled model are considered negligible for the purpose of this research as only global effects are of interest.

In a boundary layer wind tunnel test *modelling of the roughness length*, which causes this atmospheric boundary layer (ABL) in 'real-life', is of high importance. For Dutch design purposes, the CUR 103 (2005) is prescribed when wind tunnel measurements are used. It is prescribed to use a roughness length z_0 which is assumed to result in the most conservative results.

Dynamic response

The dynamic response of a structure is mostly influenced by the fundamental frequency and damping, which are both subject to uncertainties. Thereby the introduction of this dynamic amplification in code and model approaches introduces several other uncertainties in wind loading.

Codification uncertainties of the dynamic properties

Variability in the fundamental frequency and structural damping may arise either from the structures spatial variations in the material properties, its fabrication or in the mathematical idealization of a structure when deriving these parameters. The latter is a source of **codification uncertainties**.

Often both fundamental frequency and damping coefficient of a structure are derived by approximation formulas and assumptions in code practice, which are empirical formulas based on full-scale measurements. This approach introduces uncertainties in these dynamic properties. In the Probabilistic Model Code (JCSS, 2001) the uncertainties in both derived parameters are individually quantified. The coefficients of variation of the fundamental frequency and damping are approximated by $COV_{n_0} = 0.3 - 0.35$ and $COV_{\zeta} = 0.4 - 0.6$. As can be noticed from these relatively high values for the coefficient of variation the uncertainties in the derived parameters are significant and should therefore be taken into account.

Mean-over-specified values of the fundamental frequency and structural damping are $\mu_{n_0} / (n_0)_s = 1/0.85$ and $\mu_{\zeta} / (\zeta)_s = 0.8^1$. The mean fundamental frequency is higher than the specified value in the codes. The code value is therefore considered to be a conservative value. However the code value of the damping is higher than the expected (mean) value, which is a non-conservative choice.

¹For ULS design situations these values are not correct, mean-over-specified values are 1/1.15 and 1.2 actually. Therefore the code value of damping is conservative and for fundamental frequency is not

More recent research (Kwon et al., 2015) has also been conducted on the uncertainties of parameters affecting the wind load on tall (dynamically sensitive) buildings the most and on comparing this to code practice (scope of this research was the ASCE7, American standards). From this research it was concluded that the current approach in ASCE7 on determining the load factor, solely based on the uncertainties belonging to rigid buildings is not adequate for dynamically sensitive buildings. The uncertainties of the damping ratio especially have an additional effect on the total uncertainty of the wind load, besides the dominant uncertainties of the wind pressure, pressure/force coefficients and several modelling and measurement uncertainties. Although his conclusions are based on the ASCE7, it should be noted that EN1991-1-4 does not distinguish between static and dynamic structures for defining a load factor as well. The load factor for wind loading γ_s is supposed to be valid for both local and global loading and both static and dynamically sensitive structures as well.

Model uncertainties of the dynamic properties

Deriving both fundamental frequency and structural damping by approximation formulas results in considerable uncertainties. Other possibilities are computing these parameters from full-scale measurements or finite element analysis. However, these computations are subject to different types of uncertainties, like **measurement and model uncertainties**. Full-scale measurements might result in the highest accuracy, but such measurements are hardly available and are therefore not considered in this research.

Estimation of the parameters through finite element calculations might result in a higher accuracy than the empirical formula, but these require a high level of detailing in the model. Often considerable simplifications are made in the model which reduce this accuracy. In addition, like mentioned before variability in the fundamental frequency and structural damping may also arise either from the structures spatial variations in the material properties and its fabrication. The finite element model will also fail to capture these full-scale phenomena. Therefore it cannot be stated that the finite element estimations will have higher accuracy than the empirical formulas, which are based on full-scale measurements on several buildings. Therefore for the purpose of this research the code formulas for deriving the dynamic properties of the structure will be utilized.

Codification uncertainties dynamic amplification approach

The approaches to global wind loading in codes as described in § 3.3 and § 3.4 for dynamic response of the structure are source of **codification uncertainties** as well.

The methods in EN1991-1-4 Annex B and C contain several assumptions and simplifications. The dynamic amplification factor approach is derived for top displacement of a cantilevered beam model. Approaching a structure by the cantilevered beam model gives rise to uncertainties, but these are considered to be small. While the approach is derived for top displacement, it is also applied to bending moments and shear forces in the structure. From Zhou and Kareem (2001) it was found that this leads to conservative values of the dynamic amplification factor for base bending moment and shear force. Thereby the simplified expressions for the background and resonance response factor in both approaches, including introduction of the mode shape in a simplistic way, introduces more uncertainties.

The Probabilistic Model Code (JCSS, 2001) provides a first indication of all uncertainties in the dynamic amplification factor. The uncertainties are defined by coefficient of variation $COV_{c_d} = 0.1 - 0.2$ and mean-over-specified $\mu_{c_d} / (c_d)_s = 1.0$. It should be noted that these values include the codification uncertainties introduced by the derivation of fundamental frequency and damping as well. This value for the coefficient of variation indicates that the uncertainties in the dynamic response are considerable and should be taken into account in the full probabilistic assessment procedure.

Response coefficients through finite element analysis

Combined load effect and dynamic response uncertainties

For the purpose of this research response coefficients are derived through finite element modelling (see chapter 6). This approach results in coefficients combining both load effect and dynamic response. Therefore the uncertainties from the dynamic response coefficients are a direct combination of the uncertainties described before for load effect coefficients and dynamic response. Therefore response coefficients obtained through a dynamic finite element analysis contain **intrinsic uncertainties** due to the turbulent character of the wind,

statistical and sampling uncertainties, modelling uncertainties due to the wind tunnel measurements and **codification uncertainties** of the dynamic response of the structure.

As the Probabilistic Model Code (JCSS, 2001) only provides a combined coefficient of variation for the dynamic amplification factor including both uncertainties in the dynamic structural properties and simplifications in the approach, the effect of both uncertainties individually is not described. A finite element model provides the possibility to check the effect of the individual uncertainties in fundamental frequency n_0 and damping ζ to the uncertainties in the dynamic amplification factor c_d .

Model uncertainties

The use of finite element analysis in the derivation of the response coefficients introduces additional **model uncertainties** due to the finite element method and its solution techniques and the modelling choices made by the user of the program. These should therefore be carefully checked.

4.1.4. Conclusion

The uncertainties in wind loading described should be combined, which results in a stochastic description of the wind load. The described uncertainties in this section are the basis of the stochastic wind loading effect model derived for the purpose of this research. This is further explained in the methodology description in chapter 6.

In the last century, extensive research has been performed on the probabilistic approaches to wind loading. Therefore, in next sections this historical development and several of the approaches are described. Last, the assessment procedure proposed by Meinen (2015) for determining the structural reliability of wind loaded static façade elements is presented.

4.2. Historical development of accounting for wind loading uncertainties

Methods in wind engineering arose quickly since the 60s of the previous century when Davenport presented his wind loading chain approach. However, at first these methods allowed little for uncertainties in wind loading. Gradually uncertainties in wind speeds were acknowledged which led to the gust-factor approach by Davenport (1961). This method introduces peak values of the response by multiplying a mean value, which is derived with mean wind speed, with a gust response factor (GRF). This method was already introduced in §3.3. This GRF increases the mean value of the response with a standard deviation multiplied by a peak factor, so a peak value of the response is found. It should be noted that this method is still in use in code practice where the peak factor is derived for top displacement of the structure.

Where after wind speed also other wind loading parameters were addressed by probabilistic approaches, these methods only treated the parameters individually and their joint effect on the uncertainties in wind loading is not considered. Therefore a probability of exceedance of the wind load could not be derived. Cook and Mayne (1979, 1980) were the first to account for uncertainties in wind loading jointly, both wind velocity and pressure coefficients. Their method is further explained in §4.3. Subsequently, also Davenport (1983a) proposed a full-probabilistic model by addressing the uncertainties in the other wind loading parameters as well. This is further elaborated on in §4.4. Finally, also the JCSS published a full probabilistic approach, which is addressed in §4.5.

4.3. Method of Cook-Mayne

The full probabilistic approach by Cook and Mayne requires slightly adapted definitions of the wind loading parameters. They based their method on the following wind load equation:

$$\hat{X} = \frac{1}{2} \rho_{air} \bar{V}^2 \hat{c} A \quad (4.2)$$

Where:

\hat{X} = Peak load

\bar{V} = Annual-maximum hourly-mean wind speed

\hat{c} = Peak loading coefficient (both minimum and maximum)

The parameter definitions in equation (4.2) on the previous page are based on the spectral gap as defined in §2.1 in figure 2.1 on page 7. This spectral gap allows subdivision of the wind velocity near a structure by a mean and turbulent component, because both macro-meteorological and micro-meteorological behaviour can be considered independent. In equation (4.2) on the previous page \bar{V} is a function of the macro-meteorological peak only. An averaging time $T = 1$ hour is chosen. In \hat{c} both micro-meteorological behaviour as wind-structure interaction is incorporated (similar to $[1 + 7I_v]c_p$ in EN1991-1-4).

Central to the approach by Cook and Mayne lies the question: 'What is the value of the loading coefficient \hat{c} that results in a design load X_d with return period N , given a wind speed \bar{V} with the same return period?' (Cook, 1990).

To answer this question the probability density function (PDF) of the peak wind load \hat{X} should be evaluated. The statistical independence of the parameters \bar{V} and \hat{c} allows the joint PDF simply to be obtained from the product of the individual PDFs, equation (4.3). The joint PDF is visualized in figure 4.1. Also plotted are lines of constant \hat{X} . A Type I generalized extreme value (GEV) distribution is assumed by Cook and Mayne for both the annual-maxima hourly-mean wind speeds as the peak loading coefficient. The theory on extreme value distributions is further presented in chapter 5.

$$f_{\bar{V},\hat{c}}(\bar{V},\hat{c}) = f_{\bar{V}}(\bar{V}) \cdot f_{\hat{c}}(\hat{c}) \quad (4.3)$$

$f_x()$ = Probability density function

The probability density of the wind load can be computed through integration of the joint PDF along a line element l of constant \hat{X} like equation (4.4).

$$f_{\hat{X}}(\hat{X}) = \frac{1}{2} \rho \int f_{\bar{V}}(\bar{V}) \cdot f_{\hat{c}}(\hat{c}) dl \quad (4.4)$$

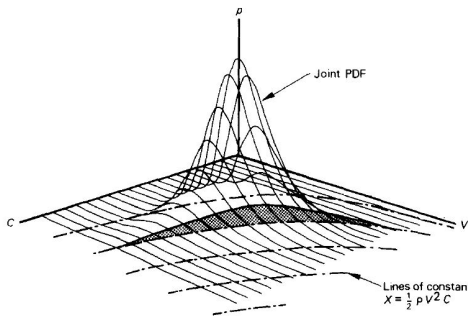


Figure 4.1: Joint probability density function of wind speed \bar{V} and peak loading coefficient \hat{c} Cook and Mayne (1979)

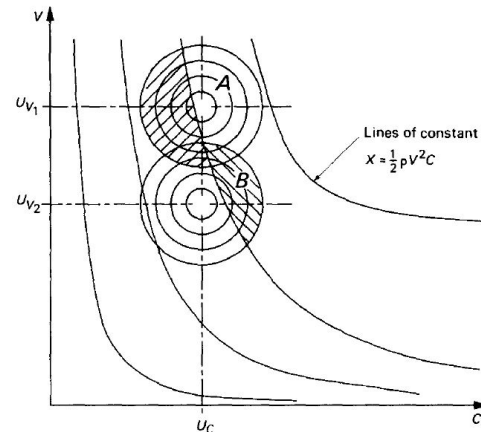


Figure 4.2: First- and second order joint probability density function of wind speed \bar{V} and peak loading coefficient \hat{c} Cook and Mayne (1980)

Next, some refinements on this first-order approach are given along with some useful implementations in wind engineering. It should be noted that these findings are based on the wind climate in the UK and a limited amount of wind measurements. The findings however will also be valid for wind climates and loading coefficient data with similar fitted distribution parameters as the parameters of the fitted UK wind speed and coefficient data.

4.3.1. Full order method

In the previous method only the annual-maximum hourly-mean wind speed with the maximum loading coefficient within that hour is considered. However, a second-strongest (or third, fourth etc.) combined with a

large peak loading coefficient could lead to higher load values than the strongest hour load. This is visualized in figure 4.2 on the preceding page. Cook and Mayne (1980) included these higher order effects by corrections of the first order method. It was found that for design purposes only corrections up to the fifth-order were of relevance.

4.3.2. 'V-c method' versus 'q-c method'

In Cook and Mayne (1982b) a further refinement of the design approach was given. It has been stated that the quality of the results by the approach are strongly dependent on the quality of the wind speed and loading coefficient data. Using the Type I GEV distributions for this data is just fitting the real data to a convenient model. Therefore the 'goodness' of fit greatly effects the accuracy of the results. In Cook and Mayne (1982a) it was found that the parent distribution of the dynamic pressure \bar{q} converges to this Type I distribution much faster than the parent distribution of the wind speeds \bar{V} . An other convenience of the method is that it linearises the problem and results in a more elegant solution.

Comparing both methods leads to the statement that the 'q-c method' underestimates compared to the 'V-c method'. For UK wind climate and 50-year return period, this underestimation is about 7%. If the Type I fit to the dynamic pressure data proves to be more accurate than to the wind speed data, the results of the 'q-c method' can be found 'correct' and the 'V-c method' overestimates. Therefore the 'V-c method' can be labelled to be the conservative method of the two and is therefore to be preferred if any doubts to the accurateness of the \bar{q} fit remains.

4.3.3. Simplified method and Cook-Mayne fractile

The method and refinements described previously still are not able to give a simple and direct answer to the question stated before. Therefore in Cook (1990) a simplified method is proposed. This method provides a direct answer to the question without the need for wind tunnel data and wind climate analysis for every design.

First the sensitivity of the full method to the variations in the parameters of the Type I GEV-distribution is tested. It was found that there is both little dependence on return period and a small range of fitted distribution parameters. A standard design value for the peak loading coefficient could therefore be defined, which is called the 'Cook-Mayne coefficient'. It was found that for UK design purposes this design value corresponds with the 0.78-fractile of the peak loading coefficient data.

4.4. Method by Davenport

4.4.1. Davenport's wind loading uncertainties

In Davenport (1983a,b) a detailed approach to relate reliability to wind loading was provided. At the basis of this approach lies the description of wind loading by the wind loading chain of Davenport. The wind load per unit area is given by:

$$w = q \cdot c_e \cdot c_p \cdot c_{str} \quad (4.5)$$

w = Wind load per unit area

q = Wind pressure (open field)

c_e = Exposure coefficient (terrain influences)

c_p = Pressure coefficient

c_{str} = Structural response factor including gust factor and dynamic response

Davenport considered uncertainties in all relevant parameters, including the model uncertainty and not only the uncertainties in wind speed and wind-structure interaction like Cook (1990). In Figure 4.3 on the following page a summary is given for rigid structures of smaller dimensions. The model uncertainty factor μ is defined as the ratio of the true wind load to the predicted wind load using local wind velocity measurements and pressure coefficients derived from wind tunnel measurements. Davenport recognized that any real data can

be subject to error. All input parameters are expressed by their mean and coefficient of variation. Under the assumption that they are independent, the mean wind load can be determined by:

$$\bar{w} = \bar{q} \cdot \bar{c}_e \cdot \bar{c}_p \cdot \bar{c}_{str} \cdot \bar{\mu} \quad (4.6)$$

And the variability of the wind load by:

$$(1 + COV_w^2) = (1 + COV_q^2) (1 + COV_{c_e}^2) (1 + COV_{c_p}^2) (1 + COV_{c_{str}}^2) (1 + COV_{\mu}^2) \quad (4.7)$$

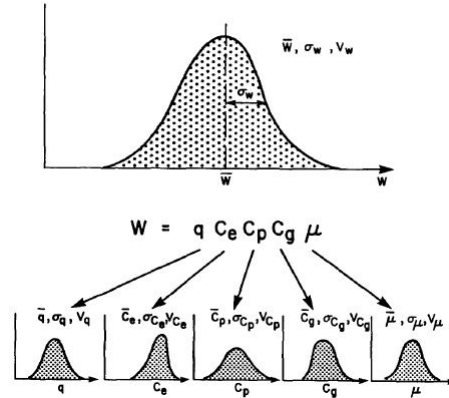


Figure 4.3: Statistical factors in Davenport's wind loading chain (Davenport, 1983a)

Davenport expressed the statistical properties of the input parameters by a mean to specified value and coefficient of variation. The mean to specified value is defined as the ratio of the specified value by the codes to the mean values of the 'true' parameters. The ratio of the specified wind load to the mean wind load can be defined by the ratios of the individual parameters:

$$\frac{\bar{w}}{(w)_s} = \frac{\bar{q}}{(q)_s} \cdot \frac{\bar{c}_e}{(c_e)_s} \cdot \frac{\bar{c}_p}{(c_p)_s} \cdot \frac{\bar{c}_{str}}{(c_{str})_s} \cdot \bar{\mu} \quad (4.8)$$

The parameters proposed by Davenport in (Davenport, 1987) are given in table 4.1.

Table 4.1: Approximate estimates of wind load uncertainty factors (Davenport, 1987)

Quantity	Mean Specified	Coefficient of variation COV
q_{50y}	0.8	0.2 - 0.3
c_e	0.8	0.1 - 0.2
c_p	0.9	0.1 - 0.2
c_{str}	1.0	0.1 - 0.2
ζ	1.0	0.4-0.5

From the proposed values it could be concluded that the uncertainties accompanying the structural and terrain effects are of the same order as the uncertainties of the pressure coefficients and can therefore be of considerable importance for the overall uncertainties in wind loading. The largest contribution to the uncertainties of c_{str} comes from the relatively large uncertainties in the damping of a structure, denoted by ζ in table 4.1.

It should be noted that these values are derived for international wind load standards (ISO). Especially for the mean-over-specified values it holds that these are not specifically derived for European Standards, but generally valid for different international codes.

4.4.2. Davenport's full probabilistic method

Davenport (1983a) also provides a full probabilistic method to determine the structural reliability of wind loaded structures. To determine the structural reliability he utilizes the 'second moment reliability' theory, which is based on the exploitation of the following two statistical results:

1. Central Limit Theorem: when independent random variables are combined, their sum or product tends toward a normal or log-normal distribution even if the original variables themselves are not normally or log-normally distributed.
2. Random variables can be characterized by a mean and standard deviation (first and second moment), which makes the algebra to determine the first and second moment of the sum or product of these independent variables straightforward, independent of their precise statistical distributions.

Next, he makes use of the 'safety factor' approach that assumes that uncertainties encountered will be accommodated by this safety factor. For the complete method reference is made to Davenport (1983a) and Meinen (2015).

4.5. Probabilistic Model Code approach

The probabilistic model code has been written by a team of experts as a first attempt 'to put together in a consistent way some - certainly not all - of the rules, regulations, and explanations that are necessary for the design of new structures, or the assessment of existing ones from a probabilistic point of view' JCSS (2001). The document contains both multiple load as resistance models, where a probabilistic wind load model is also included. The wind load model is based on the wind load model by Davenport.

The wind load per unit area of a structure sensitive to dynamic effects is determined by:

$$w = c_d c_a c_g c_r q_{ref,m} = c_d c_a c_e q_{ref,m} \quad (4.9)$$

w = Wind load per unit area
 c_d = Dynamic response factor
 c_a = Aerodynamic shape coefficient (force or pressure)
 c_g = Gust factor
 c_r = Terrain roughness factor
 c_e = Exposure coefficient (terrain influences)
 q = Wind pressure (open field)

When considering the uncertainties in the wind loading, the wind load and the individual parameters can be described by a mean value and their coefficient of variation. The mean wind load effect is given by:

$$\bar{w} = \bar{c}_d \cdot \bar{c}_a \cdot \bar{c}_e \cdot \overline{q_{ref,m}} \quad (4.10)$$

And the variability of the wind load by:

$$COV_w^2 = COV_{c_d}^2 + COV_{c_a}^2 + COV_{c_e}^2 + COV_q^2 \quad (4.11)$$

In contrast to the probabilistic approach by Davenport, the Probabilistic Model Code does not consider model uncertainties directly in their wind loading model. It should be noted however, that model uncertainty factors θ_R are prescribed when calculating the load effect, like structural moments and forces. Both mean-to-specified as coefficient of variation for the individual parameters proposed are presented in table 4.2 on the following page. These values are strongly based on the values proposed by Davenport (1967). Where Davenport did not provide a full description of these parameters, the Probabilistic Model Code JCSS (2001) does recommend the usage of a lognormal distribution for each of the factors. However a different distribution function could be determined as well.

Table 4.2: Approximate estimates of wind load uncertainty factors (Davenport, 1987), (Vanmarcke, 1992)

Quantity	Mean Specified	Coefficient of variation COV
$q_{ref,m}$	0.8	0.2 - 0.3
c_r	0.8	0.1 - 0.2
$c_{a,p}$	1.0	0.1 - 0.3
$c_{a,f}$	1.0	0.1 - 0.15
c_g	1.0	0.1 - 0.15
c_d	1.0	0.1 - 0.2
n	0.85	0.3-0.35
ζ	0.8	0.4-0.6
θ_R	1.0	0.1

4.6. Structural reliability assessment procedure by Meinen (2015)

Cook (1990) only accounted for the uncertainties in the extreme wind speeds and peak loading coefficient in a full probabilistic way including a probabilistic description of these parameters, where Davenport (1983a) also accounted for the uncertainties in the other parameters in the wind loading chain. However, a full probabilistic description of these factors is not provided as they are only described by a mean-to-specified value and coefficient of variation. In the Probabilistic Model Code distribution types are recommended, but only on an approximative basis.

In Meinen (2015) it was ought to provide a full probabilistic assessment procedure for wind loaded façade elements by extending the probabilistic description of the wind loads of Cook (1990) by the other stochastic parameters according to Davenport (1983a). Thereby most recent knowledge on the stochastic description of the extreme wind speeds, pressure coefficients and other parameters was taken into account. By combining the knowledge of existing literature, Meinen (2015) provides a generally applicable assessment procedure that is able to determine the structural reliability of wind loaded façade elements in terms of the failure probability, or reliability index. Both uncertainties on the loading as resistance side of the reliability calculation are taken into account, although the latter only simplistically. Wind-directionality effects are taken into account explicitly.

The approach by Meinen (2015) is summarized in figure C.1 on page 126 in appendix C. The stochastic wind load model is given by:

$$S(z, \theta_i) = \frac{1}{2} \rho_{air} \cdot v_{1hr,N}(\theta_i)^2 \cdot S_v(\theta_i)^2 \cdot c_r(z, \theta_i)^2 \cdot \hat{c}_{pe,1hr}(\theta_i) \cdot A_{ref} \cdot \chi_{model} \quad (4.12)$$

- $S(z, \theta_i)$ = Direction dependent N -yearly extreme wind load
- θ_i = Incident wind direction
- $v_{1hr,N}(\theta_i)$ = Direction dependent N -yearly extreme hourly-mean wind speed at height $z_{ref} = 10$ m
- S_v = Direction dependent factor considering sampling uncertainties of basic wind velocity modelling
- $c_r(\theta_i)$ = Direction dependent roughness factor correcting for height z
- $c_{pe,1hr}(\theta_i)$ = Direction dependent hourly extreme peak external pressure coefficient
- A_{ref} = Reference area of the façade element
- χ_{model} = Model uncertainty factor

The procedure takes into account full-probabilistically the direction dependent N -yearly extreme hourly-mean wind speed $v_{1hr,N}(\theta_i)$ including sampling uncertainties $S_v(\theta_i)$, the direction dependent roughness factor $c_r(\theta_i)$, the direction dependent hourly extreme peak external pressure coefficient $c_{pe,1hr}(\theta_i)$ and the model uncertainties χ_{model} . The uncertainties on the resistance side R are taken into account in a simplistic manner. A summary of the description of these stochastic variables can be found in table 4.3 on the facing page.

Table 4.3: Input parameters for the direction dependent limit state function $Z(\theta_i)$

Variable	Distribution type	Parameters	Remarks
$v_{1hr,N}(\theta_i)$	Type I GEV (Gumbel), Three-parameter- lognormal	Situation dependent	Based on 64 years of measurements at Schiphol airport
$S_v(\theta_i)$	Normal	Situation dependent	Derived by 'bootstrap-design point' method
$c_r^2(\theta_i)$	Lognormal	$\mu/(c_r^2)_s = 0.8$, $COV = 0.15$	Specified value according to EN1991-1-4
$c_{pe,1hr}(\theta_i)$	Type I GEV (Gumbel), Three-parameter- lognormal	Meinen (2015)	Based on boundary layer wind tunnel test
χ_{model}	Normal	$\mu = 1$ [-], $COV = 0.1$ [-]	
R	Lognormal	Situation dependent, $COV = 0.1$ [-]	Derived from EN1991-1-4 design value. It is assumed that this Level I design value corresponds to a probability of non-exceedance of $\phi(\alpha_R\beta)$, with $\alpha_R = -0.8$ and $\beta = 3.8$.

5

Theory on modelling of extremes

Description of the stochastic wind load requires the modelling of extremes of the wind speeds and pressure or response coefficients. In this chapter the basics on modelling of extremes is presented. In §5.1 some general description methods and requirements of sample data are presented. In §5.2 the univariate theorem is given. Finally, in §5.3 the generalized extreme value distribution is described, which is commonly used in the modelling of extremes. In this section also some choices within this modelling for the purpose of this research are explained. In §5.4 the method in this research for incorporating sampling uncertainties is explained.

5.1. General description and requirements of sample data

Similar to the description of analytical distribution functions, the sample data can also be described by the moments. For sample data this includes the sample mean, the unbiased sample standard deviation or coefficient of variation, and the unbiased sample skewness. Both definitions of the mean and standard deviation are considered known to the reader, but the sample skewness does provide important additional information when modelling of extremes. The sample skewness provides information concerning the asymmetry of the data. It is sensitive to large deviations from the sample mean and gives therefore valuable information on the tail behaviour of the distribution.

An other important summary of the sample data is the empirical cumulative distribution function (ECDF). For the purpose of this research the following definition is utilized:

$$F_N(X_i) = \frac{i}{N+1} \quad (5.1)$$

For the modelling of distributions based on sample data the quality of the sample needs to be checked to two requirements. First, the sample data should be identically distributed, or stationary, which means that systematic errors, due to sampling or observation, need to be minimized. Second, the sample data should also contain only statistically independent data.

5.2. Univariate theorem

The univariate theorem follows from this last assumption of independent and identically distributed samples, or in this case random stochastic variables. It states that the distribution of the T -extremes can be derived by the distribution of the t -extremes. This is very useful when limited data is available and the distribution of the T -extremes can not be derived accurately. The univariate theorem is defined by:

$$\begin{aligned} P(X \leq \hat{X})_T &= P(X \leq \hat{X})_t^{T/t} \\ F_T(X) &= F_t(X)^{T/t} \end{aligned} \quad (5.2)$$

5.3. Generalized extreme value distribution

For the modelling of extremes usually use is made of the generalized extreme value (GEV) distribution. In this section this type of distribution is explained. Methods in fitting this distribution and implications for wind engineering are also presented.

5.3.1. Definition of the generalized extreme value distribution

The cumulative distribution function of this type of distribution is given by:

$$F_x(X) = \exp \left\{ - \left[1 + \xi \left(\frac{X - \mu}{\sigma} \right) \right]^{-1/\xi} \right\} \quad (5.3)$$

This model has three parameters; a location parameter μ , a scale parameter σ and a shape parameter ξ . This last parameter describes the tail behaviour of the distribution and depending on the value of this parameter, three types of GEV families are distinguished. The Type II and Type III classes of the GEV distribution correspond to the cases where the shape parameter is given by $\xi > 0$ and $\xi < 0$ respectively and are also widely known as the Fréchet and Weibull families. The case where $\xi = 0$ is denoted as the Type I distribution, or Gumbel distribution. Its cumulative distribution function is defined as the limiting case of equation (5.3) for $\xi \rightarrow \infty$. The differences between the three types of GEV distributions are visualised in figure 5.1.

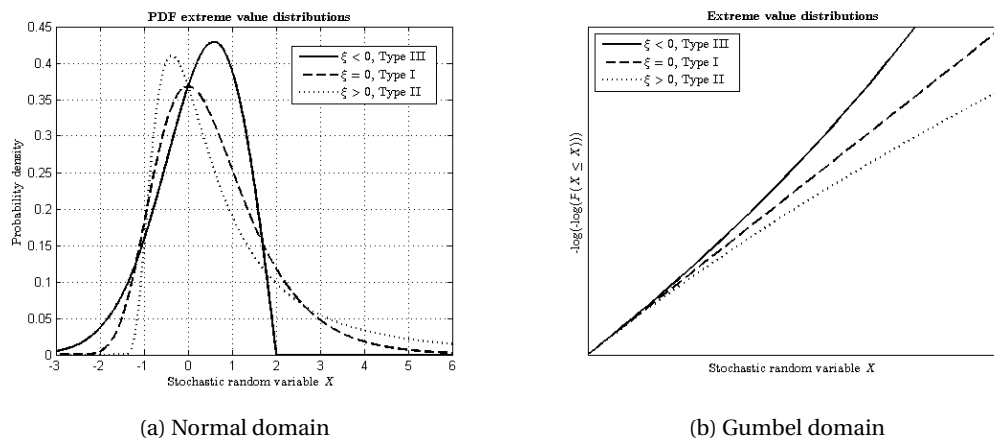


Figure 5.1: The three types of generalized extreme value distributions: the PDF and the CDF in the Gumbel domain (Meinen, 2015).

Due to the definitions of the different distributions it can be seen that the Type III distribution has an upper limit, where the Type II distribution has a lower limit. The parameters are estimated by fitting the distribution to the sample data by means of an estimator. An estimator is a rule for calculating the model parameters based on the observed sample data. These include e.g. moment-based techniques in which functions of model moments are equated with their sample data equivalents and likelihood-based methods. Each technique has its pros and cons, but for the purpose of this research the maximum likelihood estimator is utilized. The maximum likelihood estimate of a model parameter is the value that maximizes the likelihood function. In Coles (2001) it is found that for the ranges of the parameters present in wind engineering this method is valid.

The extremes of the data can either be derived by a block method or peak-over-threshold method. For the latter a generalized Pareto distribution should be used instead of the generalized extreme value distribution (the parameters are related). For the purpose of this research the block method is utilized.

5.3.2. Block method

In order to derive the extremes from the sample data to which a GEV distribution can be fitted, the block method is utilized. The data is blocked into sequences of observation length t and for each of these blocks the maximum observed value is derived. This generates a series of block maxima to which the GEV distribution can be fitted. Using this block method it is important that the chosen block duration ensures statistically

independent extremes. The optimal choice of block duration is always a trade-off between independent extremes and sufficient extremes to minimize sampling uncertainties.

5.3.3. GEV distributions in the field of wind engineering

As discussed before for the GEV distributions three types of distribution functions are to be distinguished; Type I, Type II and Type III. Whichever of the types is best to describe extremes in wind engineering is still a topic of discussion in the scientific community. In Meinen (2015) a complete discussion on this choice for both the wind speeds and peak pressure coefficients can be found. It is agreed that when the Type II is fitted this is generally indicative of a mixed climate which should therefore be decomposed. Therefore this Type II distribution is generally not found in the field of wind engineering. Disagreement can be found between scientists when comparing the Type I and Type III GEV distribution. The Type I GEV distribution is conventional in wind engineering, but it is argued that the Type III GEV distribution should be used as it better describes the skewness of the wind data according to several researches. Therefore for the purpose of this research both distribution types are used. By comparing both methods the effect of the statistical uncertainties can be incorporated in the reliability assessment.

5.4. Sampling uncertainties: Bootstrap design-point method

Like discussed in §4.1.2 sampling uncertainties play a significant role in the description of extreme wind speeds due to the modelling of extreme wind speeds using measurements. A slightly different set of sample data realized from the same 'true' distribution will result in different estimated parameters. Especially the skewness is very sensitive to small deviations in the sample. Therefore the Type III GEV distributions tends to be more sensitive to sampling uncertainties than the Type I GEV distribution as the latter has a fixed skewness. In Meinen (2015) the nonparametric Bootstrap design-point method is defined to account for sampling uncertainties. This method uses a resampling approach and assumes nothing at all about the shape of the distribution. For the purpose of this research the same method will be used. In Meinen (2015) a detailed description is given, but a summary is provided next.

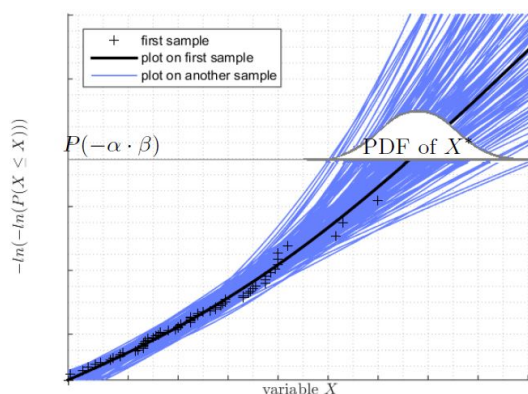


Figure 5.2: Visualization of the Bootstrap design-point method (Meinen, 2015)

In figure 5.2 a graphical summary of the method is given. First, the original dataset is resampled with replacement and model parameters are derived for each sample. Second, the coefficient of variation of the Level I design values of the bootstrapped distribution fits is determined. The Level I design values are the values that correspond to the Level I probability fractile, $P(X \leq \hat{X}) = \Phi(-\alpha\beta)$, with $\alpha = -0.7$ and $\beta = 3.8$. This procedure will be used to define a variable S with mean $\mu = 1.0$ and the obtained coefficient of variation. The sampling uncertainties are therefore separately taken into account. It should be noted that the true design point can only be obtained through a Level II or III calculation, but in Meinen (2015) it was found that the coefficient of variation is nearly insensitive for the chosen fractile of the used extreme wind speeds. Therefore the proposed procedure provides a good estimation of the statistical uncertainties.

II

Development of the probabilistic assessment procedure

6

Methodology for the assessment procedure

In this chapter the approach followed in current research and what it adds to previous research is explained. Thereby it is stated to what extent the proposed assessment procedure will be applicable. Therefore in § 6.1 it is explained which approach is followed in the development of the assessment procedure for global response. The uncertainties accounted for in this assessment procedure are briefly explained and the focus of this research is indicated. Second, in § 6.2 the applicability of the proposed assessment procedure is stated.

6.1. General methodology for the probabilistic assessment procedure

The full-probabilistic assessment procedure developed in this research should be able to determine the reliability level for global response of the main bearing structure of dynamically sensitive buildings subjected to wind loading. This in contrast to previous research (Meinen, 2015) where a full-probabilistic assessment procedure for wind loaded façade elements was developed which is only valid for local loading and static response. The developed procedure in this research links the uncertainties in wind climate, terrain effects, global dynamic response of buildings and resistance full-probabilistically. Therefore both a stochastic wind load model and a stochastic resistance model are developed and the stochastic parameters in these models are quantified. For the resistance model both a simplified model and a material and failure mode specific model are defined and compared, which is explained in chapter 8. The stochastic wind load model should represent the 'true' wind load effect for global response of the building's main bearing structure at foundation level as accurately as possible. In § 4.1 the uncertainties in global wind loading for dynamically sensitive buildings were described and evaluated. Several of these uncertainties are taken into account in the development of the stochastic wind load effect model.

Uncertainties in wind climate

In order to account for the intrinsic uncertainties in the basic wind velocity, this parameter is described by a stochastic random variable. For this purpose location-specific wind speed measurements are used. Modelling the basic wind velocity by a stochastic random variable requires the modelling of extremes, for which reference is made to chapter 5. Both statistical and sampling uncertainties in the basic wind velocity are accounted for as usually measurement periods are relatively small. Statistical uncertainties are introduced by comparing two distribution types for the modelling of extremes. Sampling uncertainties are accounted for through the bootstrap design-point method (§ 5.4).

Uncertainties in wind-structure interaction and structural effects

For evaluating global response of a dynamically sensitive building to wind loading, a new method is proposed where the combined effect of simultaneously measured pressures over both windward and leeward face of the building and the resulting dynamic response of the structure is evaluated by so-called response coefficients. This in contrast to conventional approaches where a spectral approach is utilized which results in a correcting structural factor that is applied to local pressures. This structural factor should correct for both size reduction effects and for dynamic amplification effects. For the correlation between windward and leeward pressures, usually a reduction factor is adopted. However, the response coefficients used in this research are defined for a specific building within a certain terrain and include the 'true' correlation of simultaneously

found pressures and accurate dynamic amplification for the response considered instead of using correcting factors. In the reliability assessment of the main bearing structure these response coefficients can be incorporated directly in the stochastic wind load model accounting for both the turbulent character of the wind and structural effects simultaneously.

For this purpose, in the proposed assessment procedure use will be made of boundary layer wind tunnel measurements of pressures at the façade of a specific building model. Through finite element analysis the combined effect of these pressures in time and space and the dynamic response of the building will be derived in the time domain. This will result in time series of the response coefficients of similar length as the wind tunnel measurements. As wind tunnel measurements are used, the short term fluctuating wind effects are incorporated in these response coefficients and these are therefore defined as peak response coefficients \hat{c}_R . In the stochastic wind load effect model the intrinsic uncertainties in the response coefficients will be accounted for by describing them as a stochastic random variable. Similar to the basic wind velocity, modelling of the peak response coefficients also requires the modelling of extremes (chapter 5). For this research the amount of peak response coefficients was maximized to reduce the effect of statistical and sampling uncertainties in the modelling of these extremes. For this purpose relatively long wind tunnel measurements are combined with methods to reduce the block duration for the block method and therefore to increase the number of extremes. Method development for the response coefficients for the purpose of this research is found in chapter 7. It is also investigated what the effect of uncertainties in the dynamic structural properties of the building is on the response. Therefore a method to incorporate the codification uncertainties in these properties and their effect on the response in the assessment procedure is also developed and explained in chapter 7 in § 7.3.2.

Other uncertainties in wind load model

Finally, several other types of uncertainties should be accounted for in the stochastic wind load effect model. Similar to the stochastic wind load model by Meinen (2015) the knowledge uncertainties in the roughness factor are taken into account by the modelling of the roughness factor as a stochastic random variable for which literature data are used. In addition, all other uncertainties which are not taken into account explicitly are represented by a model uncertainty factor, which is also based on literature.

Summary

A summary of all the uncertainties accounted for in the developed full-probabilistic assessment procedure is provided below:

- Intrinsic uncertainties in the basic wind velocity v_b
- Statistical and sampling uncertainties in the basic wind velocity v_b
- Intrinsic uncertainties in the peak response coefficients \hat{c}_R
- Statistical and sampling uncertainties in the peak response coefficients \hat{c}_R
- Codification uncertainties in fundamental frequency n_0 and damping coefficient ζ
- Knowledge uncertainties in the roughness factor c_r
- Model uncertainty factor to combine all other types of uncertainties implicitly
- Uncertainties in the resistance R

In figure 6.1 on the facing page the context for the previously described approach for the full-probabilistic assessment procedure is summarized and the focus of this research is indicated. In chapters 7 and 8 this scheme is followed to develop a reliability based assessment procedure for global response of wind-loaded dynamically sensitive buildings.

The developed assessment procedure allows for the determination of the reliability index β of wind-loaded dynamically sensitive buildings for global response. This reliability index can be used to assess the safety level of a building designed by the EN1991-1-4 procedure for wind loading and can be compared to code target reliabilities. A detailed description of the developed full-probabilistic assessment procedure and the stochastic resistance and wind load model is given in chapter 8. This chapter also provides a quantification for all stochastic parameters in the developed wind load model.

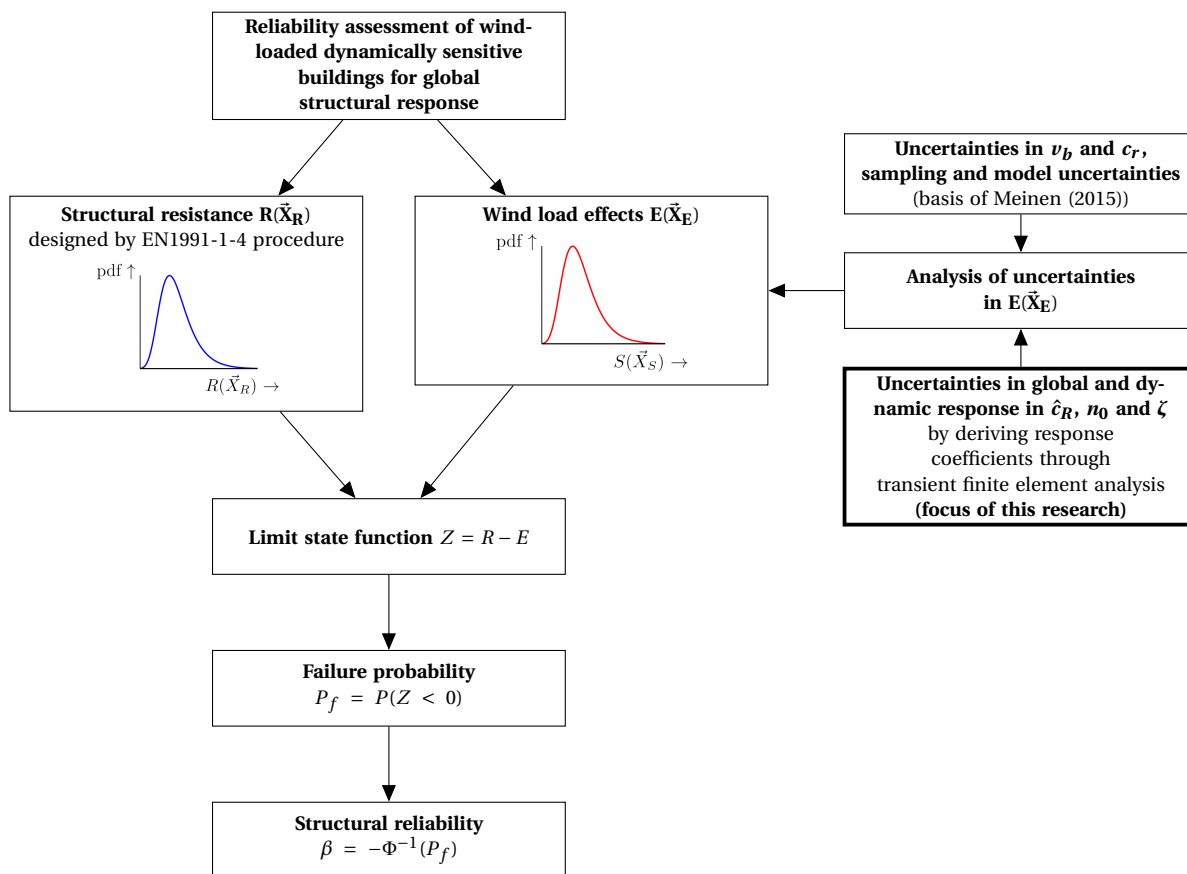


Figure 6.1: Overview of the focus of this research

6.2. Applicability of the assessment procedure

6.2.1. General remarks

The general scope of the research was addressed in § 1.3. In this section the implications of this scope on the applicability of the assessment procedure are described, together with other assumptions that have been derived from the literature study presented previously.

Within the category of dynamically sensitive buildings several building types can be distinguished. For the purpose of this research the methods were developed for one such building typology. Slender high rise buildings are considered with a concrete core as main bearing structure of the horizontal loading (see figure 6.2 on the next page).

The assessment procedure is thereby developed for standard design situations, which correspond to consequence class CC2, ultimate limit state (ULS) and a 50 year reference period. Through some straightforward adaptations of the procedure also other design situations can be considered. A different consequence class only requires a reconsidered load factor γ_s , because of a different target reliability β_{target} . A change of reference period requires an adaptation of the design wind speed in EN1991-1-4 (through c_{prob}) and an adapted definition of the wind velocity in the stochastic wind load effect model.

6.2.2. Load effects and combinations

For a building subjected to wind loading different types of responses can be found e.g. alongwind, an acrosswind (e.g. due to vortex shedding) and torsional response. By Tamura et al. (2008) it was found that there was a high correlation between several structural responses, like the maximum alongwind force and the maximum torsional moment. Only considering the alongwind response in most building codes, like the Eurocode, can lead to a significant underestimation of the response. However, for the sake of limiting complexity and correspondence to the Eurocode approach only alongwind response will be considered in this research, like

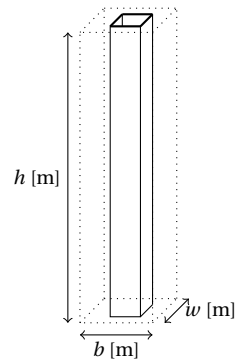


Figure 6.2: Considered building typology

previously discussed in chapter 1. Other dynamic responses like vortex shedding are also not within the scope of this assessment procedure. Thereby wind loading is considered to be the dominant type of loading for the building. Load combinations (e.g. with self-weight or other variable loads) are not taken into account.

6.2.3. Wind directionality

Kasperski (2007) amongst other researchers like Davenport (1983a) discusses the relevance of directionality of the peak wind pressures on the structural response. He concludes that for the bending moment in a low-rise structure only considering the most unfavourable direction leads to an overestimation of the design value, but for that specific case only in the order of 5 – 10%. He also shows that only a few wind directions contribute to the exceedance probability of the design value considered. This conclusion was also made by Meinen (2015).

For the purpose of this research only long-term wind tunnel measurements are available for a 0° angle of attack. The availability of these long-term measurements contributes to the robustness of the results. Thereby, when considering directionality without taking into account other responses besides the alongwind response would not add to the accuracy of the calculations so directionality will be left out of the scope of this assessment procedure.

7

Method development in derivation response coefficients

In this chapter the methods for deriving the response coefficients are derived and explained. For the derivation of the response coefficients pressure measurements are obtained from a boundary layer wind tunnel test. These measured pressures need to be processed appropriately to derive representative pressures for the transient finite element analysis. Therefore in § 7.1 the methods for obtaining these representative pressures are derived. In § 7.2 the finite element methods are derived and choices are explained. Then in § 7.3 the methods on probabilistic modelling of the response coefficients are presented. Some methods are derived on the basis of a case study approach and are therefore presented accordingly. Most methods are thereby illustrated with the case study results. However, the methods described are generally applicable to other buildings of similar typology. The case study is presented in chapter 9, but the exact description is not of true relevance for the methods derived in this chapter. In § 7.4 a summary of the derived methodology is presented that is generally applicable to buildings of similar typology.

7.1. Representative pressures

Through a boundary layer wind tunnel test pressures can be measured at façade level of the building model at specific locations where pressure taps are placed. The measured pressures are therefore very local pressures which are only representative for the area of the pressure tap. The pressure taps on a building model are distributed over the surface and each have a tributary area for which a representative pressure should be derived. In § 3.1 it was found that the correlation of pressures decays with increasing distance between two points on the façade. In conventional wind engineering procedures this lack of full correlation is accounted for by the aerodynamic admittance. However, in wind tunnel tests it is found convenient to process locally measured pressures by a moving average filter that filters out the high frequency fluctuations which have low correlation for the entire tributary area.

In this moving average filter an averaging time for the pressures is defined that results in this filtering when applied on the time series of the wind pressure data. This moving average filter concept should resemble the aerodynamic admittance and will therefore be configured accordingly. This should lead to an accurate expression of the averaging time (equation (3.8) on page 20). An accurate formulation of the aerodynamic admittance can be derived through pressure measurements or through the existing formulations in literature, e.g. the expression in equation (3.30) on page 26 (Dyrbye and Hansen, 1999). The decay constants C_r in this expression are prescribed to be $C_r = 11.5$ in EN1991-1-4. However, it was found in literature that lower constants should be used as pressures on the façade are more correlated than the dynamic velocity pressure q where the original value of 11.5 was derived for. E.g. in Newberry et al. (1967) a value of $C_r = 4.5$ was proposed from full-scale measurements on high-rise buildings. Therefore, for the purpose of this research, methods to derive this decay constant from available wind tunnel measurements are presented in § 7.1.1. In § 7.1.2 methods to obtain the required averaging constant C_T for the averaging time of the wind tunnel measurements are given. The methods are illustrated and explained by means of the case study wind tunnel measurements, but can be executed for other measurements as well. For the purpose of this research also an

evaluation of the required constants, C_r and C_T , for the case study building is presented.

7.1.1. Coherence and decay constant

The coherence of the pressure measurements is used to evaluate the decay constant in the low-pass filters. For this purpose the root-coherence (square root of the coherence or normalized co-spectrum) of the pressure measurements (equation (3.3) on page 18) should be compared to the proposed exponential decay function by Davenport (equation (3.4) on page 18). To fit this decay function to the data different choices can be made e.g. an enveloping decay function or a least square fit to the data can be derived. To arrive at the root-coherences of the measurements an average spectrum should be used by dividing the total wind tunnel registration in several segments using the non-parametric spectral estimation method by Welch based on the periodogram method (Stoica and Moses, 2005). It has been shown that the periodogram is a poor estimation of the power spectral density (PSD) of a discrete signal. Therefore the segment averaging is used to reduce the variance of the estimate PSD. Subsequently a frequency averaging technique is applied to reduce the data storage and to smooth the data. The numerical techniques mentioned are elaborated on in appendix D. An example of the results of this procedure is shown in figure 7.1 on the facing page¹. In these figures also the exponential decay function with $C_r = 4.5$ proposed by Newberry et al. (1967) is plotted for comparison.

From these figures it can be seen that the coherence between taps at the edges of the building model and the other taps is considerably lower than when considering the coherence of the middle taps with all others. Especially the coherence between two edge taps is very low and shows no relation with an exponential decay function. This is to be expected for other wind tunnel building models as well.

A conservative approach is to choose an enveloping decay function, not to underestimate the coherence of the pressures. For the evaluation of an appropriate decay function both horizontal as vertical coherences should be plotted together. On a note, in Geurts (1997) it has been found that one should be careful to compare the coherence in the wind tunnel and the one in full scale. He concluded for his measurements that there is a higher coherence in the wind tunnel than in full scale. However, in many cases there are no full-scale measurements available. Therefore, using the wind tunnel pressure coherence, is expected to result in a conservative value for the decay constant. An example of all horizontal and vertical coherences and the fitted exponential decay functions is found in figure 7.2 on the facing page².

Decay constant for this research

From figure 7.2b on the next page a value of 4.5 for the decay constant is already a reasonable choice for the vertical coherence, while the horizontal coherence in figure 7.2a on the facing page suggests a decay constant of the order 2.0. However, the data is very scattered and the fit to the data is very different from the enveloping decay function. Therefore choice is made to adopt a decay constant of 4.5, as for current wind tunnel measurements this is a quite reasonable enveloping value. This way a not too conservative value is adopted as Geurts (1997) gave reason to believe that the coherence in the wind tunnel can be higher than in the full-scale situation. Besides, this value for the decay constant has also been found by Newberry et al. (1967) from full-scale measurements on high-rise buildings.

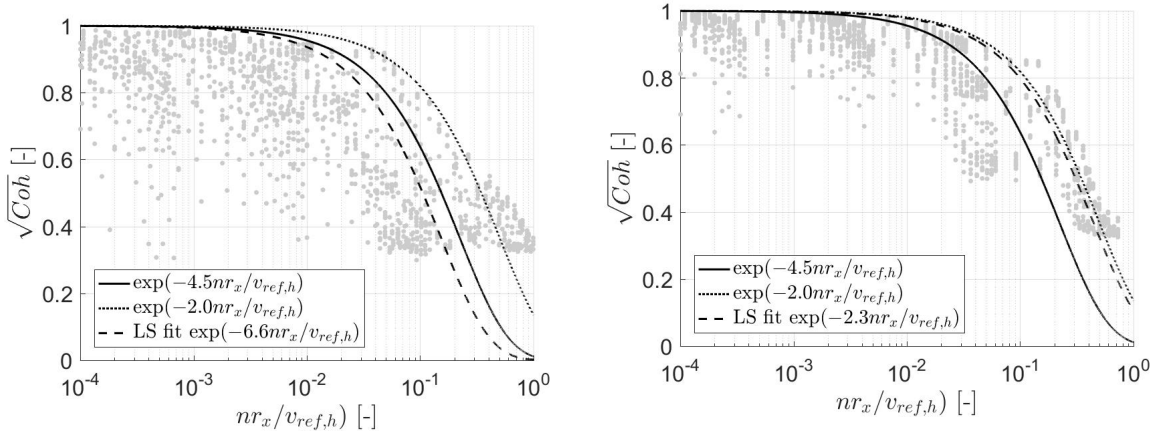
7.1.2. Moving average filter and averaging constant

Both Lawson (1976) and Cook (1985) proposed $C_T = 4.5$ as averaging constant. However, several researches have led to a smaller constant value as a value of 4.5 would not provide a sufficient safe averaging time. In Dyrbye and Hansen (1999) a value of 1.5 is proposed and Holmes (1997) proposed a value of 1.0 for a square area. For a line structure even a lower value of 0.75 was found.

For high-rise building models the tributary areas of the pressure taps often have a rectangular shape. The perpendicular lines are used to determine these areas. This choice should be evaluated later. For these rectangular shaped areas the characteristic dimension is chosen to be the height of the tributary area of the pressure tap, because all areas are considerably longer than wide. An example of the tributary areas can be seen in

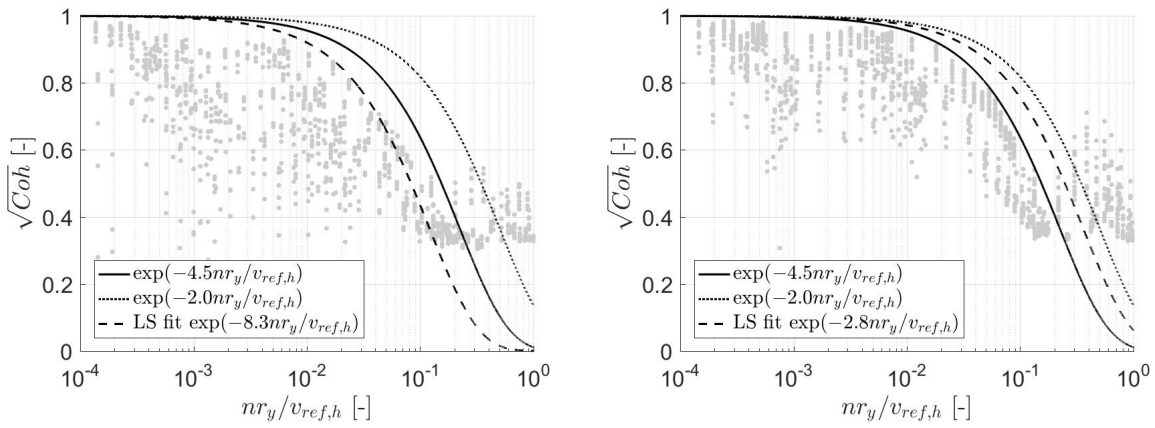
¹These figures are plotted for the case study pressure measurements. For these measurements an inconsistency at a full-scale frequency of 0.6 Hz is found, which is most clear in figure 7.1d. In the pressure spectra a dip in the spectral density can be found at this frequency which is shown in figure E.1 on page 131. This results in a peak in the coherence at the same location. Therefore the highest frequencies are not considered in the further analysis of the decay constant for this data.

²Figures are plotted for the case study pressure measurements. The high frequencies are left out (see note 1)



(a) Horizontal coherence between the side pressure taps and other taps on that horizontal line with $r_x = 2.5 - 27.5$ m

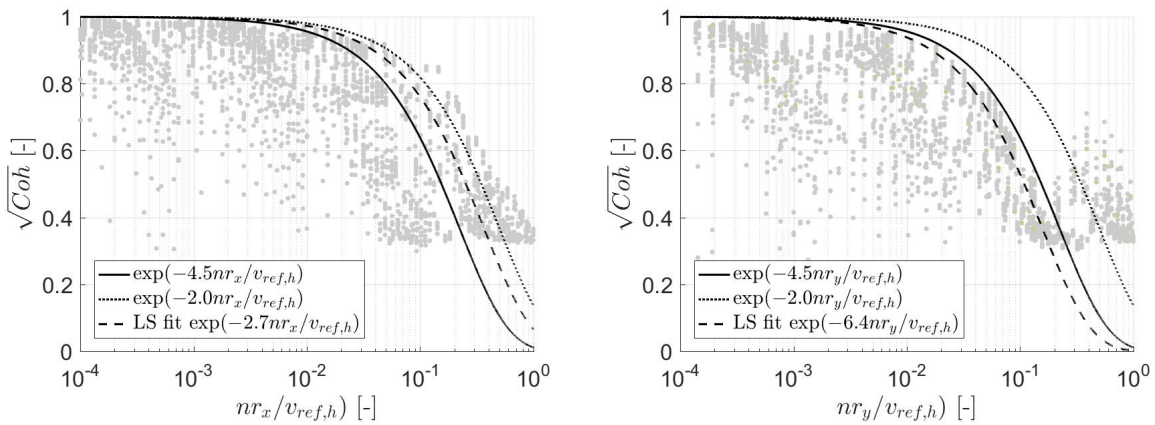
(b) Horizontal coherence between the middle pressure taps and other taps on that horizontal line with $r_x = 7.5 - 13.75$ m



(c) Vertical coherence between the top pressure taps and other taps on their vertical line with $r_y = 18.75 - 87.75$ m

(d) Vertical coherence between the middle pressure taps and other taps on their vertical line with $r_y = 20 - 40$ m

Figure 7.1: Root coherence

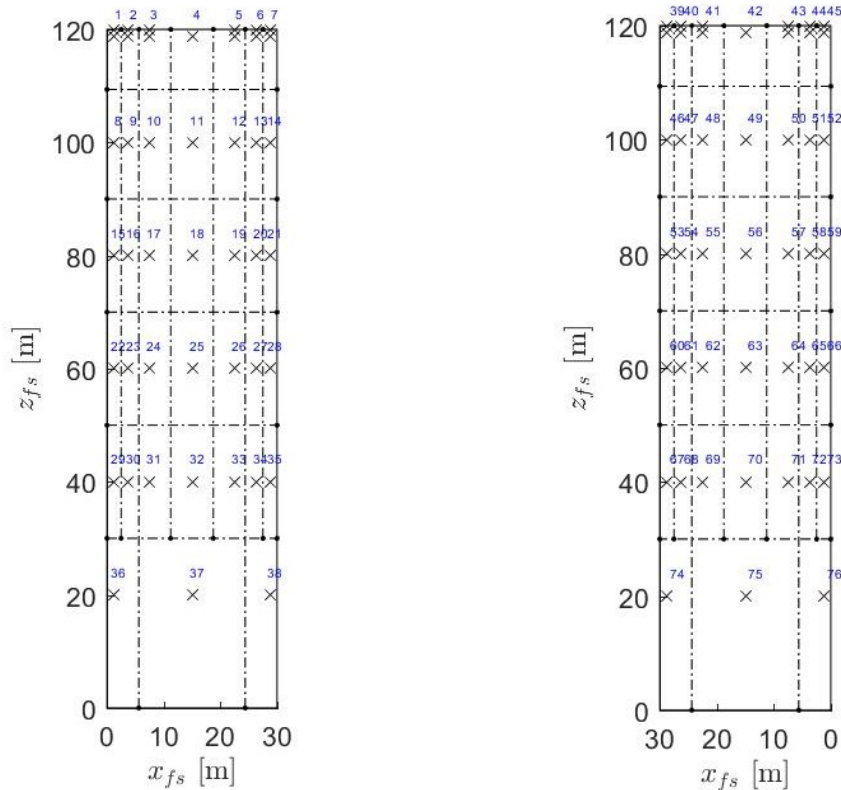


(a) Horizontal coherence between pressure taps with $r_x = 2.5 - 27.5$ m

(b) Vertical coherence between pressure taps $r_y = 18.75 - 87.75$ m

Figure 7.2: Root coherence of all taps up to a frequency of 0.6 Hz

figure 7.3³. To derive the required averaging constant the methods of Holmes (1997) and Dyrbye and Hansen (1999) should be repeated for the tributary areas of the pressure taps of the used wind tunnel test.



(a) Tributary areas for pressure taps at windward face (b) Tributary areas for pressure taps at leeward face

Figure 7.3: Tributary areas

First, for a representative area of the façade, the aerodynamic admittance approximation of equation 3.30 is to be compared to the moving average filter. This is shown in figure 7.4.⁴ The equivalent moving filter is plotted for both the values of $C_T = 4.5$ and $C_T = 1.5$. The latter value is proposed in Dyrbye and Hansen (1999). This value has been derived by means of a visual approach in a log-scale plot as the equivalent moving average filter should resemble the aerodynamic admittance in the frequency range of interest⁵. From this figure it can be seen that for the frequency range of interest a value of $C_T = 4.5$ in the equivalent moving average filter underestimates the aerodynamic admittance considerably.

Also the aerodynamic admittance based on the pressure measurements in the wind tunnel is presented in this figure. This aerodynamic admittance is only plotted as an indication of the true shape of the admittance function. From Geurts (1997) it was concluded that the aerodynamic admittance derived from wind tunnel measurements is not consistent with the full-scale situation as values above 1.0 can be found, which is impossible by definition. This is often the case for wind tunnel results because the aerodynamic admittance is derived with equation (3.6) on page 20 using a given wind speed spectrum e.g. the EN1991-1-4 spectrum. In wind tunnel testing the wind speed spectrum present in the wind tunnel, is not exactly the same as this spectrum. The theoretical expression by Dyrbye and Hansen (1999) is therefore considered to be a more accurate representation of 'reality' than the derived aerodynamic admittance from the wind tunnel data. It is noted that when using wind tunnel data the wind tunnel should represent the 'true' boundary layer accurately. For the wind tunnel data used in this research this is considered the case.

³Tributary areas for the case study building model.

⁴Figure plotted for the case study pressure measurements of tap 18. For location of this tap, see figure 7.3

⁵ $\phi = C_T \ln/U$ of interest for buildings is up to a value of around 1.0

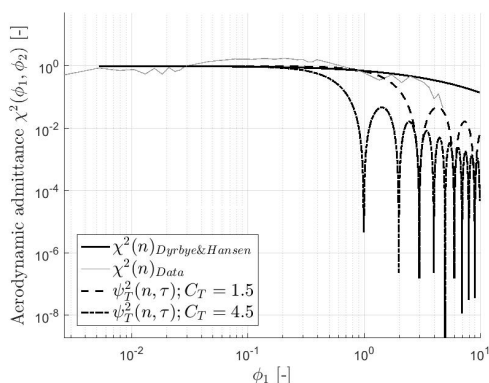


Figure 7.4: Aerodynamic admittance and equivalent moving filter by method of Dyrbye and Hansen (1999) for a pressure tap in the middle of the façade

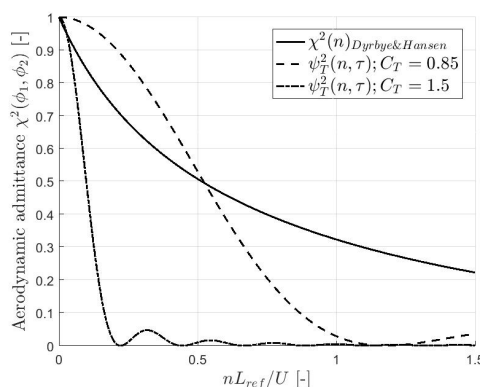


Figure 7.5: Aerodynamic admittance and equivalent average moving filter derived by the method of Holmes (1997) for a pressure tap in the middle of the façade

The method of Holmes (1997) is a more mathematical method to calibrate the value of the averaging constant. He states that a rational approach of matching the aerodynamic admittance to the moving average filter is by matching the enclosed areas or matching the 'half-power' frequencies. This means that both plots of the filters, the aerodynamic admittance and the moving average filter, should intersect at $|\chi_u|^2 = 0.5$. He chooses this last method to calibrate the constant value.

For the same representative area of the façade an example of the results of this method is shown in figure 7.5.⁶ From this figure it can also be seen that an averaging constant value of 4.5 for the moving average filter underestimates the aerodynamic admittance for the tributary area. Both methods clearly suggest a lower constant value than proposed by Lawson (1976) and figure 7.4 and 7.5 show similar findings as in Dyrbye and Hansen (1999) and Holmes (1997). Therefore this is to be expected for other measurements as well.

To check this method and the choice for taking the perpendicular lines for defining the tributary areas, the cross-correlation of the pressures should be evaluated. Sufficient high correlations should be present within the tributary areas ($R_{\chi_y} = 0.7 - 0.8$) after averaging of the pressures.⁷

Averaging constant for this research

From figure 7.4 it was found that an averaging constant value $C_T = 1.5$ results in better resemblance of the moving averaging filter and aerodynamic admittance in the frequency range of interest. In figure 7.5 a constant of 0.85 results in matching the 'half-power' frequencies using the method of Holmes. As significantly lower averaging constant values are found than $C_T = 4.5$ as proposed by Lawson (1976), for this research a lower value will be used. Choice has been made to use a value of 1.5, similar to Dyrbye and Hansen (1999), as the shape of the equivalent moving average filter resembles the aerodynamic admittance quite accurately in the frequency range of interest.

7.2. Response coefficients through finite element modelling

7.2.1. General finite element model method development

The dynamic and size effect on the global response is analysed using finite element modelling. In this section the choices and assumptions made in this model are stated. The methodology for the purpose of this research is derived with FE program DIANA, but similar programs could have been used.

⁶Figure plotted for the case study pressure measurements of tap 18. For location of this tap, see figure 7.3 on the facing page

⁷For the case study purpose it was found that sufficiently high correlations were found between pressures in a tributary area. The figures can be found in appendix F. Therefore the choice to use the perpendicular lines to determine the tributary areas and the proposed methods lead to sufficient correlation between the pressures on every area.

Finite element program description

The dynamic behaviour is evaluated using finite element program DIANA. DIANA is a finite element code based on the displacement method and can be used for multiple purposes, three-dimensional and nonlinear analysis (DIANA, 2016). As described in Cook (1995), a finite element method divides a structure in multiple elements of which a field quantity is interpolated from values at the nodes. When connecting the elements, the field quantity becomes interpolated over the entire structure. The displayed values of the field quantity at the nodes are the ones solved from a set of equations that follow from minimizing a certain function, e.g. total energy.

Time domain analysis

In case of a dynamic transient analysis a time integration method needs to be specified, as well as the type of matrices. The mass matrix is specified by the default method, namely a consistent mass matrix including rotational terms. For the damping matrix a viscous type of damping is specified, which is for this case Rayleigh damping. This results in an updated damping matrix for every time step as it is defined as a linear combination of the mass and stiffness matrix. Rayleigh damping is further explained in appendix E.

As time integration method a method belonging to the Newmark family is used by default in DIANA with $\gamma = \frac{1}{2}$ and $\beta = \frac{1}{4}$ (for meaning of these constants and definition of the integration method, see appendix E). This is also commonly known as the trapezoidal rule, which is an implicit time integration scheme. The method is unconditionally stable and $O(\Delta t^2)$ accurate, but requires a large matrix decomposition. This choice of γ also means that no numerical damping is applied, so spurious high frequency modes are not controlled. This has to be checked in the results. The method is energy conserving, so no extra energy is put into the system that influences the results.

Model schematization

The dynamic behaviour of the structure should be analysed through a simplified beam model as for the along-wind buffeting response this is considered an accurate representation for the building typology considered (see § 3.2.1). The effect of boundary conditions on the dynamic response is investigated through implementation of several boundary conditions at the base of the model. This is achieved through a step-by-step approach.

The first step involves a simple beam model that is similar to the theoretical approach of the dynamic behaviour of a structure. Therefore the building is modelled as a cantilevered beam structure. Beam elements are used, which are two-node, two-dimensional elements based on the Bernoulli beam theory. This element has three degrees of freedom (DOFs) in every node, the translations u_x , u_y and the rotation ϕ_z . At the base of the building these DOFs are constrained to simulate a fixed support.

Next, it is evaluated if a more realistic foundation stiffness instead of a fixed support has a considerable effect on the response of the structure. Therefore the results after this adjustment of the model are compared to the results of step 1. In step 2, the cantilevered beam model of step 1 is updated with a horizontal spring and dashpot element at foundation level to simulate a less rigid support like a pile foundation. In step 3 also a rotational spring and dashpot is included to simulate the less rigid support.

Elements

Element type

Simple class-I beam elements are used according to the Bernoulli theorem (L6BEN in DIANA). Timoshenko shear theory is an option in these elements. According to the DIANA manual (DIANA, 2016) these elements are not fit for physic nonlinear analysis, only for generalized stress-strain diagrams. A different option for physical nonlinear analysis are Class-II elements (do not consider Timoshenko theorem) or Class-III Mindlin-Reissner elements (shear deformation is included). For beam elements it is possible to calculate forces and moments in the nodes and cross-sections and Cauchy stresses in the Gauss points. The possibility of having the internal forces as a direct output is convenient for the purpose of this research to derive global response coefficients at foundation level. By default a 2 point Gauss integration scheme is used along the bar axis.

Mesh size

For both the cantilevered beam model of step 1 and the model of step 2 a study to determine the required

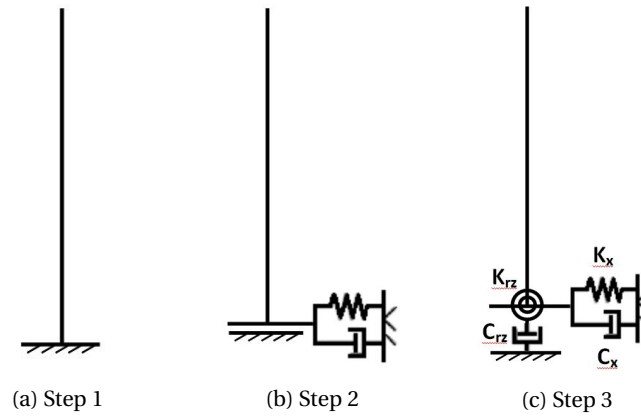


Figure 7.6: Mechanic scheme case study building

mesh size has been performed using the results of a linear-static analysis.⁸ Due to the use of beam elements and the fact that only results are required at the base of the model, only a few elements are sufficient. Also a mesh study to the fundamental frequency is performed. No considerable changes in evaluated frequency are found. Therefore the same number of elements should be used as the number of load fields (number of pressure taps on the wind tunnel model) present over the height of the building⁹.

Loads

Wind tunnel pressure measurements are usually available at multiple locations per building face. As simple beam elements are used the load can only be varied along the height-axis of the building. Therefore the pressure measurements along the width are averaged as in figure 7.7. For only considering alongwind response this simplification is justified. A distributed unit load of should placed on all pressure fields. Using time dependent factors per pressure field different pressure values are attributed to the fields at different times. This should be done both at windward and leeward side of the building model.

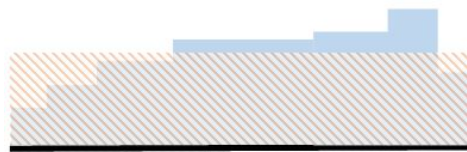


Figure 7.7: Measured pressure distribution and averaged distribution

The measured pressures at the pressure taps on the façades of the wind tunnel model are normalized using the reference pressure measured at the reference taps of the building model. This results in time series of pressure coefficients for every pressure tap. These pressure coefficients are converted to full scale pressures that can be used for the finite element analysis. This is done by multiplying the pressure coefficients by a reference pressure of the building in full scale. Both reference pressures should be defined at the same height. For the purpose of this research the reference pressure was measured at the height of the structure. The used pressures should be processed with the averaging technique described in § 7.1. The full-scale pressures are given by:

$$p(z, t) = \frac{1}{2} \rho_{air} v_{ref,h}^2 c_p(z, t) \quad (7.1)$$

Where:

⁸This evaluation was performed for the case study building, but is valid for other buildings as well.

⁹For the case study building therefore 6 elements are used.

- p = Distributed load
 ρ_{air} = Air density
 $v_{ref,h}$ = Wind velocity at reference height
 c_p = Pressure coefficient

With the wind velocity at reference height being the top of the building, defined by:

$$v_{ref,h} = k_r \cdot \ln\left(\frac{h}{z_0}\right) \cdot v_b = 0.19 \cdot \left(\frac{z_0}{z_{0,II}}\right)^{0.07} \cdot \ln\left(\frac{h}{z_0}\right) \cdot v_b \quad (7.2)$$

Where:

- k_r = Terrain factor depending on roughness length z_0
 z_0 = Roughness length in full scale, but consistent with the wind tunnel environment
 $z_{0,II}$ = Reference roughness length (terrain category II in EN1991-1-4): 0.05 m
 $v_{b,EN}$ = Design wind velocity as specified in the National Annex to EN1991-1-4: $\sqrt{\gamma_s} v_{b,0}$

Material properties

The width of the beam should be chosen such that the fundamental frequency of the model complies with the natural frequency of the full-scale building based on the estimation formula derived from full-scale measurements by Newberry et al. (1973). The same formula is used in EN1991-1-4 ($n_0 = 46/h$). The damping coefficient should be chosen comparable to the damping ratio as specified in EN1991-1-4 for concrete, $\zeta = 0.016$. This value agrees well with the damping ratio prescribed in CEB (1991) for tall reinforced concrete buildings, $\zeta = 0.015$. Only material damping in the form of Rayleigh damping is applied, as from the methodology in EN1991-1-4 Annex F it follows that the aerodynamic damping for the fundamental mode is negligible for buildings of considered typology.

The spring stiffness and dash-pot properties for the more detailed foundation models can be derived using a dynamic analysis of a pile foundation in Dynapile (Roesset et al., 2016). This program allows for an analysis in the frequency domain of a detailed pile foundation including soil layers which results in a single dynamic stiffness of the entire pile group. The real part of this dynamic stiffness is considered to represent the spring stiffness and the imaginary part the damping coefficient. Soil properties can be extracted from cone penetration test measurements at the building location.

Response coefficients

Through the transient FE-analysis of the model with the time dependent loads, time series of the base bending moment and shear force can be obtained. These responses should be transformed to dimensionless response coefficients to be used in further analysis. The base bending moment and shear coefficients are derived through:

$$c_M = \frac{M}{\frac{1}{2} \rho_{air} v_{ref,h}^2 A_{ref} h} \quad (7.3)$$

$$c_Q = \frac{Q}{\frac{1}{2} \rho_{air} v_{ref,h}^2 A_{ref}} \quad (7.4)$$

- M = Base bending moment
 Q = Base shear force
 A_{ref} = Reference area
 h = Height of the building

In figure 7.8 an example of the results of the base bending moment coefficient of the cantilevered beam model for the first few minutes is given¹⁰. Both the model with resonance (dynamic) and without resonance (static)

¹⁰Results are presented for the case study building

response are displayed. It can be seen that there is a slight dynamic adjustment period at the beginning of the loading sequence. Therefore the first part should not be considered in further analysis of the results. Furthermore, it is seen clearly that the dynamic model has an additional fluctuating response around the response of the static model. From the design procedure of EN1991-1-4 also the design base moment coefficient is derived and plotted in the figure as an indication of magnitude.

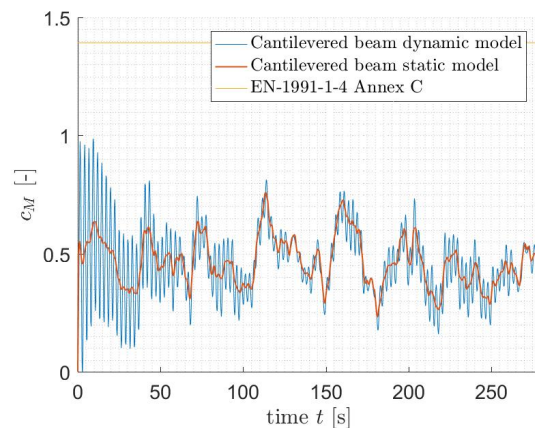


Figure 7.8: Timeseries for the static and simple dynamic model

Through this transient FE-analysis response coefficients can be derived for the entire duration of the wind tunnel test. However, when this test has very long duration computation time could be considered too long. Therefore an assessment of the required time series of response coefficient needs to be made.¹¹

7.2.2. Evaluation of model choices

To derive the representative response coefficients, the effect of different model choices should be evaluated. Therefore, first the results of the model should be verified by hand calculations to check if the model performs correctly. Next, the effect of the different boundary conditions at foundation level should be investigated. Thereby also the possibility of nonlinear material behaviour and dependence on the wind speed should be checked. The latter is necessary as in the wind loading chain by Davenport that is used as a basis for the reliability assessment it is assumed that the structural response is independent of the wind speed. This independence is therefore checked using the finite element model. For these checks and evaluations a short duration transient FE-analysis is sufficient, so computation time is reduced.

In this section these checks are performed using a specific building model as they could not have been performed without a specific case considered. For this purpose the case study building of Part III of this thesis is used. However, most conclusions drawn in this section are generally applicable or else it is stated clearly. The methodology for deriving the response coefficients described in previous section is followed.

Model and material properties

For the case study the properties in table 7.1 are assigned to the FE model for all model steps (1, 2 and 3). A fundamental frequency of $n_0 = 0.4$ Hz is found for the case study building. The building is assumed to be situated near Schiphol, which means that a value of the wind velocity for wind area II of EN1991-1-4 should be used. As no seasonal and directional effects are taken into account for the basic wind velocity a value of $v_b = 27.0$ m/s holds.

The properties of the pile foundation for models steps 2 and 3 are based on the foundation of a reference building. Details on the input for the Dynapile analysis can be found in appendix G. The damping coefficients are entered as a function of the frequency as a quite big range can be found; $3.0 \cdot 10^7 - 5.5 \cdot 10^{10}$ Ns/m for the horizontal dash-pot and $8.3 \cdot 10^9 - 1.5 \cdot 10^{13}$ Nsm/rad for the rotational dash-pot.

¹¹For the case study situation a very long test duration of more than 170 hours in full-scale was available. It was found that 24 hours of response coefficients was sufficient for the modelling of these response coefficients in the stochastic wind load model.

Table 7.1: Properties FE model of the case study building

Property	Value	Unit
ρ_{air}	1.225	kg/m ³
$\rho_{concrete}$	2400	kg/m ³
$E_{concrete}$	$3.0 \cdot 10^{10}$	N/m ²
h	120	m
b	10 (11.5 for step 3)	m
ζ	0.016	-
n_0	0.40	Hz
$v_{ref,h}$	32.3	m/s
K_{xx}	$1.0 \cdot 10^{10}$	N/m
C_{xx}	$f(n)$	Ns/m
K_{rz}	$5.2 \cdot 10^{12}$	Nm/rad
C_{rz}	$f(n)$	Nsm/rad

Verification checks

By means of a linear static calculation the cross-sectional forces at the base of the simple beam model are compared to the forces that follow from a hand calculation. Pressure measurements of the first time step are used for this calculation. This results in a 3% higher base bending moment for the hand calculations and a 0% higher shear force. The cross-sectional forces of the FE-model therefore comply with the hand calculations.

The dynamic response of the model is compared to the theoretical response of a single-degree-of-freedom (SDOF) system in the frequency domain. The results can be found in appendix E. Good agreement is found between the dynamic finite element model and the theoretical SDOF-system.

These checks should always be performed for the FE-model to ensure accurate modelling and reduce the possibility of errors.

Evaluation required detailing

In addition to the response coefficients of the cantilevered beam model, also for step 2 and step 3 the response coefficients are evaluated. Time-series of those can be found in appendix E. The figures are very similar to figure 7.8 on the preceding page and no considerable differences can be noticed visually. Therefore the dynamic amplification factors are evaluated numerically.

The dynamic factor for the base moment coefficients (defined as the ratio of the maximum dynamic bending moment coefficient and the maximum static bending moment coefficient in the sample) of all models for the first 15000 time steps (one hour in full-scale) of the transient analysis are found in table 7.2.

Table 7.2: Dynamic factors for different modelling steps for the first 15000 time steps (one hour in full-scale)

Model characteristic	Fundamental frequency [Hz]	Dynamic factor c_d [-]
Step 1 (Bernoulli beam elements) $b = 10$ m	0.397	1.118
Step 1 (Timoshenko beam elements) $b = 10$ m	0.395	1.114
Step 2 $b = 10$ m	0.394	1.127
Step 3 $b = 11.5$ m	0.399	1.114

The differences between the dynamic factor between all models can be explained by the slight difference in fundamental frequency of the models. As the fundamental frequency is manually directed for, introducing a more detailed model is of no use. This will be the case until a much more detailed model is used to determine the actual fundamental frequency of the building. From previous research, however, it has been found that the estimation formula for the fundamental frequency of a multi-story building does not lead to less appropriate approximations than detailed finite element models. It is of more use to determine the effect of the uncertainty in fundamental frequency (and damping) on the dynamic response of the structure. Therefore a

sensitivity study is included in § 7.3.2.

As this is the case for other building models as well, it can be concluded that a cantilevered beam model is sufficient for deriving response coefficients at foundation level of the building.

Nonlinear material behaviour

To evaluate the global structural response of the structure it should also be determined if nonlinear material behaviour plays a role for the domain of wind loading. Therefore an estimation of the stresses in the main load bearing structure of the case study building is made, based on the base moment response of the cantilevered beam model and $v_{ref,h} = 32.3$ m/s. A load factor is applied by multiplying this wind speed with factor $\sqrt{1.5}$ to evaluate the loading in the design situation. The concrete core is the main load bearing structure of the building. The properties of the building and the concrete core can be found in table 7.3. These properties are based on general rules of thumb for design and reference buildings.

Table 7.3: Properties case study reference building

Property	Value	Unit
b_{core}	10	m
t_{core}	0.5	m
N_{floors}	40	-
h_{floor}	0.5	m
ratio m_{floor} to core	0.4	-
μ	181000	kg/m

The stresses are calculated based on maximum base bending moment due to the wind loading and normal force at foundation level due to self-weight of the structure. It is considered that only 40% of the mass of the floors is carried by the concrete core as a different load bearing system of columns is assumed for most of the vertical load bearing. The stresses in the outer fibres of the concrete core are given by:

$$\sigma_{max} = \frac{M \cdot \frac{1}{2} b_c}{I_{cross}} - \frac{F_G}{A_{cross}} \quad (7.5)$$

σ_{max} = Stress in the outer fibre

M = Base bending moment

b_c = Width concrete core

I = Area moment of inertia

F_G = Normal force due to self-weight

A_c = Cross-sectional area concrete core

In table 7.4 the minimum and maximum stresses in the outer fibres of the concrete core are presented. The maximum stress is defined as being the stress at the 'tensile' side of the concrete core due to the wind loading. The largest absolute stresses are found at the compression side of the building. Even at the 'tensile' side due to wind loading only compressive stresses are found due to the governing effect of the self-weight. As no tensile stresses are found and the compressive stresses are still in the linear domain of the concrete material, nonlinear material behaviour will not have to be taken into account.

Table 7.4: Maximum/minimum stresses for the first 15000 time steps

	σ [MPa]
Max	-10
Min	-34

In general it can be assumed that nonlinear material behaviour does not have to be taken into account as self-weight will most likely be dominant in any case of concrete core high-rise structures. The compressive stresses could reach the nonlinear domain of concrete. However, in general this is not considered governing as usually simple design adjustments would solve this problem e.g. a higher concrete class.

Dependence dynamic response on wind speed

To check the independence of the structural response to the wind speed, the model is also run for a lower wind speed of 27.0 m/s. In table 7.5 the dynamic factor for both the original wind speed and the lower wind speed are given.

Table 7.5: Dynamic factors for different wind speeds for the first 15000 time steps

Wind speed	Fundamental frequency [Hz]	Dynamic factor c_d [-]
$v_{ref,h} = 32.3$ m/s	0.397	1.118
$v_{ref,h} = 27.0$ m/s	0.397	1.121

It can be seen that the dynamic structural behaviour is not completely independent of the wind speed as a small difference in dynamic factor is found. However this difference is so small ($< 1\%$) that independence of the structural behaviour with the wind speed is assumed in the range of the expected design wind speed. This is expected to be the case for other building models as well.

Conclusion

From this evaluation of the case study results it can be concluded in general that a cantilevered beam model is sufficient for deriving response coefficients at foundation level of the building. Thereby nonlinear material behaviour does not need to be considered and independence of the structural response to the wind speed can be assumed.

7.3. Probabilistic modelling of extreme response coefficients

To include the derived response coefficients in the full probabilistic assessment procedure requires the modelling of the extreme response coefficients by fitting an appropriate distribution function. For this procedure sufficient independent extremes need to be derived. In this research the block method will be applied as explained in chapter 5. For the purpose of this research a relatively long wind tunnel test is used to minimize statistical and sampling uncertainties in the response coefficient modelling. As wind tunnel tests or the time domain finite element analysis have only a limited duration because of cost considerations a block duration will have to be derived that ensures both independent extremes and sufficient data for the fitting of the distributions. Both these methods result in a maximized number of extremes used for the modelling. Therefore in § 7.3.1 the method for deriving this required block duration will be presented. In § 7.3.2 the approach on incorporating the uncertainties of the dynamic structural properties, fundamental frequency n_0 and damping ζ , and their combined effect on the response coefficients will be described.

7.3.1. Block duration

Two methods are applied for determining the required block duration. First the autocorrelation method and second the reversed univariate method (Meinen, 2015) are described.

Autocorrelation method

Correlation of response components in time can be described by the autocorrelation function. With this method the dependence of the samples at one time with the samples at another time can be given a numerical value. In figure 7.9 on the next page an example for the autocorrelation of every other hour of both static (moment) response coefficients as dynamic (moment) response coefficients are shown¹². The hour time lag ensures fully independent runs. The static response coefficients are derived through integration of the pressures obtained from a wind tunnel test, without application of a finite element model, so resonance behaviour is not taken into account. The autocorrelation of the static response coefficients is plotted as these can also be used when the wind tunnel test duration is longer than the duration for the transient FE-analysis.¹³ This results in more autocorrelation plots and therefore a higher accuracy.

¹²The figures are plotted for the case study response coefficients. The autocorrelation of the shear force coefficients are similar and can be found in Appendix F.

¹³For the case study building 24 hourly runs (so 12 autocorrelation plots) of response coefficients including resonance behaviour are available. However, for static response coefficients more than 170 hourly runs are available

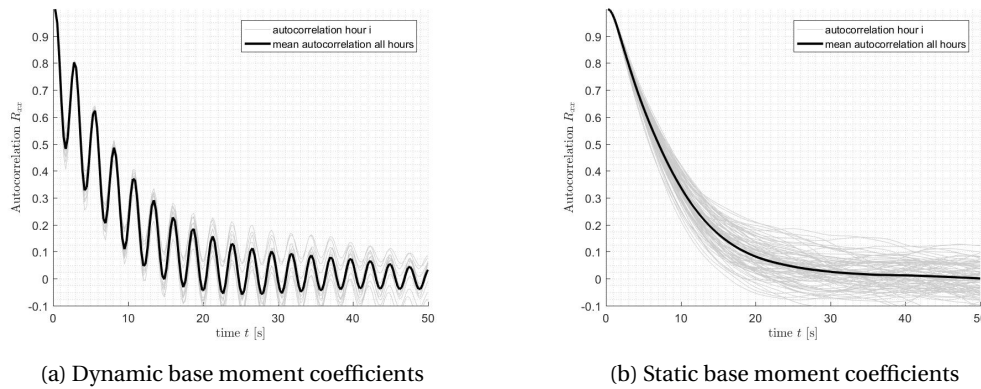


Figure 7.9: Autocorrelation base moment coefficients

The choice of block duration should be made by taking into consideration the necessity of sufficient sample data in the extreme value analysis and a low degree of dependence between successive peaks. It is assumed that for a correlation coefficient $\rho \leq 0.3$ a low degree of dependence is found (Holický, 2013). It should be noted that this value is only indicative and not based on any objective criteria.

Reversed univariate method (Meinen, 2015)

This method is based on the univariate theorem (equation (5.2) on page 43) which states that for independent and identically distributed random stochastic variables the distribution function of the extremes of reference duration T can be derived by the distribution function of the extremes with reference duration t . Here this method is utilised in a reversed way where it is stated that if the distribution function of the T -extremes is represented well by the shifted distribution of the t -extremes, the extreme coefficients were independent and identically distributed. The goodness of the fit can be evaluated using both visual judgement and the relative error in the Cook-Mayne fractile.

Use is made of the relative error in the Cook-Mayne fractile to give a quantification of the goodness of the fit. However, a complete study of the tail behaviour is necessary, because it is not sure whether the design value of the response coefficient coincides with this fractile value. This design point follows from a full reliability assessment. It is to be expected that the design point lies in the tail with the higher coefficients, so goodness of fit of this upper tail behaviour is of specific interest.

In figure 7.10 this method is illustrated by the plotted shifted t -extremes and hourly-extremes of the static moment coefficients for different block durations t .¹⁴ A choice is made for the static moment coefficients because of the lack of sufficient number of dynamic hourly extreme moment coefficients results in an unreliable empirical cumulative distribution function (ECDF) of the hourly data. It is expected that the response coefficients including resonance show similar behaviour. In this figure it can be seen that a shifted 10s- or 20s-extremes ECDF results in a good fit for the hourly extremes, especially for the upper tail behaviour.

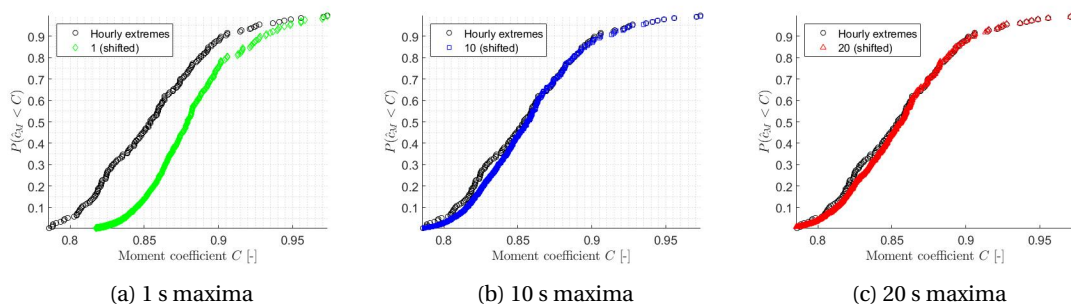


Figure 7.10: Shifted t -extremes vs hourly-extremes of static moment coefficients in the Normal domain

¹⁴Figure was plotted for the case study results.

Choice of block duration for this research

Next, based on the methods described previously and the figures presented in this section an evaluation of the required block duration for the case study purpose is made.

From figure 7.9 on the preceding page an estimation of the required block duration of the response coefficients for the case study is made to be $t = 20$ s. For both the dynamic as static response coefficients this block duration leads to a low degree of dependence of the individual extremes.

The relative error in the Cook-Mayne fractile for the t -extremes is investigated for the reversed univariate method. It is found that from a block duration of $t = 10$ s, no big differences in the Cook-Mayne fractile value of the moment coefficients can be found. The same is found for the shear force coefficients. As it is not sure that the design value of the coefficients lies at the Cook-Mayne fractile value a more detailed investigation to the upper tail behaviour of the distributions is necessary. Therefore in figure 7.11 again the ECDF of the 10s- or 20s-extremes is plotted, but this time there has been zoomed in on the upper tail of the distribution in the Gumbel domain. From this figure it can be seen that the 20s-extremes result in a slightly better correspondence with the hourly extremes for the entire upper tail.

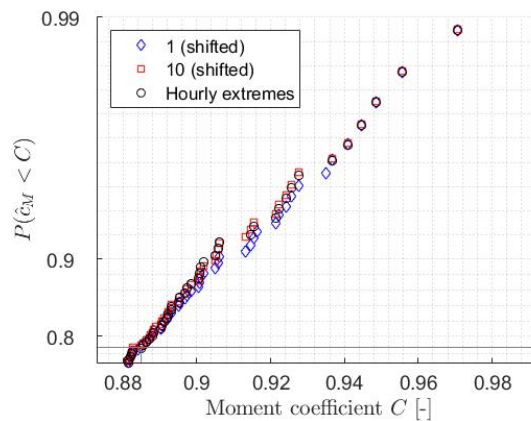


Figure 7.11: Zoom of the upper tail behaviour in the ECDF of the shifted t -extremes vs hourly-extremes of static moment coefficients in the Gumbel domain.

By application of both methods described before a block duration can be found that ensures sufficient independent extremes to use in further analysis. For the wind tunnel measurements used in this research a time lag between successive extremes of 10-20 s appears to be sufficient to ensure independence. A block duration $t = 20$ s is chosen, because a reasonably long sequence of response coefficients from the transient finite element analysis of the case study is available¹⁵.

7.3.2. Uncertainties of dynamic properties

The time series of response coefficients that are generated using the finite element model are only valid for one set of fundamental frequency and damping coefficient considered representative for the building. Both parameters are subject to uncertainties, which leads to the question of how sensitive the coefficients are to these uncertainties and how these uncertainties should be incorporated in the reliability analysis. The Probabilistic Model Code (JCSS, 2001) gives an indication of the individual uncertainties and their combined effect in the dynamic factor c_d . For the purpose of this research a reduced Monte Carlo simulation is performed by running the transient finite element analysis for different combinations of fundamental frequency and damping coefficient to evaluate the statistical properties of the combined effect and compare this to literature. These combinations have been determined using the method of Latin hypercube sampling to reduce the amount of combinations by eliminating the most unlikely events.

¹⁵This results in a sample of more than 4000 peaks, which is considered to be sufficient.

Latin hypercube sampling

Latin hypercube sampling (LHS) was first described by McKay et al. (1979). It is a technique that creates a sample of parameter values with underlying distributions, but avoids clustering of the sample in some parts of the sample space. For n variables, the range of each variable is divided into m equally probable intervals, where m is the required number of realizations. LHS ensures that e.g. for a two-dimensional sample space only one sample will be realized in each row and column (Latin square). For n dimensions this concept is called a Latin hypercube. Therefore m will be the number of realized samples irrespective of the number of dimensions n .

Sample realization

In this case only two parameters, fundamental frequency and damping coefficient, are sampled which leads to a very straightforward Latin hypercube sampling. For both parameters a lognormal distribution can be assumed of which the statistics can be found in table 7.6 which are based on values from the Probabilistic Model Code (JCSS, 2001). The description of their combined effect by the dynamic factor c_d is also found in this table. These stochastic properties are also compared to other literature. Mean values of both parameters are comparable in Solari (1996). For the COV of the damping coefficient similar values are found in literature e.g. Solari (1996) and Kwon et al. (2015). For the COV of the fundamental frequency a larger range of values is found, where most of them are less than the proposed value by JCSS. However, the value in the Probabilistic Model Code will be used as it is on the conservative side of the range of literature values. Using the mean-over-specified values in table 7.6 assumes that for fundamental frequency a conservative value is specified in codes, where the specified value for damping is considered non-conservative.

Table 7.6: Statistics of dynamic structural parameters according to JCSS (2001)

	Mean Specified ¹⁶	COV
n	1/0.85	0.30
ζ	0.80	0.50
c_d	1.0	0.1-0.2

The statistics of the dynamic structural properties are applied on the specified properties of $n = 46/h$ [Hz] and $\zeta = 0.016$ for concrete high-rise buildings. In figure 7.12 an example of 6 of such Latin hypercube realizations can be found that are used in the multiple finite element runs¹⁷. The mean (or expected) values of the parameters are indicated by the dotted lines.

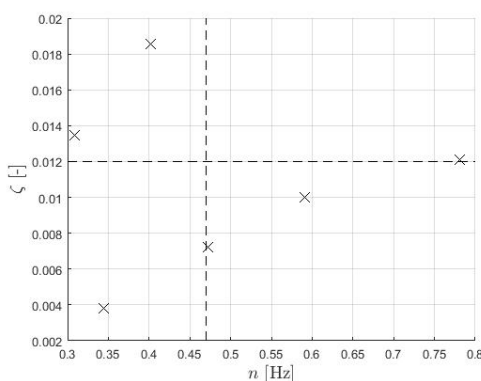


Figure 7.12: Realizations and means of the structural dynamic properties samples in the two-dimensional sample space

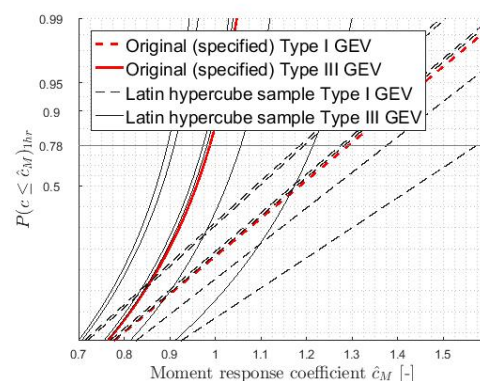


Figure 7.13: Fitted cumulative distribution functions on the hourly extreme moment coefficients for the different dynamic structural properties

¹⁶The values presented here are not correct for ultimate limit state design. The mean-to-specified ratios for the ULS should be 1/1.15 and 1.2, respectively. In further research this should be altered and the effect on the conclusions should be investigated.

¹⁷These realizations are based on the case study building with $n_0 = 0.40$ Hz and $\zeta = 0.016$.

Stochastic description of uncertainties in dynamic properties

The transient finite element analysis should be run for all combinations of parameter values derived by the Latin hypercube sampling. The natural frequency only depends on the width of the finite element cantilevered beam model, therefore this width should be altered in the model. Both the change in natural frequency as the change in damping ratio affect the Rayleigh damping parameters. Therefore these should be altered accordingly.

An example of the fitted cumulative distribution functions for the extreme base moment coefficients of the different runs (the run for the specified (or original) values is shown in red) can be found in figure 7.13 on the previous page¹⁸. The effect of the uncertainties in the dynamic properties on the distributions is investigated at the Cook-Mayne fractile. It is assumed that the design value of the response coefficients will be found around this value. The exact design point can only be found through a Level II or Level III analysis, so this assumption has to be checked after the reliability analysis. For the representation of the combined effect of uncertainties in both dynamic properties in the stochastic wind load model it has been chosen to define a separate parameter χ_{c_d} accounting for these uncertainties. For the description of this parameter a mean-over-specified and a coefficient of variation should be defined.

Both dynamic structural properties are considered to be lognormally distributed as well as their combined effect in the dynamic factor c_d according to JCSS (2001). Therefore a lognormal distribution is also assumed for the Cook-Mayne fractile values of the response coefficients.¹⁹ The COV for a lognormally distributed variable is computed as follows:

$$\text{COV}_{\log} = \sqrt{e^{s_{ln}^2} - 1} \quad (7.6)$$

With:

s_{ln} = Sample standard deviation of the data X after a natural log transformation

Derivation of properties for the dynamic property uncertainty factor for this research

The method described before was used for the case study building and an evaluation of the combined effect of the uncertainties in both dynamic structural properties is given next. It has been chosen to do a reduced Monte Carlo simulation to compare the finite element results with literature. The properties of χ_{c_d} are then determined based on both the case study results, but also on literature. The defined properties are therefore not case study specific and could be used in general.

The design value of the coefficients belonging to the specified dynamic properties, the mean design value, the mean-over-specified value and the coefficient of variation of this design point for all different realizations in figure 7.12 on the previous page are presented in table 7.7.

Table 7.7: Coefficient of variation and specified design value of the response coefficients in the Cook fractile

	Type I \hat{c}_M	Type III \hat{c}_M	Type I \hat{c}_Q	Type III \hat{c}_Q
Specified Cook-Mayne design value	1.29	0.99	2.32	1.82
Mean Cook-Mayne design value	1.32	1.01	2.35	1.84
Mean Specified	≈ 1.0	≈ 1.0	≈ 1.0	≈ 1.0
COV	0.11	0.12	0.08	0.07

It can be seen that there is no big difference in computed COV between the Type I and Type III distribution functions, but there is a substantial difference between the base moment and shear coefficients. The computed COV can be compared to the value as given in the Probabilistic Model Code (JCSS, 2001) presented in table 7.6 on the previous page. In this code only a COV for the dynamic amplification factor c_d is given,

¹⁸Figure is plotted for the case study results.

¹⁹The results for the case study building in figure 7.13 on the preceding page confirm this assumption.

including uncertainties in the dynamic properties as well as codification uncertainties in the determination of c_d . However, the computed COV and the proposed JCSS COV can be compared as they should have a similar order of magnitude. The value for the COV in the Probabilistic Model Code is slightly higher than the value computed for the 6 different finite element runs. It is to be noted that 6 runs might not be sufficient to compute a COV with a low enough variance. Larger sample sizes result in a smaller variance of the computed coefficient of variation. Additionally, for a small number of samples the COV can be underestimated as it is a biased estimate of the population COV. A second reason for the difference is the fact that COV_{c_d} also includes other types of uncertainties, like discussed before.

A mean-over-specified value of $\mu/(\chi_{c_d})_s = 1.0$ is found, which is the same as the mean-over-specified value for c_d in the Probabilistic Model Code. However, in practice usually a conservative value for fundamental frequency as well as damping is determined. This could result in a lower mean-over-specified value for χ_{c_d} for these cases.

Conclusion

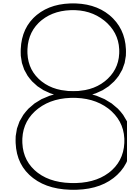
Choice is made to describe the uncertainties in the dynamic properties by a separate stochastic variable χ_{c_d} with a mean-over-specified $\mu/(\chi_{c_d})_s = 1.0$ and $\text{COV}_{\chi_{c_d}} = 0.15$. This choice is considered to be conservative with respect to the computed values in this research, as only a small sample size is used. This choice of COV is consistent with the Probabilistic Model Code JCSS (2001) and is therefore also generally applicable and not case study specific.

7.4. Summary of methods in deriving response coefficients

In this chapter the methods for deriving the response coefficients were developed and explained and illustrated by means of the case study. From this a general method can be defined, which is summarized in this section.

1. Representative pressures per tributary area of the pressure taps need to be derived from wind tunnel pressure measurements through the moving average filter concept. Therefore the required averaging time τ for the pressure measurements needs to be derived.
2. The averaging constant C_T in this averaging time has to be calibrated for the moving average filter to represent the aerodynamic admittance correctly, in which the correlation of wind pressures over the façade is taken into account. This should be done by a visual approach on letting the moving average filter and aerodynamic admittance function correspond in the frequency range of interest for high-rise buildings.
3. An accurate description of the aerodynamic admittance needs to be formed. For the purpose of this research the estimation formula by Dyrbye and Hansen (1999) is used. The decay constants in this formula should be carefully addressed and calibrated to the pressure measurements available. Therefore the root-coherence of the wind pressures at different locations of the building (equation (3.3) on page 18) has to be plotted against an enveloping exponential decay formula with decay constant C_r , as proposed by Davenport (equation (3.4) on page 18).
4. For the response at foundation level of a concrete core high-rise building a cantilevered beam finite element model has to be used with all degrees of freedom constraint at the base. The width of the concrete should be determined such that the fundamental frequency of the beam model complies with the fundamental frequency of the building. This frequency can be determined through full-scale measurements or estimation formulas (e.g. $n_0 = 46/h$). Rayleigh damping should be applied that complies with the natural frequencies and damping ratio $\zeta = 0.016$ of the building.
5. Over the width pressures should be averaged and over the height several load fields have to be applied to the FE-model that correspond to the amount of pressure taps over the height of the wind tunnel model.
6. A transient FE-analysis has to be performed with a time series of pressures applied that is derived with equation (7.1) on page 59 and equation (7.2) on page 60. No nonlinear material behaviour has to be taken into account for the building typology considered.

7. From the derived time series of cross-sectional forces at foundation level, response coefficients should be derived through equation (7.3) on page 60 and equation (7.4) on page 60.
8. For the modelling of the extreme response coefficients the T -extremes (e.g. hourly extremes) should be derived using a block method. To reduce the effect of statistical and sampling uncertainties it is recommended to use a relatively long wind tunnel test. To maximize the number of extremes used for the modelling, a block duration t must be derived that ensures both sufficient and independent extremes. For this both the autocorrelation and reversed univariate method (Meinen, 2015) are utilized.
9. Both a Type I and Type III generalized extreme value distribution are fitted to the t -extreme data. These distributions should then be shifted by means of the univariate theorem (equation (5.2) on page 43) to represent the T -extreme distribution.
10. By repeating steps 4 to 9 for different fundamental frequencies and damping coefficients in step 4 the influence of these properties can be investigated. Therefore a proper distribution of both these properties should lead to representative combinations of the properties to be implemented in the FE-model e.g. by means of Latin hypercube sampling. The Cook-Mayne design response coefficients of the different combinations should be used to determine both mean-over-specified value and coefficient of variation of a separate factor χ_{c_d} accounting for the uncertainties in dynamic properties in the reliability assessment. When less computation time is required, the choice can be made to use the value proposed in this research ($\mu/(\chi_{c_d})_s = 1.0$ and $\text{COV}_{\chi_{c_d}} = 0.15$) which are considered generally applicable as they are found consistent with the Probabilistic Model Code (JCSS, 2001).



Reliability assessment procedure

In this chapter the full-probabilistic assessment procedure for determining the structural reliability of the main bearing structure (concrete core) at foundation level of dynamically sensitive buildings is described. In §8.1 the general assessment procedure is presented. In §8.2 the methods on the resistance side of this assessment are explained and in §8.3 the used stochastic wind loading effect model and its parameters are described.

8.1. General assessment procedure

To assess the reliability of the structure the failure probability should be evaluated which relates to a reliability index β . This probability can be determined by evaluating the limit state function of the situation. The limit state function for the reliability analysis of the main bearing structure at foundation level with respect to wind loading is given in equation (8.1). Evaluating this limit state function can be done by either a Level II or Level III analysis which are explained in appendix A.

$$Z = R_{foundation\ level} - E_{wind} \quad (8.1)$$

Where:

$$\begin{aligned} R_{foundation\ level} &= \text{Shear or moment resistance of the main bearing structure at foundation level} \\ E_{wind} &= \text{Wind loading effect at foundation level} \end{aligned}$$

Both resistance and loading effect model are elaborated on in the next sections. As directional-independent resistance and loading effect are considered, evaluating the limit state function leads to a directional-independent failure probability P_f .

The reliability index of the main bearing structure at foundation level is then determined by:

$$\beta = -\Phi^{-1}(P_f) \quad (8.2)$$

8.2. Resistance

A simplified procedure is adopted for determining the resistance for the reliability calculation. For this purpose it is assumed that the main bearing structure is designed with unity check $UC = 1.0$. This means that the design load according to code procedures is equal to the structures design resistance:

$$UC = \frac{R_d}{E_d} = 1.0 \quad \longrightarrow \quad R_d = E_d \quad (8.3)$$

Where:

$$E_d = \gamma_{wind} \cdot E_{k,code} \quad (8.4)$$

Several methods to derive the stochastic description of the resistance are defined and compared for the purpose of this research. These will be explained next.

8.2.1. Simplified stochastic resistance model

A basic way to incorporate the uncertainties in the resistance in a simplified manner is based on the Level I procedure. It is assumed that the required design value of the resistance is equal to the Level I design value with $\alpha_R = -0.8$, β the minimum required reliability index, in the case for CC2 $\beta = 3.8$ and probability of non-exceedance $P_f = \Phi(-\alpha_R\beta)$. With these values the mean μ_R and standard deviation σ_R of the resistance can be derived when a type of distribution and coefficient of variation are assumed. In figure 8.1 this method is visualized for an assumed lognormal distribution and coefficient of variation $V = 0.10$ for concrete and steel members in bending.

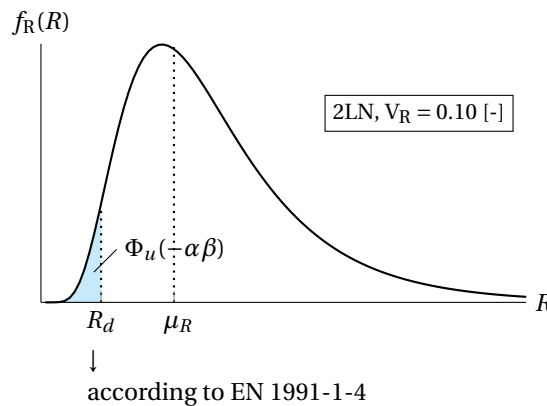


Figure 8.1: Probability density function of the structural resistance R based on the Level I procedure (Meinen, 2015)

The assumption made in this method that the design point coincides with the Level I design point with $\alpha_R = -0.8$ is not necessarily correct. E.g. from a Level II calculation a different sensitivity factor for the resistance can be found, which results in a different probability of non-exceedance and therefore a different distribution function.

8.2.2. Characteristic value resistance model procedure

A less simplified way would be to evaluate the characteristic value of the resistance as this is by definition the 5%-fractile value when a low value of the material property is unfavourable. The distance between the design and characteristic value is defined by the material factor. This method is very useful for materials like steel, but becomes less straightforward for reinforced concrete or other composite materials as not only one material factor is defined.

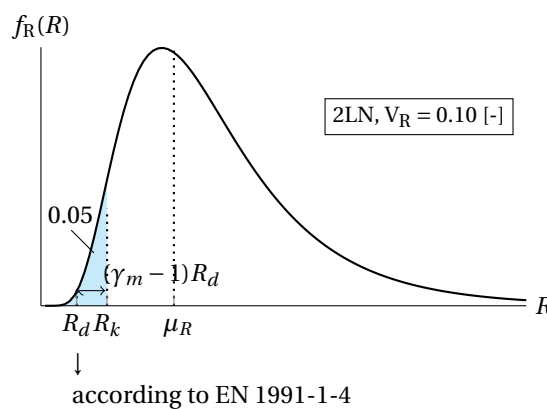


Figure 8.2: Probability density function of the structural resistance R based on the characteristic value procedure

8.2.3. Full-probabilistic resistance model

A more elaborate way that could also be used on composite materials would be to calculate the overall resistance including all stochastic material parameters for specific materials and failure modes. The procedure given is applied to reinforced concrete bending members, but could also be derived for different materials.

Both resistance models for bending moment and shear force respectively need to be derived separately for this procedure. The full-probabilistic resistance model for a beam subjected to bending is given by:

$$R_M = \chi_{R,M} \rho_s A_c f_y (b_c - 0.39 x_u) \quad (8.5)$$

R_M = Bending moment resistance
 χ_R = Resistance uncertainty factor
 ρ_s = Reinforcement ratio
 A_c = Cross-sectional area concrete core
 f_y = Yield strength reinforcement steel
 b_c = Width concrete core without reinforcement cover
 x_u = Length concrete compression zone

As the concrete core of the high-rise building of the case study is not a massive concrete beam, but a rectangular hollow beam, the determination of the concrete compression zone is not straightforward. Therefore it is first assumed that the compression zone is only present in the flange of the core. This assumption has to be checked. If the assumption is found to be correct, the resistance model for a concrete hollow core becomes:

$$R_M = \chi_{R,M} \rho_s (b_c^2 - (b_c - 2t)^2) f_y \left(b_c - 0.39 \frac{\rho_s f_y (b_c^2 - (b_c - 2t)^2)}{0.75 f_c b_c} \right) \quad (8.6)$$

t = Thickness concrete core
 f_c = Compressive strength concrete

As stated before, it is assumed that the design resistance of the concrete core in both bending and shear is equal to the design load effects. Design values of all parameters except for the core width are assumed and solving this equation for b gives the design value of the core width. It could also be solved to flange width t by assuming a core width b . The equation that needs to be solved is as follows:

$$E_{d,M} = \rho_s (b_c^2 - (b_c - 2t)^2) \frac{f_{yk}}{\gamma_{m,s}} \left(b_c - 0.39 \frac{\rho_s \frac{f_{yk}}{\gamma_{m,s}} (b_c^2 - (b_c - 2t)^2)}{0.75 \frac{f_{ck}}{\gamma_{m,c}} b_c} \right) \quad (8.7)$$

γ_m = Material factor

After solving for b or t , all parameters can be viewed as stochastic parameters in equation (8.6) and distributions of these parameters can be incorporated in the reliability calculation.

For shear loading the resistance of a beam, assuming shear reinforcement, is given by:

$$R_Q = \chi_{R,Q} \frac{A_{sw}}{s} (b_c - 0.39 x_u) \cot(\theta) f_y \quad (8.8)$$

R_Q = Shear force resistance
 χ_R = Resistance uncertainty factor
 A_{sw} = Shear reinforcement area
 s = Shear reinforcement spacing
 θ = Strut angle

For design situations it is assumed that $\cot(\theta) = 2.5$ and that the concrete compression zone is present in the flange of the hollow core. The resistance model then becomes:

$$R_Q = \chi_{R,Q} \frac{A_{sw}}{s} \left(b_c - 0.39 \frac{\rho_s f_y (b_c^2 - (b_c - 2t)^2)}{0.75 f_c b_c} \right) 2.5 f_y \quad (8.9)$$

Assuming the width b and flange width t of the bending beam and $R_d = S_d$, equation (8.10) can be solved for $\frac{A_{sw}}{s}$.

$$E_{d,Q} = \frac{A_{sw}}{s} \left(b_c - 0.39 \frac{\rho_s \frac{f_{yk}}{\gamma_{m,s}} (b_c^2 - (b_c - 2t)^2)}{0.75 \frac{f_{ck}}{\gamma_{m,c}} b_c} \right) 2.5 \frac{f_{yk}}{\gamma_{m,s}} \quad (8.10)$$

8.2.4. Conclusion

For the purpose of this research both the simplified as the full-probabilistic resistance model procedure will be compared in chapter 12. The characteristic value procedure will only be used to validate the latter.

8.3. Wind loading effect model

All different parameters that are incorporated in the wind loading effect model are based on Davenport's wind loading chain and the EN1991-1-4 wind loading model. The wind loading effect model is an adaptation on the wind loading model proposed by Meinen (2015) to include global and dynamic effects. The uncertainties in wind loading introduced in section § 4.1 are evaluated and incorporated in the wind loading effect model. The uncertainties accounted for are presented in chapter 6. A summary of the model is given by:

$$\begin{aligned} E_{wind} &= \frac{1}{2} \cdot \rho_{air} \cdot v_{pot}^2 \cdot S_v^2 \cdot c_r (h_{ref})^2 \cdot \hat{c}_{M,t} \cdot S_{\hat{c}_M} \cdot \chi_{c_d} \cdot A_{ref} \cdot h \cdot \chi_{model} && \text{(Base moments)} \\ E_{wind} &= \frac{1}{2} \cdot \rho_{air} \cdot v_{pot}^2 \cdot S_v^2 \cdot c_r (h_{ref})^2 \cdot \hat{c}_{Q,t} \cdot S_{\hat{c}_Q} \cdot \chi_{c_d} \cdot A_{ref} \cdot \chi_{model} && \text{(Base shear)} \end{aligned} \quad (8.11)$$

- ρ_{air} = Air density
- v_{pot} = Basic wind velocity: t minute mean wind speeds at $z = 10$ m and for terrain roughness $z_{0,ref}$ m
- S_v = Factor considering sampling uncertainties of basic wind velocity modelling
- $c_r(h_{ref})$ = Terrain roughness factor at the reference height of the structure h_{ref} correcting for $z_{0,ref}$ m.
 $h_{ref} = \frac{2}{3}h$ for base bending moment and $h_{ref} = \frac{1}{2}h$ for base shear
- $\hat{c}_{R,t}$ = Peak response coefficient: t minute extreme
- $S_{\hat{c}_R}$ = Factor considering sampling uncertainties of response coefficient modelling
- χ_{c_d} = Dynamic properties uncertainty factor
- A_{ref} = Reference area for global loading: frontal area of building
- h = Height of the building
- χ_{model} = Model uncertainty factor

v_{pot} , c_r and \hat{c}_R should have consistent definitions. So when the wind speeds are defined as 10 minute mean wind speeds with terrain roughness $z_{0,ref} = 0.05$ m, equivalent to the wind speeds the response coefficients \hat{c}_R should also be 10 minute extremes and the terrain roughness factor c_r should correct for $z_{0,ref} = 0.05$ m. If wind data with different characteristics are used, the definition of c_r and \hat{c}_R should be altered accordingly or the wind data should be transformed.

8.3.1. Air density ρ_{air}

The air density ρ_{air} is only taken into account in a deterministic manner. The uncertainties in ρ_{air} are not considered in the reliability analysis as they are assumed to be negligible compared to uncertainties in the other parameters in the wind loading chain.

8.3.2. Wind speed v_{pot}

On the basis of the modelling of the wind climate, lie location-specific wind speed measurements. The reference period of the structures considered is $T = 50$ year. Therefore the distribution of v_{pot} should resemble the distribution of the 50-yearly extreme wind speeds. However, measurement data lengths are not long enough to determine sufficient extremes with a 50-year block duration. Therefore of these measurement data the yearly extremes should be derived and these will be modelled by both Type I and Type III generalized extreme value (GEV) distributions to account for statistical uncertainties. The maximum-likelihood estimation technique is used to derive the distribution parameters. The required distribution is obtained by the shifting of the yearly-extremes to the 50-yearly extremes by application of the univariate theorem (equation (5.2) on page 43). Sampling uncertainties should be taken into account through a separate factor S_v with mean $\mu = 1.0$ and coefficient of variation derived by means of the bootstrap-design point method (§ 5.4).

8.3.3. Roughness factor c_r

The roughness factor is described as a stochastic parameter because of the considerable coefficient of variation specified in literature. As no additional research is performed on this parameter in wind loading, c_r is modelled by a mean-to-specified value of 0.80 and a coefficient of variation $COV_{c_r^2} = 0.15$. These parameters are based on the Probabilistic Model Code (JCSS, 2001) ($COV = 0.1 - 0.2$ [-]). Due to definition differences the roughness factor specified in the Probabilistic Model Code is considered equal to the factor c_r^2 in the stochastic wind loading effect model based on the EN1991-1-4 wind loading model.

8.3.4. Response coefficient \hat{c}_M, \hat{c}_Q

The response coefficients are derived through transient finite element analysis of a cantilevered beam model subjected to wind pressures measured in a long duration boundary layer wind tunnel test. Statistical uncertainties are incorporated by modelling the extreme response coefficients by Type I and Type III generalized extreme value (GEV) distribution. The maximum-likelihood estimation technique is used to derive the distribution parameters. For the determination of the extremes the block method is applied and a proper block duration should be determined that ensures independence of the individual extremes and sufficient extremes for modelling purposes. The fitted distribution of the t -extremes should be shifted to the distribution of the required extremes to resemble the wind speed data by utilizing the univariate theorem. For the total methodology of deriving the response coefficients reference is made to § 7.4, where a step-by-step procedure is provided that is generally applicable to buildings of considered typology. Sampling uncertainties should be taken into account through a separate factor $S_{\hat{c}}$ with mean $\mu = 1.0$ and coefficient of variation derived by means of the bootstrap-design point method (§ 5.4).

8.3.5. Dynamic properties uncertainty factor χ_{c_d}

The dynamic amplification of the response is implicitly incorporated in the peak response coefficients, therefore the uncertainties in the dynamic response are described by a separate stochastic parameter with $\mu = 1.0$ [-]. In the Probabilistic Model Code (JCSS, 2001) a coefficient of variation $COV_{\chi_{c_d}} = 0.1 - 0.2$ [-] is proposed.

Dynamic properties of the structure include fundamental frequency and damping coefficient. Based on literature the fundamental frequency can be described by a parameter with mean-to-specified value of 0.85^1 and $COV_n = 0.3 - 0.35$ [-] and the damping coefficient with a mean-to-specified value of 0.8^2 and $COV_n = 0.4 - 0.6$ [-]. In § 7.3.2 the relation between the specified uncertainties of the dynamic properties and the dynamic amplification factor in the Probabilistic Model Code is checked. For the purpose of this research a $COV_{\chi_{c_d}} = 0.15$ [-] and $\mu = 1.0$ is chosen which is generally applicable for all buildings of considered typology.

8.3.6. Model uncertainty factor χ_{model}

The model uncertainty factor combines all uncertainties that can not be quantified independently and is modelled by a normally distributed stochastic variable with $\mu = 1.0$ and $COV_{\chi} = 0.1$ [-].

¹For ULS design situations this value is not correct, mean-over-specified value is 1.15 actually

²For ULS design situations this value is not correct, mean-over-specified value is 1.2 actually

III

Reliability assessment of the case study

Description case study

In this chapter a description of the case study building and the data used for the reliability analysis is given. First the case study building and its location is described in § 9.1. Next, in § 9.2 and § 9.3 the location-specific wind speed measurements and wind tunnel pressure measurements are described, respectively.

9.1. Case study building

For the reliability assessment a case study was used. For the purpose of this research a case study was defined for which both representative full scale wind speed measurements and wind tunnel pressure measurements were available. Since this research focusses on dynamically sensitive structures the wind tunnel measurements have been derived for a high-rise slender building model. Therefore measurements were used that were derived for a building with rectangular plan (30x30 m) and a height of 120 m. The case study building is located at the location of the wind speed measurement station at Schiphol Airport. This location was chosen, because a relatively long run of measurements is available and the fundamental basic wind velocity of wind area II in the Dutch National Annex of EN1991-1-4 is also based on these measurements.

It should be noted that this building is not actually present at this location and is only defined for the purpose of this research. In figure 9.1 a graphical description of the case study building is given.

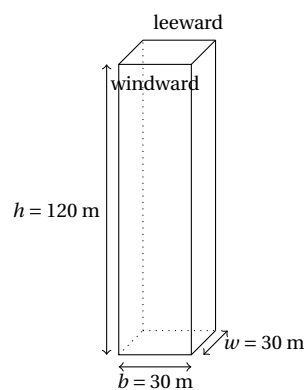


Figure 9.1: Case study building

9.2. Wind speed data

Potential wind speed data v_{pot} are obtained from the KNMI-measurement station at Schiphol Airport. These potential wind speeds are defined as the hourly mean wind speed at a height of 10 m above ground with terrain roughness $z_0 = 0.03$ m. The measurement period covers 64 years and measurements are documented every hour. Also wind direction is documented for discretized wind speed sections of 10° . A summary is provided in table 9.1 on the next page, together with additional details of the measurement station.

Table 9.1: Measurement station and measurement data details

Location	Schiphol Airport (X: 110.750; Y: 482.550)
Station nr. KNMI	240
Period	01/01/51 - 31/12/2014 (64 year) ¹
Recording	Every hour
Directions	Every 10° relative to north
Additional documentation	Can be found in Verkaik (2001)
Source	Free downloadable from knmi.nl

Implementation in stochastic wind load effect model

Due to the available wind speed data of hourly means with given terrain roughness, the other parameters in the stochastic wind load effect model should be altered accordingly. Therefore the terrain roughness factor c_r should correct for a terrain roughness of $z_0 = 0.03$ m and the response coefficients should correspond to hourly extremes as well.

9.3. Wind tunnel measurement data

For the derivation of the response coefficients pressure measurements are used from the open-circuit atmospheric boundary layer wind tunnel of TNO. The raw measurement data are processed according to the CUR 103 (2005) guidelines. A simple static (wooden) building model was used with scale $\lambda_g = 1 : 250$. The terrain roughness used to model the atmospheric boundary layer is $z_0 = 0.8$ m. In the Dutch National Annex to EN1991-1-4 this terrain roughness can not be assigned in the design of wind loaded buildings. Therefore for the design a terrain roughness of $z_0 = 0.5$ m is used, which is considered a conservative choice.

86 pressure taps are distributed across the windward (38), leeward (38) and top face (10) of the building model. For short duration runs (30 minutes in full-scale) the model is turned so different angles of attack are documented and also pressures for the side faces of the model are measured by a 90° angle of attack. For the purpose of this research only the long run measurements (176 hours in full-scale) are used which have an angle of attack of 0°. The measurements from the top face taps are not used. Two reference taps (87,88) measure the dynamic pressure at reference height, which is equal to the building height h . Details of the wind tunnel tests are found in table 9.2. The distribution of the pressure taps can be found in figure 7.3 on page 56.

Table 9.2: Wind tunnel and measurement data details

Wind tunnel and incident flow	Dimensions	13.5x3x2 m
	ρ_{air}	1.225 kg/m ³
	$v_{ref,h}$	14.7 m/s
Scaled model	Dimensions	0.48x0.12 m
	Scale λ_g	1:250
	Taps	[1:38] windward; [39:76] leeward; [77:86] top; [87:88] reference pressures
Test	Sampling duration	≈ 94 min
	Full-scale duration	≈ 176 hr
	Angle of attack	frontal, 0°
	Sampling frequency	400 Hz

¹Same data is used as in Meinen (2015). Data is not extracted again.

10

Description wind speeds

In this chapter the gathered data of wind speeds at Schiphol Airport is processed and a probabilistic description for the yearly wind speeds is given in § 10.1. Possible distributions are fitted to the data and are compared in § 10.2. The distribution of the 50-yearly wind speeds will be used in the reliability assessment of the case study building. In § 10.3 the sampling uncertainties are considered and a way to incorporate them in the reliability analysis is provided. In § 10.4 some conclusions on the found results and implications for the reliability analysis are given.

10.1. Description of the wind speed data

From § 9.2 it was found that there is a total of 64 years of hourly mean wind speeds around Schiphol Airport available from the KNMI wind velocity data. From this data yearly maxima are extracted and dependence of these maxima is checked. Maxima are considered independent when the time between two successive maxima is more than 6 hours, which is the short-range storm dependency (Cook, 1985). It was found that the 64 yearly maxima can be considered independent. The data is also considered stationary (Meinen, 2015). Both these checks have been performed, because the yearly extreme data will have to be transformed to 50-yearly extreme data for the reliability analysis in the ULS. For this purpose the univariate theorem of § 5.2 will be used and for this theorem to hold the data should be both independent and stationary.

The original data is divided into wind speed directions of 10° . Only alongwind buffeting response is considered in this thesis and separate wind directions are not accounted for. Therefore wind speeds from all directions are used in this analysis. In Meinen (2015) it was found that the ECDF of all wind directions is almost the same as the one from the governing wind direction, which is South-West around Schiphol Airport (and in the Netherlands in general). The wind speeds were divided into wind sections of 30° and of all 12 resulting sections the yearly maxima were gathered. The ECDF's of these wind speed sections as well as the one for all directions can be seen in figure 10.1. From this it can be concluded that considering wind speeds irrespective of their direction is a conservative choice.

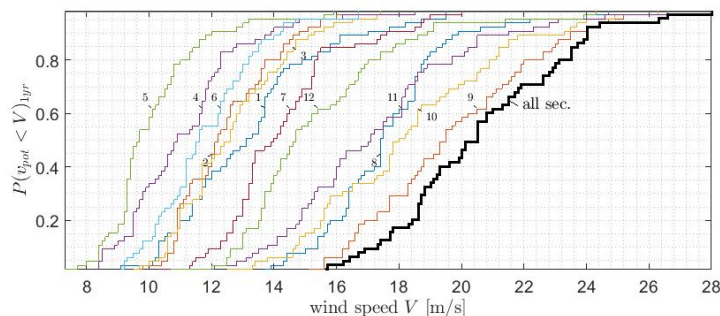


Figure 10.1: ECDF of yearly extreme wind speeds of 12 different wind directions and independent of wind direction (Meinen, 2015)

The moments of the yearly maximum wind speed data irrespective of their direction are given in table 10.1. This data is used to fit distribution functions in the next section that can be used in the reliability calculation.

Table 10.1: Probabilistic description of the 64 measured direction independent yearly extreme wind speeds at Schiphol Airport

	$\hat{\mu}$ [m/s]	$\hat{\sigma}$ [m/s]	$\hat{\alpha}$ [-]
Yearly extremes v_{pot}	20.5	2.7	0.43

10.2. Distribution fitting of the wind speed data

Two types of distributions are fitted on the yearly extreme data, both members of the family of the Generalised Extreme Value distribution; a Type I (Gumbel) and a Type III (Weibull) GEV distribution. These distributions and the reasons for considering these were described in chapter 5.

10.2.1. Distribution fitting

In figure 10.2a both distribution fits are displayed together with the sample data. From this figure it can not be concluded whether one fit is 'better' than the other. Therefore in figure 10.2b also a few fits for bootstrapped samples are presented. It can be seen that the data does not suggest one of the two distribution types to be a better fit than the other as a different set of sample data could result in both a Type I or Type III GEV distribution fitted to this data.

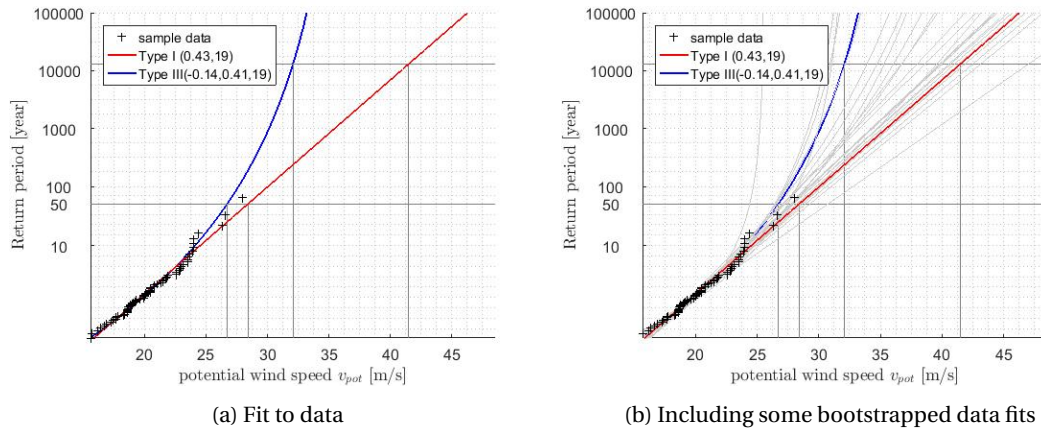


Figure 10.2: ECDF annual maxima of wind speed and fitted Type I and III extreme value distributions

In the range of the sample data both distribution types do not deviate that much from one another. However, in reliability analysis those wind speeds relevant for design are generally found in the upper tail of the distribution. Therefore the Level I characteristic and design value of the wind speed are indicated and explained in next section. It should be noted that the true design wind speeds can only be computed through a Level II or Level III reliability calculation, but the Level I values do give a first indication.

10.2.2. Level I characteristic and design wind speeds

The characteristic value corresponds to the wind velocity that is exceeded once during the lifetime of the structure, which is 50 years for the purpose of this research. The Level I design value corresponds to the Level I probability fractile with a reliability index for CC2 of $\beta = 3.8$. The wind speed is considered to be the governing load-parameter and has therefore sensitivity factor $\alpha_S = 0.7$. These probabilities of exceedance correspond to the 50-yearly extreme distribution and can be transformed to corresponding probabilities of the yearly extreme distributions. The yearly probabilities of non-exceedance are therefore given by:

$$\begin{aligned}
 P(v \leq v_{pot,k})_1 &= 1 - \frac{P(v > v_{pot,k})_{50}}{50} = 0.98 \\
 P(v \leq v_{pot,d})_1 &= 1 - \frac{\Phi_u(-0.7 \cdot 3.8)}{50} = 0.99992
 \end{aligned}
 \tag{10.1}$$

These correspond to a return period of 50 and 12500 years, respectively. In figure 10.2a on the facing page it can be seen that around the Level I design value the two distribution plots show entirely different behaviour. The obtained design value will therefore depend considerably on the chosen statistical method.

In Meinen (2015) a detailed comparison of the derived Level I design values with the EN1991-1-4 design values is provided. It was found that the characteristic wind speeds do not deviate that much, due to the fact that this value has a return period of 50 years and 64 years of data is available. In current research a Type III GEV distribution is utilized instead of a Three Parameter Lognormal distribution. It is found that a similar conclusion can be drawn for the Type III GEV distribution. It was also found that the design values do depend greatly on the statistical method and that the derived values can deviate from the EN1991-1-4 considerably as well. For the detailed analysis reference is made to Meinen (2015).

10.2.3. Parameters distribution fits

In table 10.2 the moments of the sample data together with the ones of the fitted distributions are given. Especially the skewness of the data and the Type I fit show different behaviour, due to the fixed skewness $\alpha = 1.14$ of the Type I GEV distribution. This skewness is important for the tail fitting. However, small changes in the data will greatly effect the skewness and therefore the fit of the Type III GEV distribution. Therefore, especially for this distribution, it is important to account for the sampling uncertainties.

Table 10.2: Moments of the sample data of the yearly extreme wind speeds and of the fitted Type I and III GEV distributions

	μ [m/s]	σ [m/s]	α [-]
Sample data yearly extremes v_{pot}	20.5	2.7	0.43
Type I yearly extremes v_{pot}	20.6	3.0	1.14
Type III yearly extremes v_{pot}	20.5	2.7	0.46

In table 10.3 the model parameters of the fitted distributions are given for the yearly extreme wind speeds. It is noted that the parameters of the distributions of the 50 yearly extreme wind speeds would be different, but for this research choice is made to numerically transform the CDF instead of analytically changing the model parameters. This shifting is done by application of the univariate theorem in § 5.2.

Table 10.3: Model parameters of the fitted Type I and III GEV distributions for the yearly extreme wind speeds

	u	α	ξ
Type I yearly extremes v_{pot}	19.24	0.43	-
Type III yearly extremes v_{pot}	19.42	0.41	-0.14

10.3. Sampling uncertainties

In figure 10.3 on the next page both Type I and Type III GEV distribution fits on the wind speeds sample data are displayed together with several 'bootstrapped' sample fits. From these figures it can be clearly seen that the Type III GEV distribution fit is more sensitive to sampling uncertainties than the Type I GEV distribution fit. The Level I design values are indicated in the figures as well. As was explained in chapter 5 in § 5.4 the Level I design points will be used in the computation of the sampling uncertainty factor S_v by means of the bootstrap-design point method (Meinen, 2015). For this purpose the coefficient of variation of the Level I design points for all 'bootstrapped' sample fits is used as the coefficient of variation of S_v . The computed coefficients of variation for both distribution types are given in table 10.4.

Table 10.4: Coefficients of variation for the Level I 'bootstrapped' design points

Distribution type	COV [-]
Type I GEV	0.04
Type III GEV	0.09

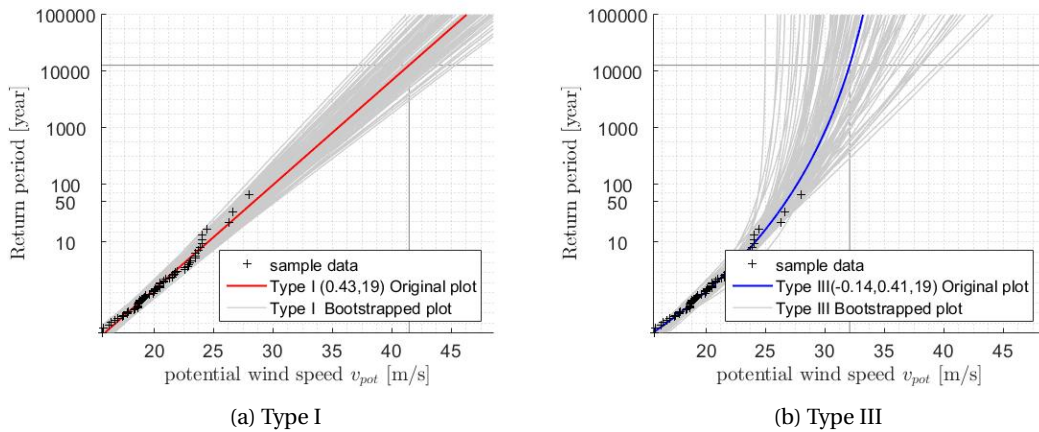


Figure 10.3: Fitted Type I and III extreme value distributions for yearly extreme wind speeds together with bootstrapped sample fits

10.4. Conclusions

- For the purpose of this research from KNMI wind speed measurements 64 yearly extremes are derived which are independent of wind direction. From Meinen (2015) it was found that this results in slightly conservative values of the wind speeds compared to the governing wind direction.
- On this data two distribution types are fitted, a Type I and Type III GEV distribution. The distributions are fitted on the yearly extremes and the obtained cumulative distribution function (CDF) will be shifted to the 50-yearly extremes distribution function by means of the univariate theorem.
- The sample skewness is highly dependent on individual extremes of the data and the Type III GEV distribution fit is therefore more sensitive to sampling uncertainties as the Type I GEV distribution has a fixed skewness. The higher coefficient of variation of the Level I 'bootstrapped' design values of the Type III distribution fits compared to the lower Type I coefficient of variation confirms this statement.

Description global response coefficients

In this chapter the derived response coefficients by means of the methods described in chapter 7 are processed and a description for the computed response coefficients is given in § 11.1. Also a comparison to the response coefficients derived from EN1991-1-4 is provided to evaluate the global effect, like in Hansen (2012). Possible distributions are fitted to the response coefficient data and are compared in § 11.2. The distribution of the hourly extreme response coefficients will be used in the reliability assessment of the case study building. In § 11.3 the sampling uncertainties are considered and in § 11.4 some conclusions on the found results and implications for the reliability analysis are given.

11.1. Description of the response coefficient data

On the wind tunnel pressure measurements described in § 9.3 the methods of chapter 7 have been applied. For the purpose of this research wind tunnel pressure measurements for a duration of 24 hours in full-scale were used to reduce the effect of statistical and sampling uncertainties. First representative pressures are derived, which have been assigned to the cantilevered beam model in finite element program DIANA. All model choices are explained in § 7.2. A transient analysis is performed which results in the response coefficient data of the base bending moment and base shear. In figure 11.1 the response coefficient for the maximum time of loading are shown. The dynamic response coefficients as designed for in EN1991-1-4 are also shown in these figures. It should be noted that these Eurocode response coefficients include the amplification factor c_d (and size factor c_s). Similar to Hansen (2012), which was explained in § 3.1, the response coefficients are found to be lower than the values proposed in EN1991-1-4 for the entire test duration. However, an extreme value analysis is required to compare both the design value in EN1991-1-4 and the design value computed through the reliability analysis.

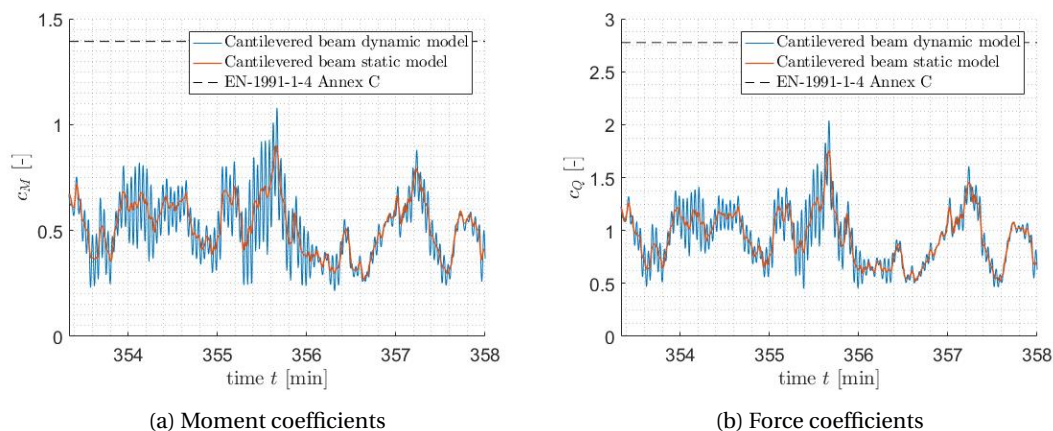


Figure 11.1: Maximum response coefficients for the entire transient analysis results. The Eurocode dynamic response coefficients are also presented.

By means of the block method described in chapter 5 the peak response coefficients are derived. For choice of block duration the autocorrelation and reversed univariate method are used as explained in § 7.3. In this section a block duration of 20 s is chosen. This choice was made to ensure both sufficient and independent extremes. The moments of the peak response coefficient data are given in table 11.1. This data is used to fit distribution functions which will be used in the reliability calculation.

Table 11.1: Probabilistic description of the 20s-extreme response coefficient data

	$\hat{\mu}$ [-]	$\hat{\sigma}$ [-]	$\hat{\alpha}$ [-]
t extremes \hat{c}_M	0.66	0.11	0.11
t extremes \hat{c}_Q	1.16	0.20	0.21

11.2. Distribution fitting of the response coefficient data

11.2.1. Distribution fitting

In figure 11.2 the fitted Type I and III GEV distributions of the 20s-extreme base moment and shear coefficients are plotted together with the ECDF of the data. From this figure it appears that the Type I GEV distribution would overestimate the design value of the response coefficients, while the Type III GEV distribution represents the skewness of the data better, but would possibly underestimate the design value slightly. This is addressed again in further analysis.

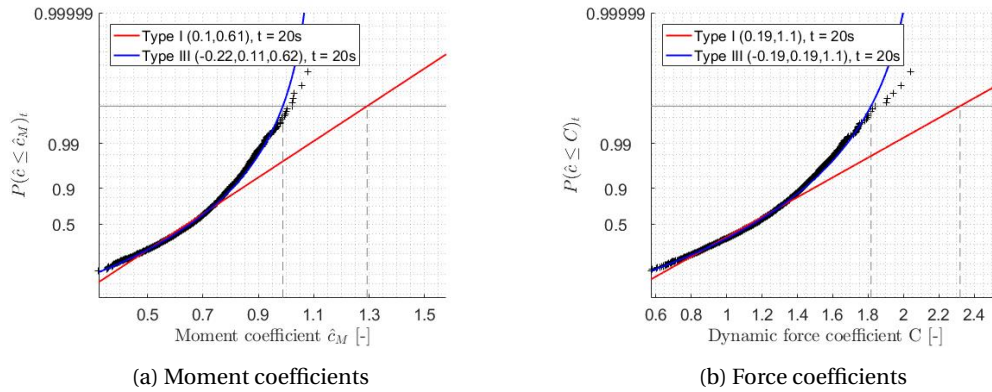


Figure 11.2: ECDF and fitted Type I and III distributions on the 20 s extremes of the response coefficients in the Gumbel domain

11.2.2. Cook-Mayne design value

A first indication of the design value of the response coefficients is the Cook-Mayne fractile which was explained in § 4.3. It should be noted that the true design value can only be computed through a Level II or Level III reliability calculation. The Cook-Mayne fractile is the 0.78 fractile and is also indicated in figure 11.2. This fractile value is valid for hourly T extreme coefficients and should therefore be transformed to the corresponding fractile of the 20s- or t -extremes:

$$P(\hat{c} \leq C)_t = 1 - \frac{0.22}{T/t} = 1 - \frac{0.22}{3600/20} = 0.9988 \quad (11.1)$$

It can be noticed that the deviation between the Type III GEV distribution and the sample data is only small for this fractile value and the effect can be considered negligible. However, it should be checked if the 'true' design value is not much larger than this Cook-Mayne fractile.

Due to the methods applied to maximise the number of extreme response coefficients for the modelling the Cook-Mayne fractile value is still within the range of the empirical cumulative distribution function. Statistical uncertainties are therefore reduced. It should be checked if the 'true' design value is in this range as well.

11.2.3. Parameters distribution fits

The moments of the data and of the fitted distributions can be found in table 11.2 which confirms the fact that the Type III GEV distribution better represents the skewness. This skewness is again important for the tail fitting. A different data set can greatly effect this skewness and therefore the fit of the Type III GEV distribution. However, for large data sets like these it should be checked if these sampling uncertainties have noticeable effect on the fit and if they should be incorporated.

Table 11.2: Moments of the sample data of the t -extreme response coefficients and of the fitted Type I and III distributions

		μ [m/s]	σ [m/s]	α [-]
\hat{c}_M	Sample data t extremes	0.66	0.11	0.11
	Type I t extremes	0.67	0.13	1.14
	Type III t extremes	0.66	0.11	0.20
\hat{c}_Q	Sample data t extremes	1.16	0.20	0.21
	Type I t extremes	1.17	0.24	1.14
	Type III t extremes	1.16	0.21	0.30

In table 11.3 the model parameters of the fitted distributions are given for the 20s-extremes. For the reliability analysis the distributions for the hourly extreme response coefficients are required. For this research choice is made to numerically transform the cumulative distribution function with the univariate theorem instead of analytically changing the model parameters.

Table 11.3: Model parameters of the fitted Type I and III distributions of the 20s-extreme response coefficients

		u	α	ξ
\hat{c}_M	Type I t extremes	0.61	9.57	-
	Type III t extremes	0.62	9.47	-0.22
\hat{c}_Q	Type I t extremes	1.06	5.24	-
	Type III t extremes	1.08	5.13	-0.19

11.2.4. Dependence of distribution fit on block duration

The shifted t -extremes are used to fit a theoretical distribution type to the data of the response coefficients. Therefore the effect of the block duration on the fit of the distribution and the evaluated Cook-Mayne fractile value is investigated. In 11.3 the fitted GEV distribution functions for the 10s-, 20s- and hourly extreme static moment coefficients are plotted to see if any noticeable differences between the fits can be found. The static moment coefficients are plotted, because a longer data set is available so enough hourly extremes are present for an accurate fit (176 extremes). For the dynamic response coefficients only 24 hourly extremes could have been derived. The static moment coefficients are the coefficients that are derived by integration of the wind tunnel pressure measurements.

Only a small difference can be noticed between the fits to the 10- and 20s-extremes and the hourly extremes for the Type III GEV, but there is a more noticeable difference between the t -extremes fit and the hourly extreme Type I GEV distribution fit. Therefore the effect around the Cook-Mayne fractile value for the different distribution fits is also evaluated. This fractile value is indicated by the gray line in figure 11.3 on the next page. This leads to the conclusion that for the Type III GEV distribution the different shapes of the fitted distribution functions do not have a considerable effect around the Cook-Mayne fractile. If the design value of the moment coefficient shows to deviate considerably from this fractile value, one must be aware of this effect. For the Type I GEV distribution there is a considerable difference in the Cook-Mayne fractile. Using the 20s block duration to fit the Type I GEV distribution leads to very conservative design values of the hourly extreme design response coefficients around the fractile value. Therefore this will be addressed in the reliability assessment in the next chapter. This deviation between the t -extreme fits and the hourly extreme fits is due to the high density of samples in the lower tail of the t -extremes. When the Type I GEV distribution would have been fitted to the upper tail of the samples, this deviation would not have been present. However, this choice was not made in this research.

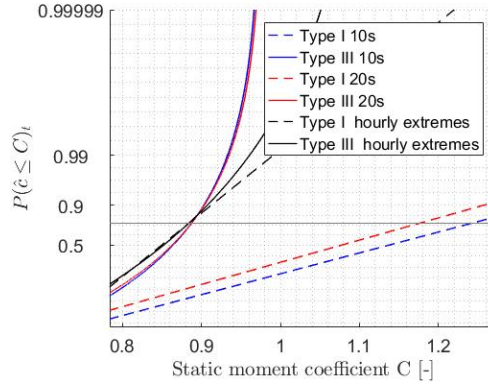


Figure 11.3: Fitted distributions of 10 and 20 s extremes versus hourly extremes of static moment coefficients

11.3. Sampling uncertainties

In figure 11.4 the fitted distributions and the sample data are plotted together with 200 bootstrapped data fits to visualize the sampling uncertainties. As expected the range for the Type I GEV distribution is not so large as for the Type III distribution. Therefore it is to be expected that the sampling uncertainties have a larger influence on the structural reliability for the Type III than for the Type I GEV distribution. However, for both distribution types the range of bootstrapped fits is very small. This leads to a low coefficient of variation and will therefore not have much effect on the reliability analysis. The sampling uncertainties in the extreme response coefficients will therefore not be accounted for in further reliability assessment.

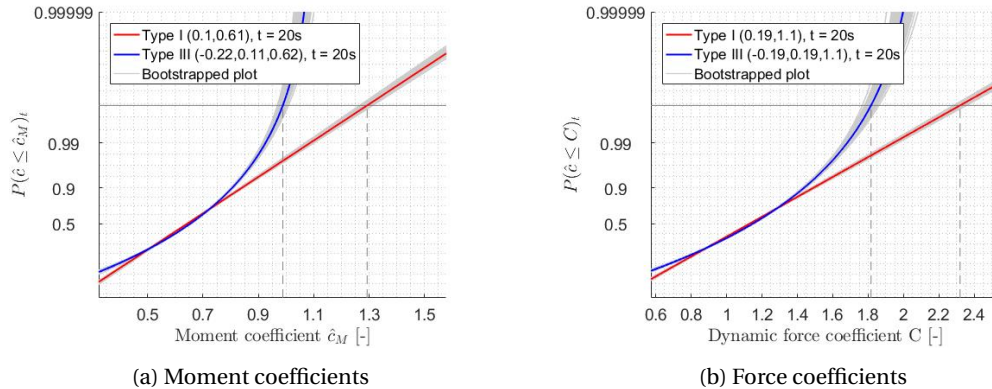


Figure 11.4: ECDF and fitted Type I and III distributions on the 20 s extremes of the response coefficients in the Gumbel domain together with the bootstrapped sample fits

11.4. Conclusions

- For the modelling of the extreme response coefficients the block method is applied with a block duration t of 20 s to maximize the amount of extremes for the modelling, but to ensure independence between the extremes.
- On this data two distribution types are fitted, a Type I and Type III GEV distribution. For the reliability analysis hourly extreme response coefficients are required which are derived by means of the univariate theorem on the t -extreme distribution fits.
- It was found that, due to its fixed skewness, the Type I GEV distribution is not able to adequately capture the naturally found skewness in the data. The Type III GEV distribution slightly overestimates the skewness of the data, but this is found to be of minor importance around the Cook-Mayne fractile.
- It was also found that the Type I fit greatly depends on the chosen block duration, which leads to very

conservative Cook-Mayne design values for this distribution type. In the next chapter it is investigated if this is the case for the 'true' design point as well.

- Due to the large data set of extreme response coefficients, both the Type I and Type III GEV distribution fits are not very sensitive to sampling uncertainties. These are therefore not taken into account in the reliability assessment.

12

Reliability assessment

Now all stochastic parameters for the case study building have been defined, in this chapter the results for the reliability assessment are presented. Therefore, in § 12.1 first a summary of the input for the reliability analysis is given and the level of calculation is given. Next, in § 12.2 the results of the reliability calculation are presented for different resistance models, also sampling uncertainties in the wind speed is accounted for. In § 12.3 the design values of the individual parameters are evaluated. This is done to check the assumption of the Cook-Mayne fractile of the response coefficients and to compare the obtained design values with the EN1991-1-4 design values. Last, in § 12.4 the sensitivity of the reliability results to the individual stochastic parameters is checked. In this section also the effect on the results of both a conservative assumed fundamental frequency and damping value is evaluated.

12.1. Input

12.1.1. Level of calculation

For the assessment of the reliability of the main bearing structure at foundation level of the case study building the limit state function in § 8.1 needs to be evaluated. Both a Level II as Level III calculation can be performed to determine the probability of failure of the structure and the design points of all the individual stochastic parameters. Both methods are explained in appendix A. Where a Level III calculation can give an exact indication of the probability of failure, a Level II calculation only gives an approximation. It is noted that this approximation is considered accurate for the β -values close to the target reliability index $\beta = 3.8$ for the situation in (Meinen, 2015). Therefore a Level II calculation procedure is chosen for this research to reduce computation time. An additional benefit of the Level II procedure is that it provides direct insight in the measure of impact of uncertainties in the individual parameters and their design values. Use is made of Prob2B for the evaluation of the limit state function, which is a TNO - developed program.

12.1.2. Description of stochastic parameters

For the assessment of the reliability of the main bearing structure at foundation level of the case study building a FORM (Level II) calculation is performed using the limit state function in chapter 8. The input for all different parameters considering a simplified probabilistic resistance model can be found in table 12.1 on the next page. For the derivation of the parameter values in R and c_r^2 see appendix H. For the full-probabilistic resistance model, the stochastic properties can be found in table 12.2 on the following page.

12.2. Reliability results

The reliability analysis is performed for both the base bending moment and base shear. The wind speed v_{pot} and response coefficients \hat{c}_R are modelled by both a Type I GEV distribution (1) and both a Type III GEV distribution (3). Also an intermediate case (2) is considered where v_{pot} is modelled by a Type I GEV distribution and \hat{c}_R by a Type III GEV distribution. The latter is performed, because in chapter 11 it was found that the Type I distribution fitted to the 20s-extremes could lead to very conservative design values of the

Table 12.1: Description of stochastic input variables for the reliability assessment of the case study building by limit state function z for a simplified stochastic resistance model

Variable	Distribution type	Parameters	Remarks
R	Lognormal	$\mu_{M,\log} = 20.3, \mu_{Q,\log} = 16.2,$ $COV = 0.1$	See appendix H
ν_{pot}	Type I GEV (Gumbel), Type III GEV (Weibull)	Type I: $u = 19.24, \alpha = 0.43;$ Type III: $u = 19.42, \alpha = 0.41,$ $\xi = -0.14$	Based on yearly extremes table 10.3 on page 83
S_v	Normal	$\mu = 1 [-], COV_I = 0.04 [-],$ $COV_{III} = 0.09 [-]$	Different COV for Type I and Type III GEV distribution of ν_{pot} , see § 10.3
c_r^2	Lognormal	$\mu_m = 1.03 [-], \mu_f = 0.91 [-],$ $COV = 0.15 [-]$	$\mu/(c_r^2)_s = 0.8$, see appendix H
\hat{c}_M	Type I GEV (Gumbel), Type III GEV (Weibull)	Type I: $u = 0.61, \alpha = 9.57;$ Type III: $u = 0.62, \alpha = 9.47,$ $\xi = -0.22$	Based on 20s extremes table 11.3 on page 87
\hat{c}_Q	Type I GEV (Gumbel), Type III GEV (Weibull)	Type I: $u = 1.06, \alpha = 5.24;$ Type III: $u = 1.08, \alpha = 5.13,$ $\xi = -0.19$	Based on 20s extremes table 11.3 on page 87
χ_{c_d}	Lognormal	$\mu = 1 [-], COV = 0.15 [-]$	$\mu/(c_d)_s = 1$
χ_{model}	Normal	$\mu = 1 [-], COV = 0.1 [-]$	
h	Deterministic	$h = 120$ m	
A	Deterministic	$A = 30 \times 120$ m ²	
z_0	Deterministic	$z_0 = 0.8$ m	

Table 12.2: Description of stochastic input variables on the resistance side for the reliability assessment of the case study building by limit state function z for the full-probabilistic resistance model method

Variable	Distribution type	Parameters	Remarks
χ_R	Lognormal	$\mu = 1.0 [-], COV = 0.06 [-]$ ¹	$\mu/(\chi_R)_s = 1$
ρ_s	Deterministic	0.01 [-]	Assumption
f_y	Lognormal	$\mu = 550$ MPa, $V = 0.05 [-]$ ²	Based on B500
f_c	Lognormal	$\mu = 48$ MPa, $V = 0.15 [-]$ ³	Based on C40/50
t	Deterministic	0.5 m	Choice: x_u lies within flange thickness
b	Deterministic	8 m	Follows from equation (8.7) on page 73
$\frac{A_{sw}}{s}$	Deterministic	0.92 mm ² /mm	Follows from equation (8.10) on page 74

response coefficients.

12.2.1. Simplified stochastic resistance model

First the reliability analysis is performed using the simplified stochastic resistance model. In figure 12.1 on the facing page the results of the reliability calculation can be found for this resistance model. Both the sensitivity factor α and reliability index β for different analyses are presented. The sensitivity factor gives a direct indication of the sensitivity of the structural reliability to the uncertainties in the specific stochastic variable. Also the target reliability for CC2 $\beta_{\text{target}} = 3.8$ is plotted in the figure.

It can be seen from figure 12.1a on the next page that when modelling the wind speed by a Type I GEV distribution the most dominant factor contributing to the reliability of the structure is this wind speed. However, when the wind speed is modelled by a Type III distribution, this dominance is not found and all other stochastic parameters in the reliability calculation gain importance. This effect is also seen in figure 12.1b on the facing page as the reliability index for the Type III distribution is a lot higher than for the Type I distribu-

¹from *fib SAG 7* document 'Reliability assessment of Existing Structures' (*fib SAG 7*)

²see footnote 1

³see footnote 1

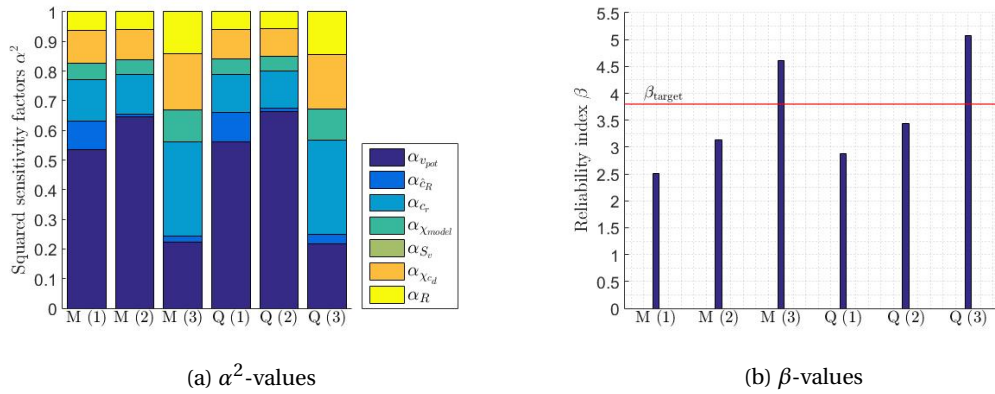


Figure 12.1: α^2 -values of the stochastic variables and β -values of the reliability calculation considering base bending moment and shear force for both the Type I and Type III distribution functions for the simplified resistance model *without sampling uncertainties*.
 (1): Both v_{pot} and $\hat{\epsilon}_R$ Type I; (2): v_{pot} Type I and $\hat{\epsilon}_R$ Type III; (3): Both v_{pot} and $\hat{\epsilon}_R$ Type III

tion. This can be explained by the fact the squared wind velocity is found in the stochastic wind load effect model. Therefore, a lower design value for the wind speed results in a considerable effect on the β -value.

Next, sampling uncertainties in the wind speeds are accounted for. The results are given in figure 12.2. The sampling uncertainties have the largest effect on the Type III GEV distribution of the wind speeds. Therefore especially the derived reliability levels of analyses (3) are influenced. However, still a beneficial effect on the β -values can be noticed when modelling the wind speed by a Type III GEV distribution.

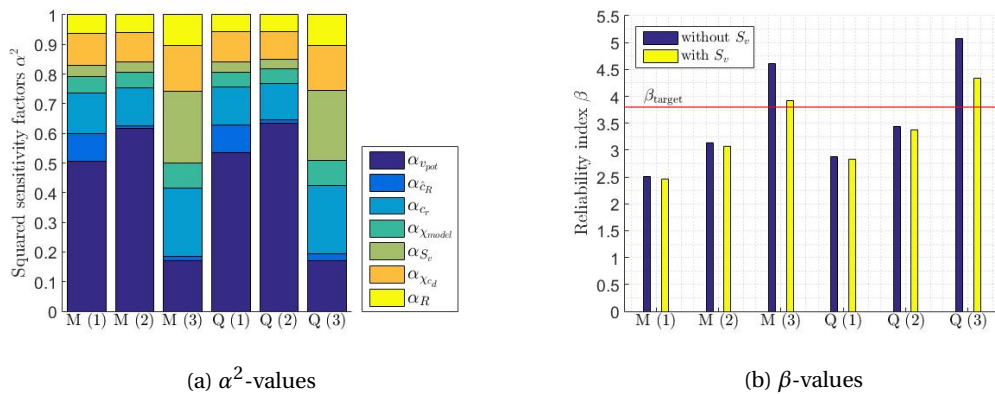


Figure 12.2: α^2 -values of the stochastic variables and β -values of the reliability calculation considering base bending moment and shear force for both the Type I and Type III distribution functions for the simplified resistance model *including sampling uncertainties*.
 (1): Both v_{pot} and $\hat{\epsilon}_R$ Type I; (2): v_{pot} Type I and $\hat{\epsilon}_R$ Type III; (3): Both v_{pot} and $\hat{\epsilon}_R$ Type III

12.2.2. Full-probabilistic resistance model

Next, the full-probabilistic resistance model is utilized in the reliability analysis. The sensitivity of the reliability analysis to all individual resistance parameters is checked by including the stochastic properties of the parameters one by one. In the first steps sampling uncertainties are *not* accounted for.

1 stochastic resistance variable

In figure 12.3 on the following page and figure 12.4 on the next page the results of the reliability calculation can be found for the full-probabilistic resistance model, only considering uncertainties in the reinforcement yield strength f_y and the characteristic procedure resistance model for dominant reinforcement steel behaviour. The latter model is used to check the behaviour of the full-probabilistic resistance model, as both methods should lead to similar results for dominant steel behaviour. It can be seen that the results are quite similar, so the full-probabilistic resistance model is considered to perform well. Furthermore, similar conclusions can be drawn as from the simplified stochastic resistance model results.

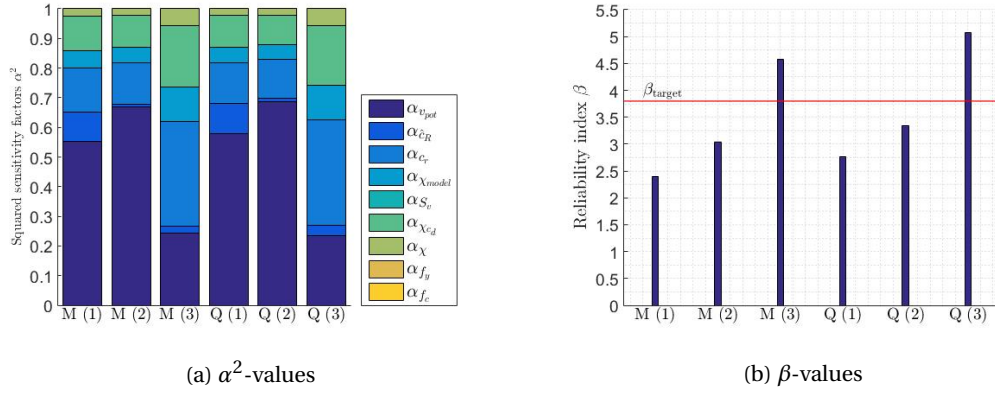


Figure 12.3: α - and β -values of the stochastic variables in the reliability calculation considering base bending moment and shear force for both the Type I and Type III distribution functions of the full-probabilistic resistance model for one stochastic resistance parameter; f_y without sampling uncertainties. (1): Both v_{pot} and $\hat{\epsilon}_R$ Type I; (2): v_{pot} Type I and $\hat{\epsilon}_R$ Type III; (3): Both v_{pot} and $\hat{\epsilon}_R$ Type III

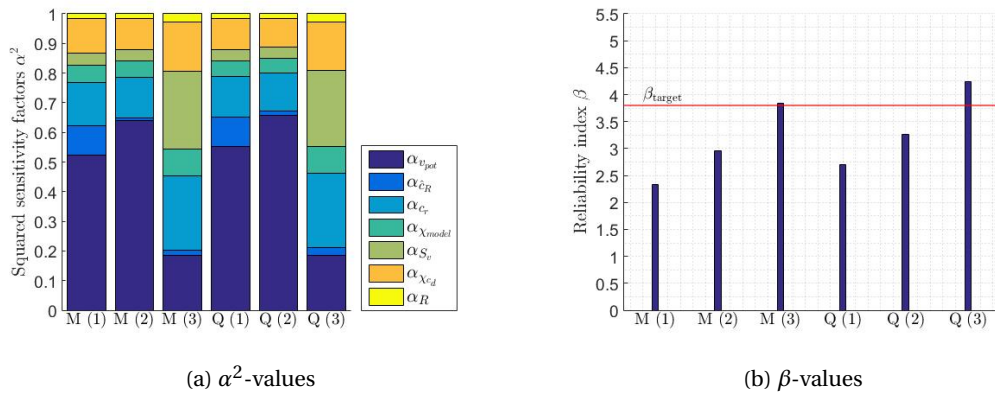


Figure 12.4: α - and β -values of the stochastic variables in the reliability calculation considering base bending moment and shear force for both the Type I and Type III distribution functions of the characteristic resistance procedure for steel dominance without sampling uncertainties. (1): Both v_{pot} and $\hat{\epsilon}_R$ Type I; (2): v_{pot} Type I and $\hat{\epsilon}_R$ Type III; (3): Both v_{pot} and $\hat{\epsilon}_R$ Type III

2 stochastic resistance variables

Next both model uncertainty factor χ_R and yield strength f_y are considered to be stochastic parameters in the resistance model. The results are found in figure 12.5.

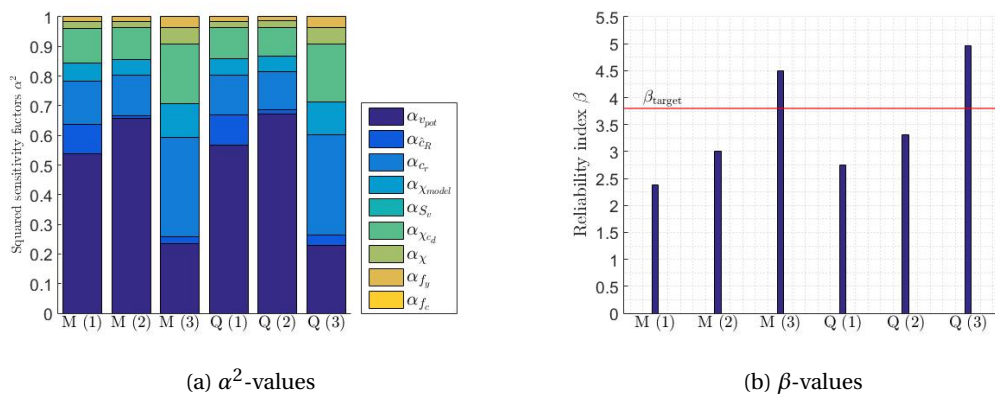


Figure 12.5: α - and β -values of the stochastic variables in the reliability calculation considering base bending moment and shear force for both the Type I and Type III distribution functions of the full-probabilistic resistance model for both θ_R and f_y stochastic parameters without sampling uncertainties. (1): Both v_{pot} and $\hat{\epsilon}_R$ Type I; (2): v_{pot} Type I and $\hat{\epsilon}_R$ Type III; (3): Both v_{pot} and $\hat{\epsilon}_R$ Type III

Only slightly lower β -values are found for the two stochastic resistance parameters. It can also be seen that the α -value of the second resistance parameters is not that high, so only small influence on the structural reliability is found.

3 stochastic resistance variables

Finally model uncertainty factor χ_R , yield strength f_y and concrete compressive strength f_c are considered all to be stochastic parameters in the resistance model. These results are found in figure 12.6. The α -value of the third parameter f_c is almost zero. Therefore the found β -values are the same as for the two parameter case.

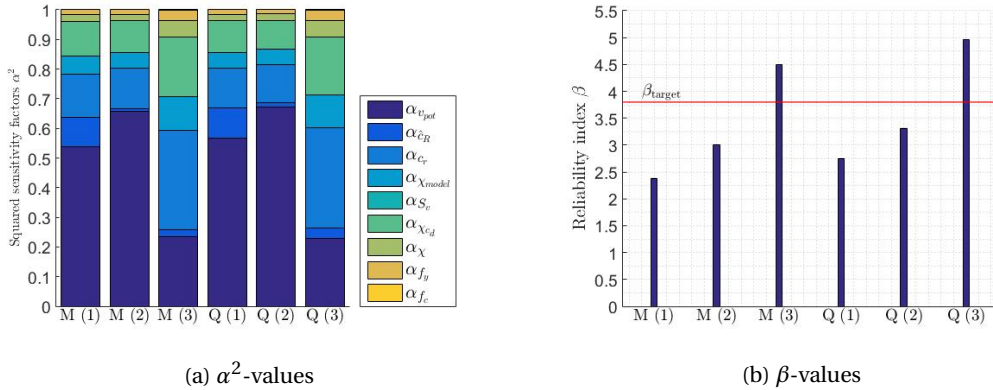


Figure 12.6: α - and β -values of the stochastic variables in the reliability calculation considering base bending moment and shear force for both the Type I and Type III distribution functions of the full-probabilistic resistance model for θ_R , f_y and f_c stochastic parameters *without sampling uncertainties*. (1): Both v_{pot} and \hat{c}_R Type I; (2): v_{pot} Type I and \hat{c}_R Type III; (3): Both v_{pot} and \hat{c}_R Type III

Effect of sampling uncertainties

Next, sampling uncertainties in the wind speed distribution fitting are considered. The results are presented in figure 12.7. The β -values of the previous analysis with 3 stochastic resistance parameters without accounting for sampling uncertainties are also displayed. It can be seen that especially the results for the Type III GEV distribution for the wind speed are sensitive to these sampling uncertainties and these reliability indices clearly decrease. However, still higher reliability levels are derived with this Type III GEV distribution for the wind speeds and response coefficients than with the Type I GEV distribution for the wind speeds.

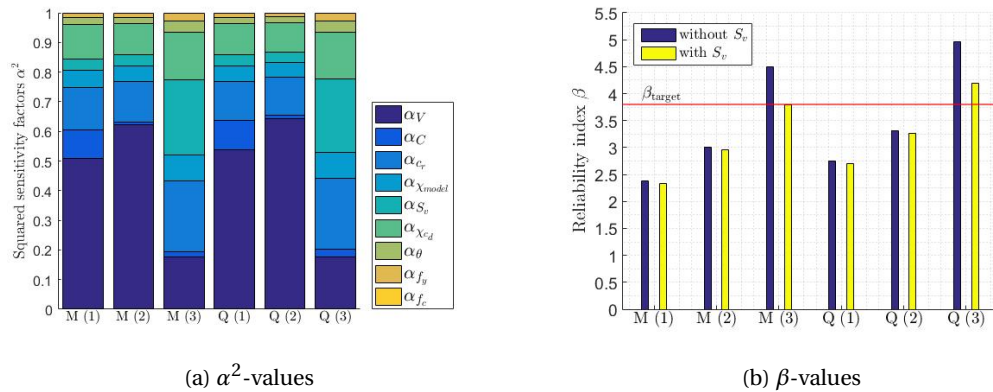


Figure 12.7: α - and β -values of the stochastic variables in the reliability calculation considering base bending moment and shear force for both the Type I and Type III distribution functions of the full-probabilistic resistance model for θ_R , f_y and f_c stochastic parameters *including sampling uncertainties*. (1): Both v_{pot} and \hat{c}_R Type I; (2): v_{pot} Type I and \hat{c}_R Type III; (3): Both v_{pot} and \hat{c}_R Type III

12.2.3. Conclusions on the first reliability results

The third stochastic parameter on the resistance side, f_c , does not influence the reliability calculation significantly. The same β -values are found for 2 and 3 stochastic parameters in the resistance model. Additionally,

when comparing the simplified stochastic resistance model and the full-probabilistic resistance model, it can be seen that slightly lower β -values are found for the latter model, but only of an order of 0.1.

From the results presented in this chapter it can be seen that the situation (1) results in the lowest β -values. For the other two situations, the derived β -values are close to the target reliability $\beta_{\text{target}} = 3.8$ in EN1990 for consequence class 2. Modelling the wind speed by a conventional Type I GEV distribution leads to reliability levels reaching β_{target} and were found to be almost insensitive to sampling uncertainties. The reliability levels for this situation (2) are still below the target reliability. However, it should be noted that it is not properly defined in literature how this target reliability was defined. Therefore for the reliability assessment of the case study it has been chosen not to use this target reliability as a hard boundary when assessing whether a structure is safe or not. A Type III GEV distribution for the wind speeds, which better represents the naturally observed skewness in the data, can only be used when sampling uncertainties are accounted for. These are found to have considerable influence on the obtained reliability levels. Reliability levels for this situation (3) are found to be around the target reliability.

In chapter 11 it was found that the Type I GEV distribution for the response coefficients can lead to overly conservative design values for these coefficients when these design values are in the range of the Cook-Mayne design value. Therefore in next section it is investigated what the design value for the response coefficients is and how this effects the reliability results. Thereby the design values for the other parameters are derived as well and compared to the EN1991-1-4 design values.

12.3. Design values

In this section, first the obtained design values for the response coefficients are checked with previous assumptions and second all design values are compared to the Eurocode wind loading model to obtain insight in the reason for the derived β -values. The computed design values are derived for the situation *with* accounting for sampling uncertainties.

12.3.1. Response coefficients design fractile

In § 11.2 it was noticed that the performance of the Type III GEV distribution for the response coefficients was dependent on the required fractile value of the response coefficients. It was found that for the Cook-Mayne fractile and lower fractile values the distribution fit performed well enough. Therefore in figure 12.8 the Cook-Mayne fractile values are indicated together with the derived design values for the response coefficients. It can be noticed that the found design values are almost the same as the Cook-Mayne fractile values.

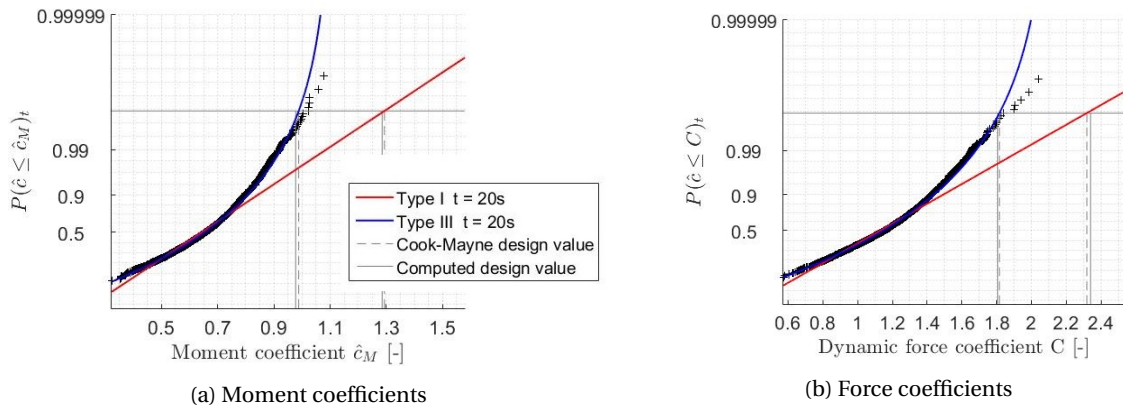


Figure 12.8: ECDF and fitted Type I and III distributions on the 20 s extremes of the response coefficients in the Gumbel domain along with computed and Cook-Mayne design value with accounting for sampling uncertainties

In § 11.2 it was also stated that the t -extreme Type I GEV fit might not represent the hourly extreme fit well enough, while the Type III GEV does perform well, especially in the Cook-Mayne fractile. As the derived design value corresponds to this fractile value the Type III GEV distribution of the t -extremes can be considered accurate. Furthermore, this design value is still in the range of the empirical cumulative distribution function

of the extreme response coefficients, which confirms this statement. However, it can be seen the Type I GEV distribution of the shifted t -extremes leads to overly conservative design values for the response coefficients. Therefore the derived β -values for the analysis (1) with the response coefficients modelled by this distribution type are also considered too conservative.

12.3.2. Derived design values and EN1991-1-4 design values

Next, the derived design values for all individual stochastic parameters are presented. This is done to evaluate the difference between the EN1991-1-4 design values and the derived design values. For the EN1991-1-4 it is assumed that the total value of the partial factor is applied to the wind speed. For the other parameters it therefore holds that the characteristic value equals the design value. The design values are given in table 12.3.

Table 12.3: Design values for the reliability calculations and EN1991-1-4 design values. (1): Both v_{pot} and \hat{c}_R Type I; (2): v_{pot} Type I and \hat{c}_R Type III; (3): Both v_{pot} and \hat{c}_R Type III

		Design value I (1)	Design value I/III (2)	Design value III/III (3)	Code value
M	v_d [m/s]	36.2	40.2	35.2	33.1^4
	\hat{c}_R [-]	1.28	0.97	0.98	1.34^5
	c_r^2 [-] at 2/3h	1.16	1.19	1.34	1.28
	χ_{model} [-]	1.06	1.07	1.11	1.0
	χ_{c_d} [-]	1.12	1.14	1.23	1.0
Q	v_d [m/s]	37.9	42.1	36.1	33.1^6
	\hat{c}_R [-]	2.34	1.78	1.81	2.78^7
	c_r^2 [-] at 1/2h	1.04	1.07	1.22	1.14
	χ_{model} [-]	1.06	1.07	1.12	1.0
	χ_{c_d} [-]	1.13	1.15	1.25	1.0

From table 12.3 it can be seen that the design values of the response coefficients \hat{c}_R and the roughness factor c_r^2 in EN1991-1-4 are conservative with respect to the full reliability calculation. However, the wind speed design value in the Dutch National Annex to EN1991-1-4 is less than the derived design value. Additionally, the full-probabilistic assessment procedure derived and used in this research uses two extra parameters χ_{model} and χ_{c_d} which are not found explicitly in the EN1991-1-4 wind loading model. Therefore the EN1991-1-4 design values of these parameters are set to 1.0. Both derived design values are more than 1.0 and especially the dynamic property uncertainty factor causes an increase in the design wind load.

12.4. Sensitivity study stochastic parameters wind loading effect model

The derived reliability levels are based on certain model choices made in previous chapters and the chosen description of the stochastic parameters. Therefore in this section first the influence of the different stochastic parameters on the structural reliability is investigated. Second, the influence of the assumptions made in the dynamic property uncertainty factor are checked.

12.4.1. Influence of the number of stochastic parameters in the reliability analysis

First, one by one the stochastic parameters are considered deterministic. Finally, all stochastic parameters apart from the response coefficients and wind speeds are considered deterministic. The results are presented in figure 12.9a on the following page. In figure 12.9b on the next page the α -values belonging to the last step in this sensitivity analysis are given.

From figure 12.9a on the following page it can be seen that the influence of every stochastic parameter on the found β -values is only small. Not considering the model factor χ_{model} , the dynamic property factor χ_{c_d} or the roughness factor c_r^2 as stochastic parameters does increase the reliability of the structure a little, but β -values do not rise considerably. When only the response coefficients and the wind speed are stochastic parameters the average increase in β is about 0.5. Only in the third case (3) the reliability index increases more when only

⁴10 min mean design wind velocity $v_d = \sqrt{1.5}v_b$, instead of hourly mean.

⁵10 min extreme design response coefficient, instead of hourly extremes.

⁶See footnote 4

⁷See footnote 5

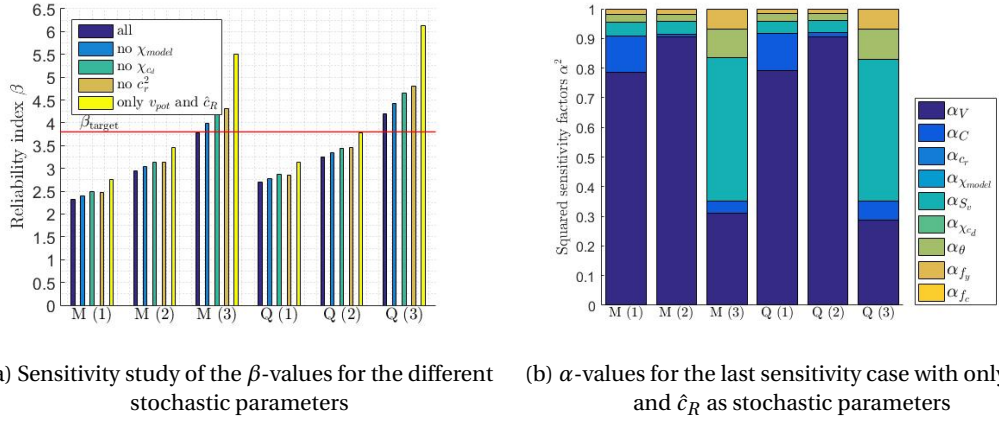


Figure 12.9: Sensitivity study of reliability results on different stochastic parameters *with accounting for sampling uncertainties*

considering v_{pot} and \hat{c}_R as stochastic parameters. It should be noted that sampling uncertainties in the wind velocities are accounted for. In figure 12.9b it can be seen that in the third case the sampling uncertainty factor is the dominant one instead of the wind speed, which results in the larger change in β -value.

The stochastic parameters considered in the sensitivity analysis do not influence the β -values considerably. Therefore, it can also be concluded that especially the wind speed, and response coefficients, have a large influence on the reliability. From figure 12.9b it can be noticed that it is the wind speed that influences the structural reliability results the most.

12.4.2. Assumptions in dynamic property uncertainty factor χ_{cd}

From the Probabilistic Model Code it was found that while for damping the code specified value is considered conservative, for the fundamental frequency this is not the case. However, in practice, when for both properties conservative values are adopted, this could have considerable influence on the reliability results. Therefore, the reliability analysis is also performed for a χ_{cd} -factor with mean-over-specified of $\mu/(\chi_{cd})_s = 0.8$. This value means that the value designed is conservative with respect to the 'true' or expected value. In figure 12.10 the derived reliability indices β are presented.

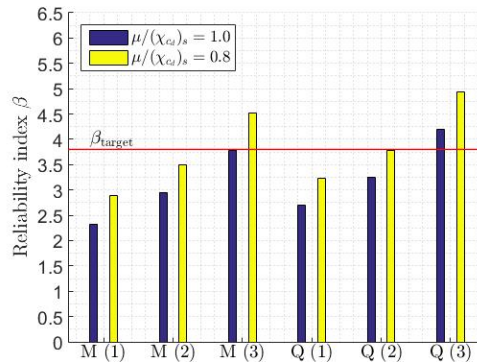


Figure 12.10: β -values for different mean-over-specified of χ_{cd} *with accounting for sampling uncertainties*. Original compared to situation when code values for both fundamental frequency as damping are considered conservative

It can be seen that the derived β -values do increase considerably compared to the case when $\mu/(\chi_{cd})_s = 1.0$ up to an order of 0.5. Therefore, it can be concluded that using a conservative estimate of both the fundamental frequency and damping in the full-probabilistic procedure presented in this thesis does indeed affect the reliability level considerably.

13

Discussion on the reliability results

In previous chapters the reliability assessment procedure was used on a case study building. All parameters were derived where required and the results of the reliability assessment were presented. In this chapter a discussion on the most important results is given.

13.1. Wind speeds

- Wind speeds were modelled by both a Type I and Type III generalized extreme value (GEV) distribution. The Type I GEV (or Gumbel) distribution is a conventional distribution type for the modelling of extreme wind speeds. The Type I distribution uses the first two moments of the data to fit its two parameters and the third, the skewness, is fixed. Another distribution type used in literature for the modelling of extreme wind speeds is the Type III GEV distribution, which requires three parameters to be fitted to the data. Therefore also three moments of the data are used including the skewness. This Type III GEV distribution better follows the data, as more parameters are fitted. However, it is also very sensitive to individual measurements, which introduces a considerable influence of sampling uncertainties for relatively small datasets.
- It was found that the Type I GEV distribution is not able to adequately capture the skewness of the used wind speed data, but will lead to a conservative distribution of the wind speeds due to its fixed skewness. However, based on a visual approach none of the two distributions can be considered a 'better' fit to the data.
- The sample skewness is highly dependent on individual extremes of the data and the Type III GEV distribution fit is therefore more sensitive to sampling uncertainties than the Type I GEV distribution fit. As a relatively small dataset of 64 yearly extreme wind speeds is used the effect of sampling uncertainties should be taken into account.

13.2. Response coefficients

- From the wind tunnel pressure data and the transient finite element model response coefficients were derived. For the entire (relatively long) duration of the test these were found to be smaller than the EN1991-1-4 response coefficients. This is consistent with expectations based on previous research by Hansen (2012). It should be noted that an extreme value analysis of the response coefficients is required to compare the actual design value to the EN1991-1-4 design values.
- The extreme response coefficients were modelled by both a Type I and Type III GEV distribution as well. It was found that, due to its fixed skewness, the Type I distribution is not able to adequately capture the naturally found skewness in the data. The Type III GEV distribution slightly overestimates the skewness of the data, but this is found to be of minor importance around the Cook-Mayne fractile (governing the design). The derived design value is found to be consistent with this fractile value, so the Type III GEV distribution is considered to perform well for the case study situation.

- A relatively large dataset was used for the modelling of the extreme response coefficients to reduce the effect of statistical and sampling uncertainties. It was found that these sampling uncertainties have a negligible effect on the distribution fit as around 4000 extreme response coefficients are used. Therefore sampling uncertainties in the modelling of the extreme response coefficients are not taken into account. It should be noted that when smaller datasets are used sampling uncertainties do have to be considered.
- It was also found that the Type I fit greatly depends on the chosen block duration and leads to conservative values of the response coefficients in the range governing the design for the block duration used in this research. As the derived design value is consistent with this fractile value, the results of the reliability assessment for a Type I GEV distribution of the shifted t -extreme response coefficients are on the very conservative side as well.
- The found design value for the response coefficients is still within the range of observed extremes due to the relatively large dataset. Therefore for the data used in this case study, a Type III GEV distribution can be considered a more accurate fit to the data than a Type I GEV distribution. So using both a relatively long set of wind tunnel measurements and using the methods to maximize the number of extreme response coefficients reduces the sampling and statistical uncertainties considerably.

13.3. Reliability assessment

- It was found that the results for the simplified probabilistic resistance model and the full-probabilistic resistance model for specific materials and failure modes do not differ much. The latter leads to slightly lower β -values, but only of an order of 0.1.
- For the full-probabilistic resistance model, the yield strength of the reinforcement steel f_y and the resistance model factor χ_R are the governing resistance parameters. Other stochastic parameters in the resistance model do not influence the results significantly.
- In general, the derived β -values are close to the target reliability $\beta_{\text{target}} = 3.8$ in EN1990 for consequence class 2. The situation when both wind speed and response coefficients are modelled by a Type I GEV distribution is considered too conservative as explained previously. There it was concluded that, for the relatively long dataset of the case study, a Type III GEV distribution for the extreme response coefficients better represents this data than a Type I GEV distribution. Modelling the wind speed by a conventional Type I GEV distribution leads to reliability levels reaching β_{target} and were found to be almost insensitive to sampling uncertainties. A Type III GEV distribution for the wind speeds, which better represents the naturally observed skewness in the data, can only be used when sampling uncertainties are accounted for. These are found to have considerable influence on the obtained reliability levels. Modelling the wind speed by a Type III GEV distribution and accounting for sampling uncertainties has a positive influence on the obtained reliability levels, where the Type I GEV distribution for the wind speeds leads to slightly lower and more conservative β -values.
- It was found that especially the wind speed influences the structural reliability. From the sensitivity factor for v_{pot} it can be concluded that the wind speed is the dominant factor. Additionally, the design value from EN1991-1-4, $v_d = \sqrt{1.5}v_b$, slightly underestimates the derived design value. However, EN1991-1-4 design values for both the response coefficient (including $c_s c_d$) and roughness factor are conservative with respect to the calculated design values.
- From the sensitivity study to the effect of all individual stochastic parameters it can also be concluded that the wind speed has the highest influence on the derived β -values. Not considering c_r^2 , χ_{c_d} and χ_{model} as stochastic parameters results in only slightly higher reliabilities than for the case with all stochastic parameters.
- Both χ_{model} and χ_{c_d} are factors that are not present in EN1991-1-4. The partial factor for wind loading $\gamma_s = 1.5$ should also incorporate these uncertainty factors. Especially the factor introducing the uncertainties in the dynamic properties χ_{c_d} , which is introduced in this research, does cause a higher design wind load than the EN1991-1-4 wind loading model.
- In practice it is often the use to adopt a conservative value for both fundamental frequency and damping. If this assumption is used in the reliability analysis, by adopting a lower mean-over-specified

value for χ_{c_d} , β -values are found that are about 0.5 higher than in the original situation, with $\mu/(\chi_{c_d})_s = 1.0$. This is a considerable increase and an accurate mean-over-specified value for χ_{c_d} should therefore be defined when applying the assessment procedure proposed in this research.

Conclusions and recommendations

14

Conclusions

In chapter 1 the main research question of this research was formulated:

How could the reliability of the main bearing structure of a dynamically sensitive building designed within the Eurocode framework be assessed in a full probabilistic way for global response through coupling of the uncertainties in wind climate, global dynamic response of the structure and resistance?

Therefore, the objective of this research was to give insight in the reliability based assessment of structures subjected to wind loading within the Eurocode framework, by first developing a probabilistic assessment procedure for global response of the main bearing structure at foundation level and second by giving an indication on this reliability by means of a case study approach. In order to answer the main research question several sub-questions have been formulated. These questions will be answered first, before reaching conclusions on the main research question.

- *What are the factors that should be incorporated in a stochastic wind load model based on literature?*
A literature study resulted in an overview of the most important factors and accompanying uncertainties that should be incorporated in the stochastic wind load effect model for the full probabilistic assessment procedure. The factors that should be incorporated in this model are; intrinsic uncertainties in basic wind velocity v_b , statistical and sampling uncertainties in basic wind velocity, intrinsic uncertainties in peak response coefficients \hat{c}_R , statistical (and sampling) uncertainties in peak response coefficients, knowledge uncertainties in roughness factor c_r , codification uncertainties in fundamental frequency n_0 and damping coefficient ζ and a model uncertainty factor.
- *How can global response at foundation level be evaluated and included directly in this model?*
For the purpose of this research response coefficients are defined that account for the relation between dynamic wind pressure in front of the building and actual response values in the main bearing structure. Therefore, methods were developed for deriving these response coefficients from building shape and terrain specific boundary layer wind tunnel pressure measurements to evaluate the global response at foundation level and include this response directly in the stochastic wind load model.
 - It is found that the combined effect of simultaneously measured pressures over both wind- and leeward façade of the building and the resulting dynamic response of the structure can be evaluated through transient finite element analysis. For this purpose a beam model was utilized as this is considered to be an accurate representation for global alongwind response of a building. A study to appropriate boundary conditions has been performed and it was investigated whether a more accurate representation of a pile foundation has an effect on the derived response coefficients. It is found that a cantilevered beam model with all degrees of freedom fully constrained at foundation level is sufficient and that less stiff boundary conditions (both horizontal and rotational) to represent the pile foundation stiffness do not have considerable effects on the response at foundation level. The beam model should have similar fundamental frequency and damping properties as the full-scale building. Nonlinear material behaviour does not have to be taken into account for wind loading. The required amount of elements is found to be equal to the amount of

pressure fields over the height of the finite element beam model which are defined for the amount of pressure taps over the height of the wind tunnel model. Over the width the pressures from the different pressure taps are averaged which is justified as only alongwind response is considered.

- To derive representative pressures belonging to the tributary area of the pressure tap in the wind tunnel test a decay constant C_r and an averaging constant C_T should be defined. In EN1991-1-4 a decay constant of $C_r = 11.5$ is adopted and in literature an averaging constant of $C_T = 4.5$ is usually found. Methods to derive and evaluate both constant values were presented in this research. By means of the proposed methods a study to the constant values was performed and the following values were derived for the case-study purpose; $C_r = 4.5$ and $C_T = 1.5$. These values are considerably lower than the proposed values and this strengthens findings of previous research where lower constant values are also suggested. Therefore this is to be expected for pressure measurements for other buildings as well and it can be generally concluded that currently prescribed constant values overestimate the size reduction effect.

- *How can all factors in the stochastic wind load model be incorporated in a full-probabilistic assessment procedure?*

In the method development of this research the methods by which all factors can be incorporated in the full-probabilistic assessment procedure were formed. The stochastic wind load model that is developed links and quantifies all previously described uncertainties full-probabilistically.

- Location-specific wind speed measurements should be used to derive an appropriate distribution of the extreme wind speeds with considered reference period. To account for statistical uncertainties, for the purpose of this research, two distribution types are considered based on literature and the available data; the Type I (conventional) and Type III generalized extreme value distribution functions. Sampling uncertainties are accounted for through a separate uncertainty parameter S_v based on the bootstrap design-point method by Meinen (2015). The knowledge uncertainties in the roughness factor are taken into account by modelling the roughness factor as a stochastic random variable for which literature data are used. Uncertainties which are not taken into account explicitly in the stochastic wind load effect model are represented by a model uncertainty factor which is also based on literature data.
- For the t -extreme response coefficients an appropriate distribution function needs to be derived. For the purpose of this research a Type I and Type III generalized extreme value distribution function are fitted. Both statistical and sampling uncertainties are reduced by utilizing a relatively long set of wind tunnel measurements and by methods reducing the block duration for extracting the extremes. It was found that the Type I fit greatly depends on the chosen block duration t , which leads to overly conservative Cook-Mayne fractile values (governing the design). Therefore when sufficient response coefficient data is available a Type III GEV distribution should be utilized if the data suggests this distribution shape. For the purpose of this research sampling uncertainties in response coefficients did not have to be taken into account as they were found to have negligible effects on the distribution fit due to the relatively large dataset.
- The uncertainties in fundamental frequency and damping should be taken into account through a separate uncertainty factor based on literature and the derived methods in this research by means of the finite element model.

- *How can the uncertainties on the resistance side of the probabilistic assessment be incorporated?*

To arrive at a full-probabilistic assessment procedure also the uncertainties on the resistance side of the calculation should be incorporated in a stochastic resistance model. For the purpose of this research a simplified probabilistic resistance model based on a Level I procedure and a full-probabilistic material and failure mode specific resistance model with all stochastic resistance parameters accounted for individually are compared. Similar reliability levels are obtained. Only two stochastic parameters in the full-probabilistic model are of relevance; yield strength of the reinforcement steel f_y and a model uncertainty factor χ_R .

- *How does the reliability of current designed buildings by EN1991-1-4 relate to the requirements in EN1990, which are expressed by a target reliability?*

The full probabilistic assessment procedure was used on a case study building to give an indication of the reliability of current designed buildings by EN1991-1-4 by means of a Level II reliability calculation.

It has also been evaluated how the total EN1991-1-4 procedure for wind loading relates to the design values of the full probabilistic procedure.

- In general, the derived β -values are close to the target reliability $\beta_{\text{target}} = 3.8$ in EN1990 for consequence class 2. Both modelling wind speed and response coefficients by a Type I GEV distribution is considered too conservative. This because it was concluded that, for the relatively long dataset of the case study, a Type III GEV distribution for the extreme response coefficients better represents this data than a Type I GEV distribution. Thereby, this Type I GEV distribution is found overly conservative when fitted to the t -extreme coefficients. Modelling the wind speed by a conventional Type I GEV distribution leads to reliability levels reaching β_{target} and were found to be almost insensitive to sampling uncertainties. A Type III GEV distribution for the wind speeds, which better represents the naturally observed skewness in the data, can only be used when sampling uncertainties are accounted for. These are found to have considerable influence on the obtained reliability levels. Modelling the wind speed by a Type III GEV distribution and accounting for sampling uncertainties has a positive influence on the obtained reliability levels, where the Type I GEV distribution for the wind speeds leads to slightly lower and more conservative β -values.
- From the sensitivity study to the effect of all individual stochastic parameters it can be concluded that the wind speed has the highest influence on the derived β -values. Not considering c_r^2 , χ_{c_d} and χ_{model} as stochastic parameters (as these parameters are very dependent on choices made) results in only slightly higher reliabilities than for the case with all stochastic parameters.
- Both χ_{model} and χ_{c_d} are factors that are not present in the EN1991-1-4 design procedure. Especially the factor introducing the uncertainties in the dynamic properties χ_{c_d} does cause a higher design wind load than the EN1991-1-4 wind loading model. In practice it is often the use to adopt a conservative value for both fundamental frequency and damping. If this assumption is used in the reliability analysis, by adopting a lower mean-over-specified value for χ_{c_d} , β -values are found that are about 0.5 higher than in the original situation, with $\mu/(\chi_{c_d})_s = 1.0$. This is a considerable increase and an accurate mean-over-specified value for χ_{c_d} should therefore be defined for the building considered when applying the assessment procedure proposed in this research.

The following conclusions are formulated when answering the main research question. These conclusions apply in general to the structural reliability assessment of dynamically sensitive buildings for global response.

- Nowhere in literature a complete probabilistic assessment procedure was found to evaluate the reliability of a dynamically sensitive building subjected to wind loading that links and quantifies uncertainties in wind climate, global pressure effects, dynamic response and resistance. Therefore in this research such a procedure was developed. For this purpose location-specific wind speed measurements, boundary layer wind tunnel pressure measurements and finite element analysis are used. Following this probabilistic assessment procedure allows for the derivation of the reliability level and for the assessment of this safety level of the main bearing structure of dynamically sensitive buildings designed within the Eurocode framework.
- It was found that using both wind tunnel pressure measurements and transient finite element analysis of a cantilevered beam model is sufficient for the evaluation of the global dynamic response of the structure at foundation level to determine the reliability level in the global situation. Less stiff boundary conditions to represent a pile foundation more accurately do not have a considerable influence on the derived response. It is recommended to use a long set of wind tunnel measurements combined with methods proposed in this research to maximise the number of computed extreme response coefficients and thereby to reduce the statistical and sampling uncertainties.
- The case study indicates that the Eurocode design procedure for global wind loading results in reliability levels close to the target reliability $\beta_{\text{target}} = 3.8$ in EN1990 for CC2. It was found that the intrinsic uncertainties in the wind speed have the highest influence on the derived reliability levels. Therefore it is to be expected that similar levels will be found for other buildings in similar wind speed conditions, which is the case for most Dutch design situations.
- One should be careful with the relatively high decay constant $C_r = 11.5$ in EN1991-1-4 and averaging constant $C_T = 4.5$ in literature describing the size effect as these are found to overestimate the size

reduction effect. For the purpose of this research values of $C_r = 4.5$ and $C_T = 1.5$ are derived. Similar constant values are to be expected for other buildings as well.

- When conservative values for both natural frequency as damping are adopted in practice, higher reliability levels β are obtained. β -values can be found to be of an order 0.5 higher. An accurate mean-over-specified value for χ_{c_d} should therefore be defined when applying the assessment procedure proposed in this research.

15

Recommendations

Based on current research recommendations for further research are:

- It was found that the reliability results by the assessment procedure depend considerably on the dynamic properties of the structure and the mean-to-specified ratio of these properties. Therefore it is recommended to investigate this mean-to-specified ratio in practice and derive these property values in an accurate way.
- Constant values for the decay and averaging constant, C_r and C_T respectively, were derived for the case study purpose based on wind tunnel measurements. By Geurts (1997) it was found that the wind tunnel results do not always represent the full-scale situation accurately. Therefore for the purpose of this research conservative values were adopted. For further research, it is recommended to evaluate these constant values by full-scale measurements as well.
- Reliability results were found to be highly dependent on the wind speed and the chosen distribution type. For the purpose of this research only 64 yearly-extremes were used for the distribution fitting and it could not be concluded if a Type I or Type III generalized extreme value distribution would be a 'better' fit. More data could lead to more information on the goodness of fit. Therefore generating more wind speed data is recommended. This could be achieved by longer measurements (which is time-consuming in practice) or a different block duration, e.g. two extremes per year instead of only one.
- Sampling uncertainties were accounted for in a rather simplistic manner by means of the non-parametric bootstrap design-point method. This only results in rough indications of these uncertainties and could lead to conservative reliability results. Other methods of accounting for these uncertainties, e.g. Bayesian updating, should be investigated and compared to the method used in current research.
- For the purpose of this research, choice was made to use a linear cantilevered beam finite element model as this was found sufficient for the evaluation of global response coefficients at foundation level. The beam model only allows for evaluation of the responses of the structure at foundation level. Responses at other levels of the main bearing structure should be evaluated with a different (and more detailed), possibly 3D, finite element model.
- Last, for the purpose of this research only alongwind buffeting response was considered. For further research it is recommended to investigate other responses, like across-wind and torsional responses as well. Thereby, load combinations and evaluation of governing wind directions for these combinations should also be subject of further research as it was found in literature that these load combinations could be governing for design.

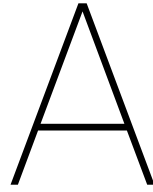
Bibliography

- CEB. Vibration problems in structures: practical guidelines. Comité Euro-International du Béton, 1991.
- Stuart Coles. *An Introduction to Statistical Modeling of Extreme Values*. Springer, 2001.
- N. J. Cook and J. R. Mayne. Towards better estimation of extreme winds. *Journal of Wind Engineering and Industrial Aerodynamics*, 9:295–323, 1982a.
- N. J. Cook and J. R. Mayne. Further development of a working approach to the assessment of wind loads for equivalent static design. *Journal of Wind Engineering and Industrial Aerodynamics*, 9:389–392, 1982b.
- N.J. Cook. *The Designer's Guide to Wind Loading for Building Structures, Part 1*. Building Research Establishment, Butterworths, 1985.
- N.J. Cook. *The Designer's Guide to Wind Loading for Building Structures, Part 2*. Building Research Establishment, Butterworths, 1990.
- N.J. Cook and J.R. Mayne. A novel working approach to the assessment of wind loads for equivalent static design. *Journal of Industrial Aerodynamics*, 4:149–164, 1979.
- N.J. Cook and J.R. Mayne. A refined working approach to the assessment of wind loads for equivalent static design. *Journal of Wind Engineering and Industrial Aerodynamics*, 6:125–137, 1980.
- R.D. Cook. *Finite Element Modeling for Stress Analysis*. John Wiley & Sons, 1995.
- A.G. Davenport. The application of statistical concepts to the wind loading of structures. In *Proceedings Institution of Civil Engineers*, number 19, pages 449–472, London, UK, 1961.
- A.G. Davenport. The buffeting of large superficial structures by atmospheric turbulence. *Annals New York Academy of Sciences*, 1964.
- A.G. Davenport. Gust loading factors. *Journal of the Structural Division, ASCE.*, 93(3):11–34, 1967.
- A.G. Davenport. On the assessment of the reliability of wind loading on low buildings. *Journal of Wind Engineering and Industrial Aerodynamics*, 11:21–37, 1983a.
- A.G. Davenport. The relationship of reliability to wind loading. *Journal of Wind Engineering and Industrial Aerodynamics*, 13:3–27, 1983b.
- A.G. Davenport. Proposed new international (iso) wind load standard. Presented at WERC Mid-Term Symposium on High Winds and Building Codes/Standards, Kansas City, November 1987.
- DIANA. *DIANA FEA User's Manual - Release 10.1*. DIANA FEA BV, 2016.
- C. Dyrbye and S.O. Hansen. *Wind Loads on Structures*. John Wiley & Sons, New York, 1999.
- C.P.W. Geurts. *Wind-induced pressure fluctuations on building façades*. phdthesis, Technische Universiteit Eindhoven, 1997. URL <https://doi.org/10.6100/IR495154>.
- S.O. Hansen. Wind actions on structures - uncertainties and bias of eurocode estimates. Workshop CEN/TC250/WG7: Partial safety factors for wind actions.
- S.O. Hansen. *Fifty Years of Wind Engineering: Prestige Lectures from the Sixth European and African Conference on Wind Engineering*, chapter Wind Loading Design Codes, pages 35–68. University of Birmingham, 2012.
- M. Holický. *Introduction to Probability and Statistics for Engineers*. Springer, 2013.

- J.D. Holmes. Equivalent time averaging in wind engineering. *Journal of Wind Engineering and Industrial Aerodynamics*, 72:411–419, 1997.
- J.D. Holmes. *Wind Loading of Structures*. Spon Press, New York, 2001.
- N. Isyumov. Alan g. davenport's mark on wind engineering. *Journal of Wind Engineering and Industrial Aerodynamics*, (104–106):12–24, 2012.
- JCSS. Probabilistic model code, part 2: Loads, 2001.
- M. Kasperski. Design wind loads for a low-rise building taking into account directional effects. *Journal of Wind Engineering and Industrial Aerodynamics*, 95:1125–1144, 2007.
- M. Kasperski. Specification of the design wind load - A critical review of code concepts. *Journal of Wind Engineering and Industrial Aerodynamics*, 97:335–357, 2009.
- H. Kawai. Pressure fluctuations on square prisms - applicability of strip and quasi-steady theories. *Journal of Wind Engineering and Industrial Aerodynamics*, 13:197–208, 1983.
- D.K Kwon, A. Kareem, R. Stansel, and B.R. Ellingwood. Wind load factor for dynamically sensitive structures with uncertainties. *Engineering Structures*, 103:53–62, 2015.
- T.V. Lawson. The design of cladding. *Building and Environment*, 11:37–38, 1976.
- M. D. McKay, W.J. Conover, and R.J. Beckman. A comparison of three methods for selecting values of input variables in the analysis of output from a computer code. *Techometrics*, 21:239 – 245, 1979.
- N.E. Meinen. A reliability based assessment of the partial factor for wind loads in the eurocode framework. Master's thesis, Delft University of Technology, 2015.
- N.E. Meinen, R. D. J. M. Steenbergen, C. P. W. Geurts, and C. A. van Bentum. Probabilistic assessment of wind-loaded façade elements. 14th International Probabilistic Workshop, August 2016.
- C.W. Newberry, K.J. Eaton, and J.R. Mayne. The nature of gust loading on tall buildings. In *Proceedings from the Second International Conference on Wind Effects on Buildings and Structures.*, volume 1, Ottawa, 1967.
- C.W. Newberry, K.J. Eaton, and J.R. Mayne. Wind loading on tall buildings - further results from royex house. *Industrial Aerodynamics Abstracts*, 4(4), 1973.
- J. Roesset, S.T. Wang, L. Vasquez, and H. Fadaifard. *Dynapile 2016 - User's Manual: Dynamic analysis of pile and drilled shafts under dynamic loading*. ENSOFT, INC., 3003 W. Howard Lane, Austin Texas, 2016.
- K.B. Rojani and Y. Wen. Effect of estimation and sampling errors in distributions of extreme wind on structural reliability. *Engineering Structures*, 2:237–243, October 1980.
- G. Solari. Along wind response estimation: closed form solution. *ASCE Journal of the Structural Division*, 108(1):225–244, 1982.
- G. Solari. Equivalent wind spectrum technique: theory and applications. *ASCE Journal of the Structural Division*, 114(6):1303–1323, 1988.
- G. Solari. Gust buffeting. i: peak wind velocity and equivalent pressure. *Journal of Structural Engineering*, 119(2):365–382, 1993a.
- G. Solari. Gust buffeting. ii: dynamic along wind response. *Journal of Structural Engineering*, 119(2):383–398, 1993b.
- G. Solari. Evaluation and role of damping and periods for the calculation of structural response under wind loads. *Journal of Wind Engineering and Industrial Aerodynamics*, 59:191–210, 1996.
- G. Solari and F. Tubino. *Wind effects on buildings and design of wind-sensitive structures.*, chapter Dynamic approach to the wind loading of structures: Alongwind, crosswind and torsional response., pages 137–166. SpringerWienNewYork., 2007.

- R.D.J.M Steenbergen, A.C.W.M. Vrouwenvelder, and C.P.W. Geurts. The use of Eurocode EN1991-1-4 procedures 1 and 2 for building dynamics, a comparative study. *Journal of Wind Engineering and Industrial Aerodynamics*, 107–108:299–306, 2012.
- P Stoica and R. Moses. *Spectral Analysis of Signals*. Prentice hall, Inc., 2005.
- Y. Tamura, H. Kikuchi, and K. Hibi. Peak normal stresses and effects of wind direction on wind load combinations for medium-rise buildings. *Journal of Wind Engineering and Industrial Aerodynamics*, 96:1043–1057, 2008.
- fib* SAG 7. Reliability assessment of existing structures. cross reference.
- J. W. Verkaik. Documentatie windmetiwind in nederland. Koninklijk Nederlands Meteorologisch Instituut Klimatologische Dienst, januari 2001.
- J. Wieringa. Updating the davenport roughness classification. *Journal of Industrial Aerodynamics*, 41(13): 357–368, 1992.
- Y. Zhou and A. Kareem. Gust loading factor: new model. *Journal of Structural Engineering*, 2:168–175, 2001.

Appendices



Basics on structural reliability

A.1. General

In structural reliability calculations the probability of failure of a structure is searched for. Therefore a limit state function is formed:

$$Z = R - S \tag{A.1}$$

Failure occurs when $R < S$, or when $Z < 0$ and the probability of failure is then given by: $P_f = P(Z < 0)$. Z is a function of multiple n stochastic variables X . For simple (one-dimensional) problems this probability of failure can be analytically calculated by integration of the n -dimensional combined probability density function, which is visualized in figure ?? on page ??.

$$P_f = \int_{Z < 0} f_X(X) dX \tag{A.2}$$

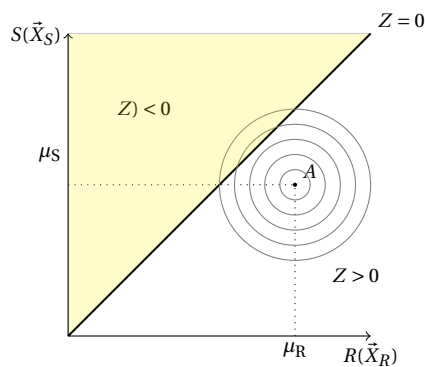


Figure A.1: Two-dimensional combined probability density function with limit state function

For more complex problems equation (A.2) can be elaborated using several methods with a different level of accuracy and complexity. These methods will be explained further on in this chapter. To gain insight on the measure of safety and to compare structures more easily one has defined the reliability index. This index is directly related to the probability of failure through the cumulative normal distribution:

$$P_f = \Phi(-\beta) \tag{A.3}$$

A.2. Level III methods

Level III methods of reliability calculation evaluate the integral of equation (A.2) on the preceding page explicitly. For up to two-dimensional problems this can easily be done through numerical integration, even for nonlinear limit state functions Z . However, for more dimensional problems this is rather difficult. Therefore for these situations Monte-Carlo simulations are used, which generate random samples. Of these random samples it is evaluated if $Z < 0$ and the probability of failure is calculated through the following equation in case that number of samples $N \rightarrow \infty$.

$$P_f = \frac{1}{N} \sum_{j=1}^N I(Z < 0) \quad (\text{A.4})$$

To improve this simulation and reduce the number of required samples for an accurate calculation several techniques are available. However, these methods will not be explained, so reference is made to other literature.

A.3. Level II methods

Level II methods make use of linear limit state functions. When this function is not linear, it will be linearized in a carefully chosen point, which is often called the design point. Thereby the stochastic random variables are considered to be normally distributed. When this is not the case, a normal distribution is adopted that represents the original one the 'best'. So for nonlinear limit state functions and non-normally distributed random variables the probability of failure using a Level II method is approximated.

If Z is a linear combination of random variables X_i (multiplied with constants a_i), the mean of Z , μ_Z is a linear combination of the mean values of X_i , μ_{X_i} (multiplied with constants a_i). The standard deviation of Z is given by:

$$\sigma_Z = \sqrt{\sum_{i=1}^n \sum_{j=1}^n a_i a_j \text{Cov}(X_i, X_j)} \quad (\text{A.5})$$

If the base variables X_i are normally distributed, Z is also normally distributed. The probability of failure is then calculated using the standard normal distribution:

$$P_f = \Phi\left(\frac{-\mu_Z}{\sigma_Z}\right) \quad (\text{A.6})$$

And the reliability index is defined by:

$$\beta = \frac{\mu_Z}{\sigma_Z} \quad (\text{A.7})$$

In case of nonlinear limit state functions, these functions are linearized around the design point by a Taylor expansion. In case of non-normally distributed random variables, these variables will be transformed to normally distributed variables by setting the probability density function and cumulative probability distribution function of the real and approximated function equal in the design point.

One advantage of the Level II methods is the direct formulation of the design point as the 'the most probable point of failure'. An other advantage is the direct formulation of sensitivity factors, which are a measure for the relative importance of the standard deviation of a basic variable to the reliability index. The general definition of the sensitivity factors α_i is:

$$\alpha = \frac{\sigma_{X_i}}{\sigma_Z} \quad (\text{A.8})$$

A property of the sensitivity factors α_i is that; $\sum \alpha_i^2 = 1$.

A.4. Level I methods

For Level I procedures standardized reliability indices β and sensitivity factors α_i are formulated. The latter for both strength and resistance parameters and for both dominant and remaining parameters. The design value of the parameters is then derived by:

$$X_i^* = \mu_{X_i} + \alpha_X \beta \sigma_{X_i} \quad (\text{A.9})$$

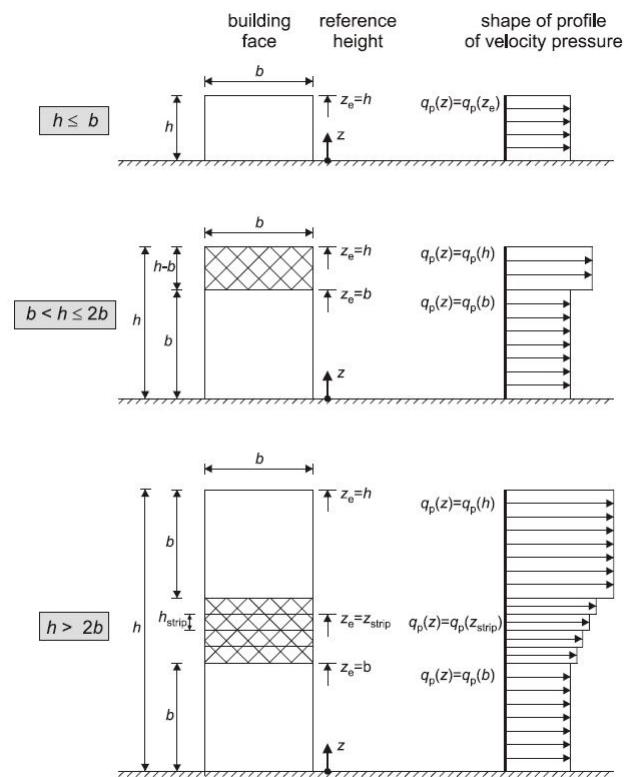
Therefore these Level I methods are not used to derive a probability of failure, but are very useful to derive design values for e.g. code practice.

A.5. Comparison Level III and Level II methods

Like discussed before Level III methods converge for a high number of samples and therefore provide accurate results for the probability of failure P_f . Also complex limit state functions and individual parameter distributions can be evaluated. However, for high accuracy in small failure probabilities a large number of simulations needs to be performed, even when using 'variance reducing' techniques. Therefore large computation effort is required. Thereby, Level III methods do not provide direct insight in design values and the effect on the failure probability of the individual parameters by means of the sensitivity factors. Level II methods do provide this direct insight. An other advantage is that the Level II methods are relatively fast compared to the Monte-Carlo simulations of the Level III methods. However, for nonlinear limit state functions and non-normally distributed random variables only an approximation of the probability of failure is provided. Therefore, this should be carefully addressed in the analysis.

B

Figures to EN1991-1-4



NOTE The velocity pressure should be assumed to be uniform over each horizontal strip considered.

Figure B.3: Reference height, z_e , depending on h and b , and corresponding velocity pressure profile (Figure 7.4 EN-1991-1-4)

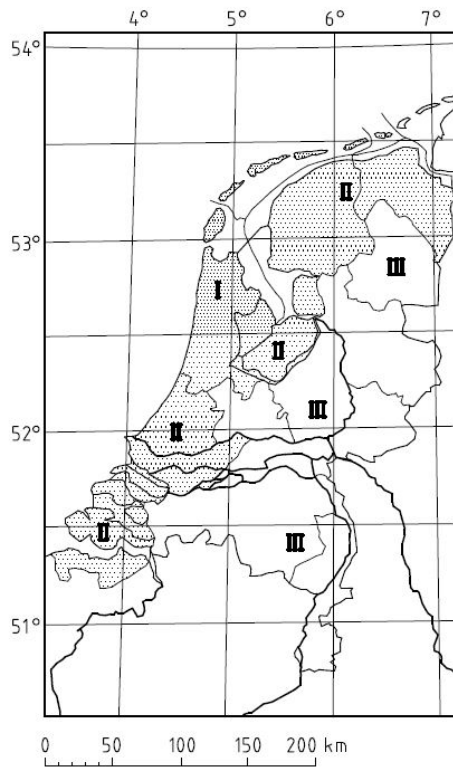
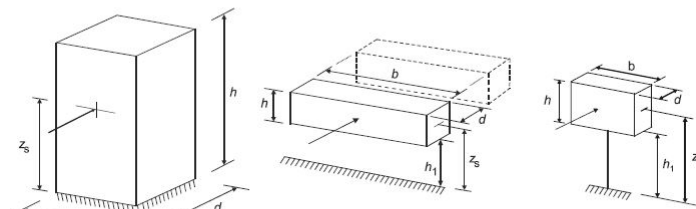


Figure B.1: Wind areas in the Netherlands, Dutch National Annex

- a) vertical structures such as buildings etc.
- b) parallel oscillator, i.e. horizontal structures such as beams etc.
- c) pointlike structures such as signboards etc.



NOTE Limitations are also given in 1.1 (2)

$$z_s = 0,6 \cdot h \geq z_{min}$$

$$z_s = h_1 + \frac{h}{2} \geq z_{min}$$

$$z_s = h_1 + \frac{h}{2} \geq z_{min}$$

Figure 6.1 — General shapes of structures covered by the design procedure. The structural dimensions and the reference height used are also shown.

Figure B.4: Reference height, z_s , for general shapes of structures covered by the design procedure to determine the structural factor (Figure 6.1 EN-1991-1-4)

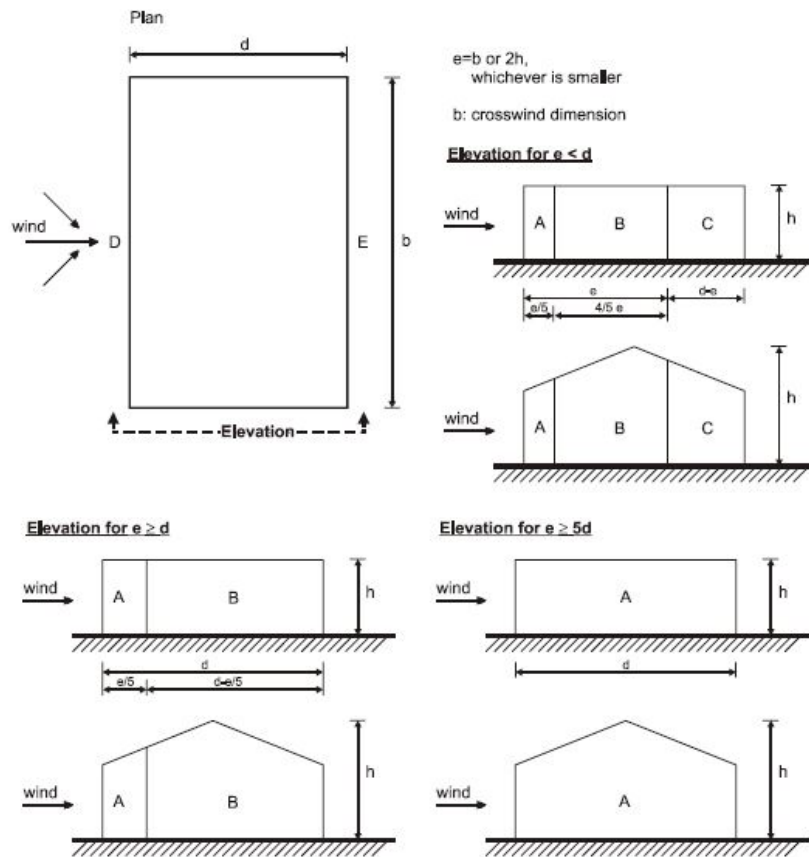


Figure 7.5 — Key for vertical walls

Figure B.2: Zonification for vertical walls (Figure 7.5 EN1991-1-4)

C

Assessment procedure Meinen (2015)

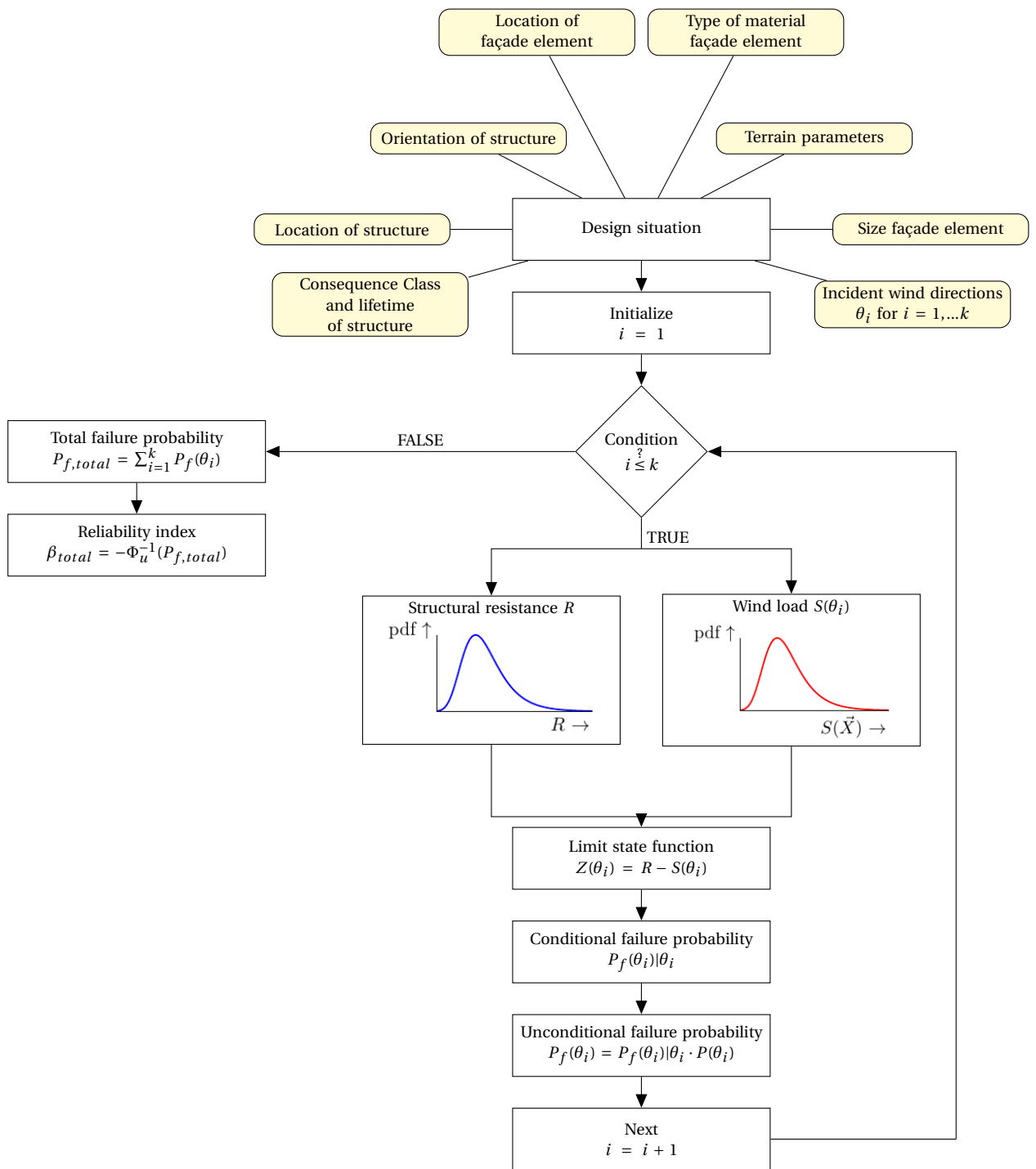


Figure C.1: Approach of assessment procedure by Meinen et al. (2016)

D

Numerical procedures

D.1. Welch's power spectral density estimation method

The power spectral density estimation method by Welch is a refined periodogram method. Using the Welch estimation method, the total sample is divided in multiple segments that are allowed to overlap. These segments are windowed to give more importance to the samples in the middle of the segment than to the two ends. Of every segment the PSD is estimated using the periodogram method and an average of the segments is used as the output PSD. The periodogram method is computed using the following:

$$\hat{S}_{xx} = \frac{1}{N} \left| \sum_{t=1}^N x(t) e^{-i\omega t} \right|^2 \quad (\text{D.1})$$

By default the total sample length is divided as close to 8 segments as possible with an overlap of 50%. A Hamming window is used to window each segment. The Hamming window is of the following shape:

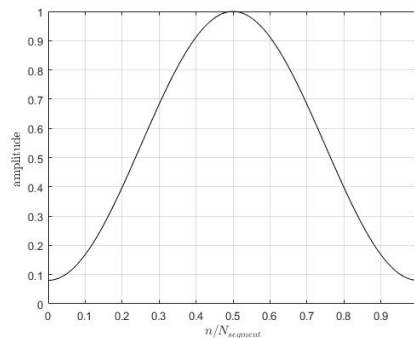


Figure D.1: Hamming window (default in Welch's PSD estimation method)

D.2. Frequency smoothing data

To smooth the data in the frequency domain an averaging procedure was followed, as proposed by Geurts (1997). This entails averaging the data over a certain frequency domain. As the data is mostly plotted on a logarithmic scale more data points are averaged over in the high frequency range than in the low frequency range. Therefore the first 12 data points are not frequency averaged, the next 12^2 points are averaged in groups of 12, the next 12^3 in groups of 12^2 etc. The averaged frequencies and spectral densities are computed as follows:

$$n_{averaged} = \frac{1}{N_{tot}} \sum_{N_i=1}^{N_{tot}} n_i \quad (\text{D.2})$$

$$S_{averaged}(n_{averaged}) = \frac{1}{N_{tot}} \sum_{N_i=1}^{N_{tot}} S(n_i) \quad (D.3)$$

An example of the result of this procedure is given in figure D.2. In this figure the normalized power spectral density of the pressures at tap 18 in the middle of the building's windward façade are plotted.

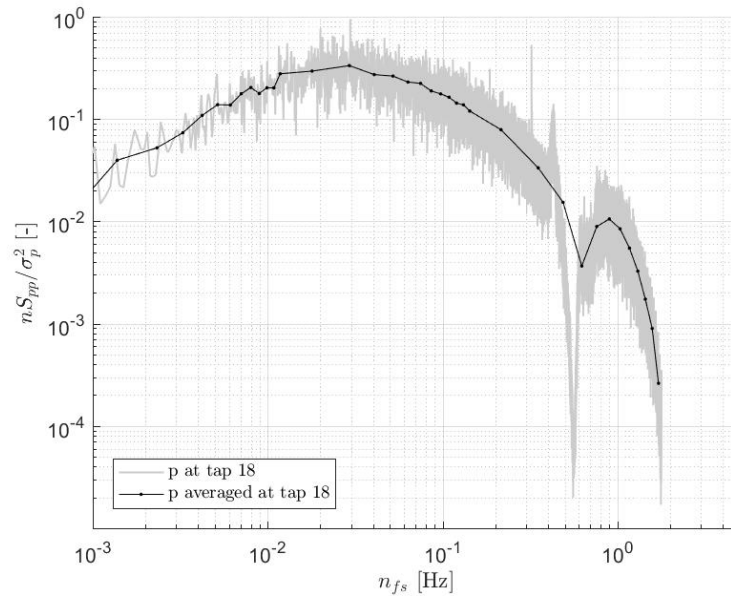
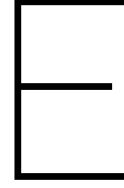


Figure D.2: Frequency averaging of power spectral density of pressures at tap 18 on the windward façade

D.3. Nonlinear least square curve fitting

Find coefficients C_i that give:

$$\min_{C_i} \sum_i (F(C_i, x_{data,i}) - y_{data,i})^2 \quad (D.4)$$



Finite element analysis

E.1. Time-dependency

Time-dependent finite element analysis requires the program to solve the following semi-discrete set of equations:

$$M\ddot{\mathbf{a}}_{n+1} + C\dot{\mathbf{a}}_{n+1} + K\mathbf{a}_{n+1} = \mathbf{f}_{n+1} \quad (\text{E.1})$$

With for $\ddot{\mathbf{a}}_{n+1}$ and $\dot{\mathbf{a}}_{n+1}$ using the trapezoidal time integration scheme:

$$\begin{aligned} \ddot{\mathbf{a}}_{n+1} &= \frac{1}{\beta\Delta t^2} (\mathbf{a}_{n+1} - \mathbf{a}_n) - \frac{1}{\beta\Delta t} \dot{\mathbf{a}}_n - \frac{1}{2\beta} \ddot{\mathbf{a}}_n + \ddot{\mathbf{a}}_n \\ \dot{\mathbf{a}}_{n+1} &= \dot{\mathbf{a}}_n + \Delta t \left((1-\gamma) \ddot{\mathbf{a}}_n + \gamma \left(\frac{1}{\beta\Delta t^2} (\mathbf{a}_{n+1} - \mathbf{a}_n) - \frac{1}{\beta\Delta t} \dot{\mathbf{a}}_n - \frac{1}{2\beta} \ddot{\mathbf{a}}_n + \ddot{\mathbf{a}}_n \right) \right) \end{aligned} \quad (\text{E.2})$$

E.2. Rayleigh damping

Rayleigh damping describes the damping matrix by a linear combination of the mass and stiffness matrices.

$$[C] = a[M] + b[K] \quad (\text{E.3})$$

The modal damping is therefore given by:

$$c_i = 2\zeta_j \omega_j = a + b\omega_j^2 \quad (\text{E.4})$$

With:

ω_j = The natural undamped circular frequency = $2\pi n_j$

ζ_j = The damping as a fraction of the critical damping

Assuming the damping ratio to remain constant for the first and second mode, the constants a and b are defined as:

$$a = \zeta \frac{2\omega_1\omega_2}{\omega_1 + \omega_2} \quad b = \zeta \frac{2}{\omega_1 + \omega_2} \quad (\text{E.5})$$

E.3. Verification dynamic model

The generalized force is derived with the use of the same measurements as the ones in the FEM model. These measurements are also scaled to pressures in full scale similarly. To derive at the generalized force using this

pressure field, the pressures are multiplied with the value of the mode shape at highest coordinate of the tributary area per pressure tap. The mode shape and eigenfrequency of the structure has been derived by means of a eigenvalue analysis in DIANA. Only the first mode will be evaluated as this is the dominant response in wind engineering.

By means of a fast Fourier transform the generalized load spectrum is derived. Using random vibration theory, the response spectrum can be derived by multiplying the load spectrum with a transfer function (or mechanical admittance) of a SDOF system.

Integration of equation 3.10 with respect to frequency results in the mean square value of the modal coordinate. As long the value of the response for a unit value of the modal coordinate is known, the mean square of the response can be derived:

$$\bar{r}'^2 = \sum_{j=1}^N \bar{a}_j'^2 R_j^2 \quad (\text{E.6})$$

With:

\bar{r}'^2 = Mean square value of the response

R_j = Response for a unit value of the modal coordinate

Again only the first mode will be considered, so only the response to a unit value of the modal coordinate for the first mode will have to be evaluated. This has been done with the use of the FEM model.

For the case study the modal shape in table E.1 is derived with the use of the finite element model.

Table E.1: Mode shape first eigenmode

z [m]	ϕ_1 [-]
118.75	0.9391
100	0.7679
80	0.5490
60	0.3437
40	0.1722
20	0.0486

The graphs in figures E.1, E.2 and E.3 show the spectral density of the generalized force, the mechanical admittance function and the response spectrum of the modal coordinate respectively.

The response spectrum clearly shows an extra peak around the eigenfrequency of the building. The mean square of the modal coordinate is determined by evaluating the area underneath the graph. The displacement response of the simple beam model in DIANA is also included. It can be seen that both spectra are quite similar. Only in the higher frequency region there is a significant deviation.

It should be noted that only the first 15000 time steps of measurements are used as only these time steps are currently used in the FEM model. This sample size agrees with about an hour in full scale. Of these 15000 time steps the first 100 steps are left out as figure 7.8 clearly shows a disturbance at the start of the loading sequence. The mean square of the response at the base of the FEM model is determined including (Rayleigh) damping of the material. The results are compared to the mean square of the base bending moment calculated by means of random vibration theory.

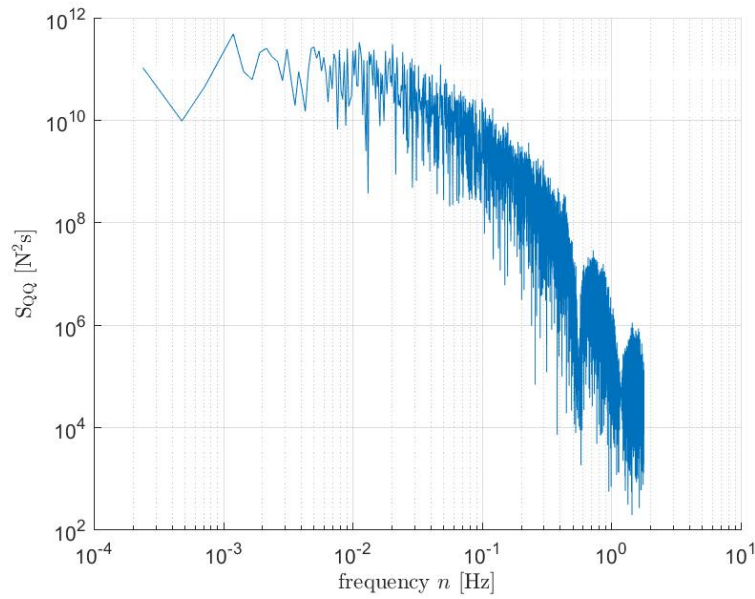


Figure E.1: Spectral density function of the generalized force derived from the wind tunnel measurements.

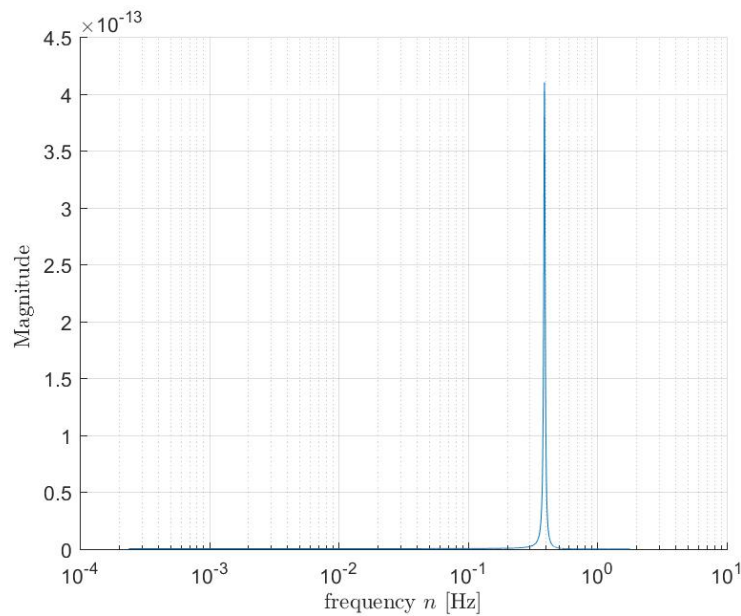


Figure E.2: Mechanical admittance function for the first mode of a SDOF system

Table E.2: Standard deviation of the base bending moment

Analysis	\bar{r}' [Nm]	Percentage of SDOF value
SDOF system	$3.69 \cdot 10^7$	-
FEM model with (Rayleigh) damping	$3.45 \cdot 10^7$	94%

E.4. Time-series of response

E.4.1. Step 2

In figure E.4 the time series of the base bending moment for the first few minutes are presented including the more detailed model of step 2. Only a small deviation can be noticed in this part of the response between the simple and the more detailed dynamic model.

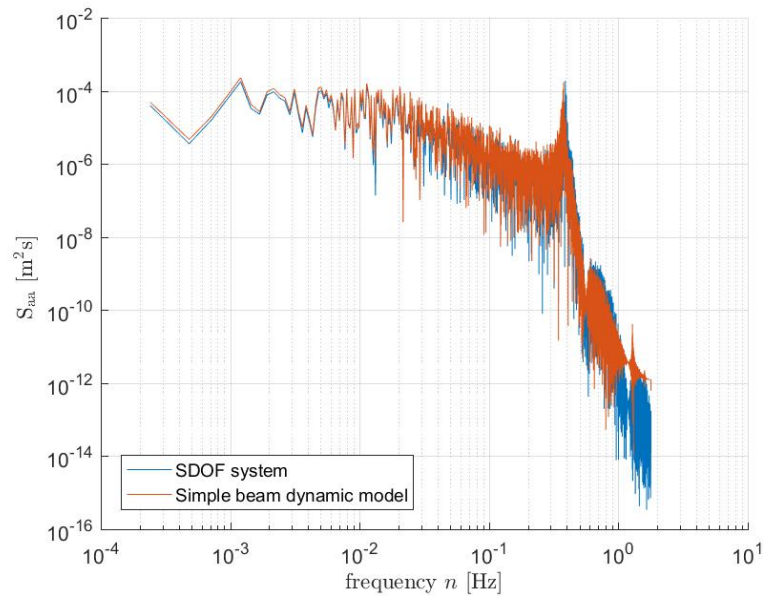


Figure E.3: Spectral density function of the response modal coordinate of a SDOF system and of the top displacement of the simple beam model in DIANA

Table E.3: Standard deviation of the top displacement

Analysis	\bar{x} [mm]	Percentage of SDOF value
SDOF system	4.3	-
FEM model with (Rayleigh) damping	4.5	105%

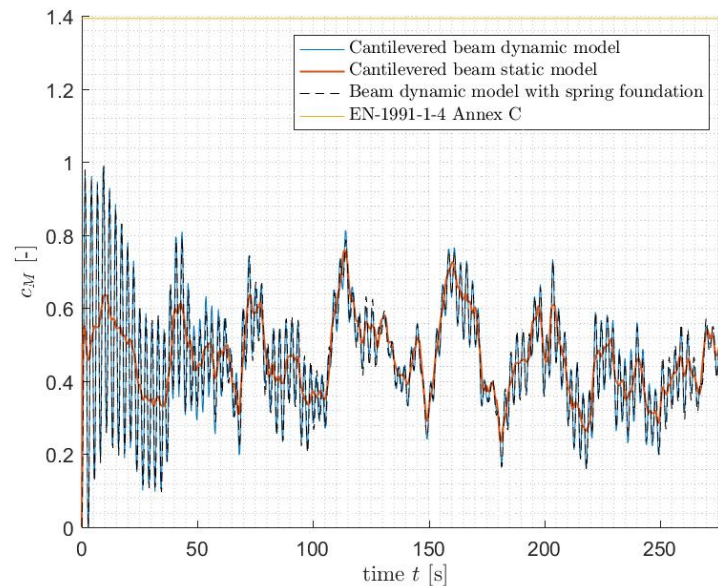


Figure E.4: Timeseries for the static model, the simple dynamic model and dynamic model of step 2

E.4.2. Step 3

In figure E.5 the base bending moment coefficients are also shown for a rotational spring foundation. Again the results are similar, because the natural frequency is again similar.

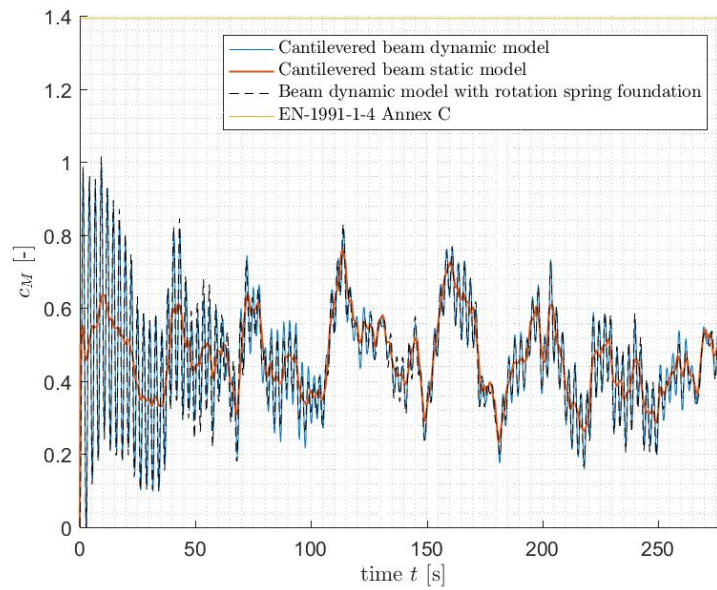


Figure E.5: Timeseries for the static model, the simple dynamic model and dynamic model of step 3

E.4.3. Timoshenko

In figure E.6 the base bending moment coefficients are also shown for the Timoshenko beam elements. Again the results are similar, because the natural frequency is again similar.

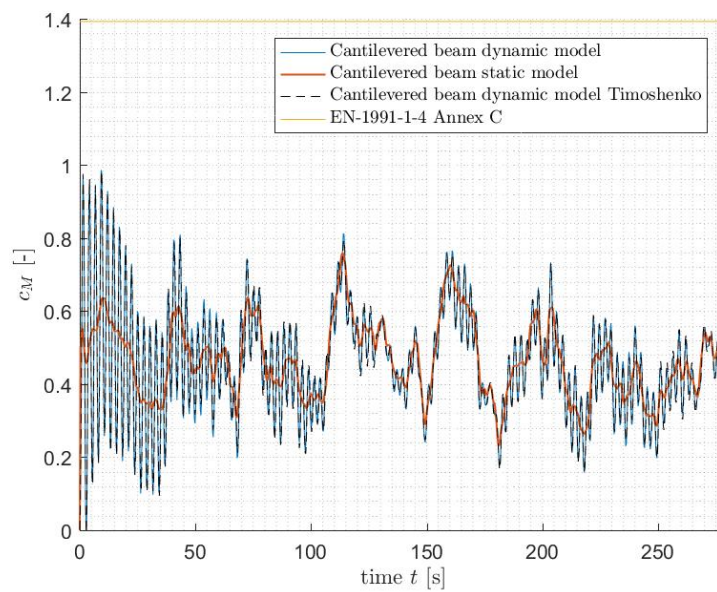
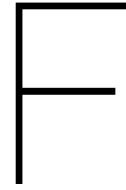


Figure E.6: Timeseries for the static model, the dynamic model and dynamic model with Timoshenko beam elements



Derivation response coefficients

F.1. Cross-correlation pressure coefficients on wind- and leeward façade

In figure E.1a the cross-correlation between the middle tap and the other taps at the windward face are shown. It can be seen that the pressures are well related within the tributary area. The cross correlation of a pressure tap at the corner of the façade with the other taps at the windward face is plotted in figure E.1b. Also at the edges of the building high correlations can be found within the tributary area of the tap considered.

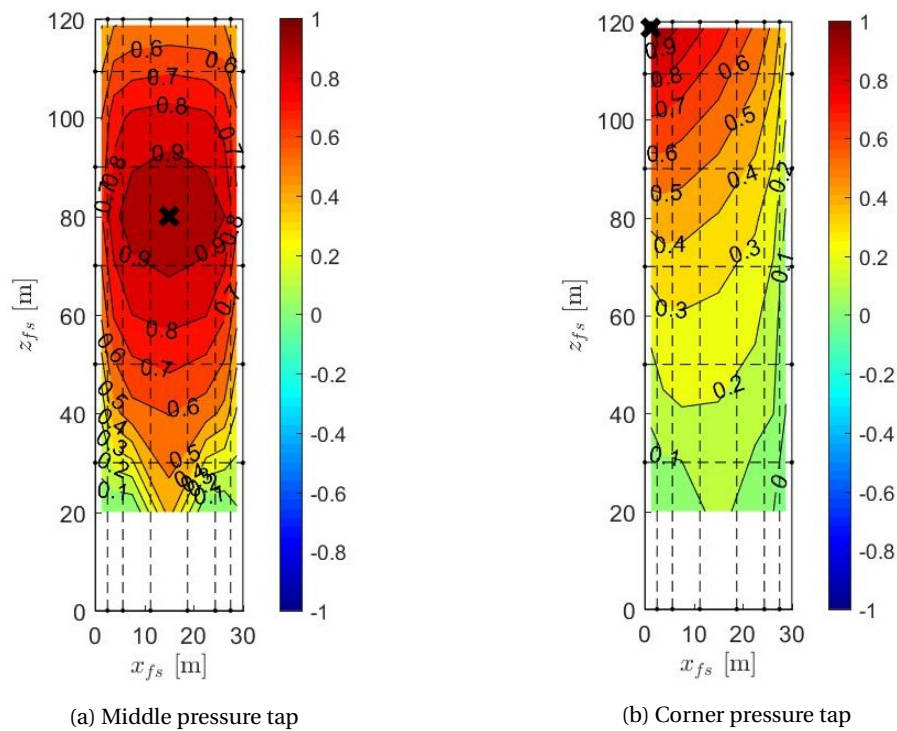


Figure E.1: Contourplot of cross-correlations of one pressure tap with the other taps at the windward face of the case study building

In figures E.2a and E.2b it can be seen that even though pressures at the leeward face of the building are less correlated, still sufficient high correlations can be found within the tributary areas ($R_{xy} = 0.7 - 0.8$).

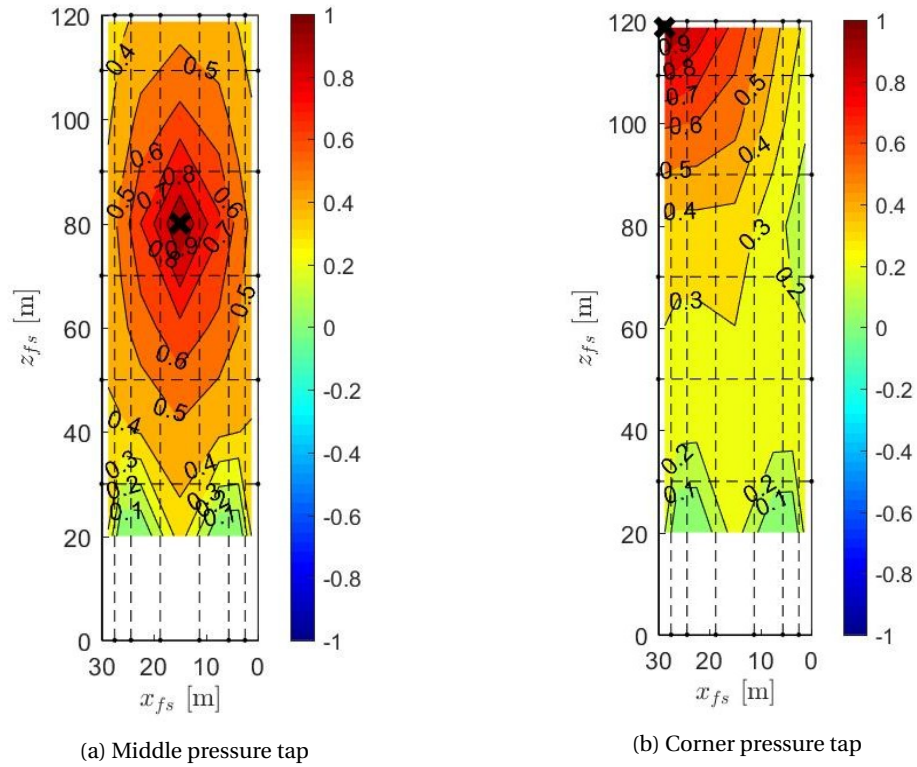


Figure E2: Contourplot of cross-correlations of one pressure tap with the other taps at the leeward face of the case study building

F.2. Autocorrelation base shear coefficients

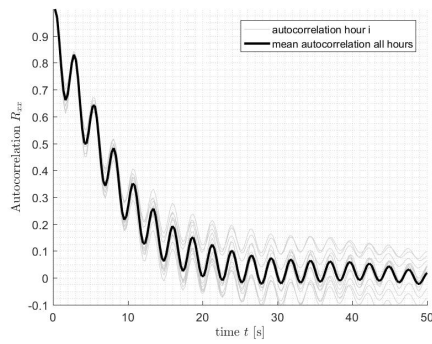


Figure F3: Autocorrelation of the dynamic base shear coefficients

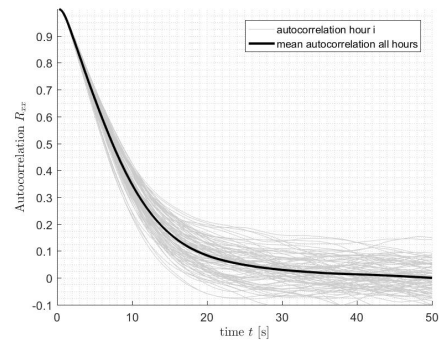


Figure F4: Autocorrelation of the static base shear coefficients



Input DynaPile

G.1. Pile properties

The case study by Meiring (2016) is taken as representative for the case study building at Schiphol. The foundation of the Erasmus Medisch Centrum is considered representative as this is a 114 [m] high building with a concrete skeleton and comparable soil layers are found in both locations.

Table G.1: Pile properties

Property	Value	Unit
Radius	0.254	m
Cross section area	0.202683	m ²
Moment of inertia	0.003269	m ⁴
Mass density	2300	kg/m ³
Poisson ratio	0.2	-
Damping ratio	0.005	-
Elastic modulus	30000000	kN/m ²
Pile length	20	m

G.2. Soil properties

For the soil properties a cone penetration test was chosen that was considered for the ground profile around Schiphol. This has been determined with the use of Dinoloket.

Layer 1: Silt

Layer thickness	6.5	m
Number of sublayers	4	-
Shear wave velocity	140	m/s
Poisson ratio	0.3	-
Mass density	2100	kg/m ³
Damping ratio	0.02	-

Layer 2: Peat

Layer thickness	0.5	m
Number of sublayers	1	-
Shear wave velocity	180	m/s
Poisson ratio	0.35	-
Mass density	1200	kg/m ³
Damping ratio	0.02	-

Layer 3: Sand fine

Layer thickness	1.0	m
Number of sublayers	2	-
Shear wave velocity	220	m/s
Poisson ratio	0.3	-
Mass density	2000	kg/m ³
Damping ratio	0.01	-

Layer 4: Sand dense

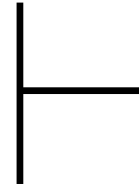
Layer thickness	3.0	m
Number of sublayers	5	-
Shear wave velocity	310	m/s
Poisson ratio	0.3	-
Mass density	2000	kg/m ³
Damping ratio	0.01	-

Layer 5: Sand medium

Layer thickness	6.5	m
Number of sublayers	9	-
Shear wave velocity	290	m/s
Poisson ratio	0.3	-
Mass density	2000	kg/m ³
Damping ratio	0.01	-

Layer 6: Sand dense

Layer thickness	7.5	m
Number of sublayers	9	-
Shear wave velocity	360	m/s
Poisson ratio	0.3	-
Mass density	2000	kg/m ³
Damping ratio	0.01	-



Definition stochastic parameters

H.1. Roughness factor

The roughness factor in the stochastic wind load effect model is determined using the EN1991-1-4 formula in figure 2.8 on page 13. Where z_e is the reference height for the determination of the roughness factor for base bending moment and shear. In EN1991-1-4 the roughness factor is determined for all heights and together with the pressures integrated over the height to reach equivalent loading at the base of the structure. However, in this research one value has to be found that is representative for type of loading. This is achieved by determining the equivalent response factor using EN1991-1-4 procedures and evaluating the required reference height for c_r to reach similar loading values at the base as for the original integration method. This results in a reference height for the base bending moment of $2/3h$ and for base shear of $1/2h$. For the case study $z_0 = 0.8$ m and $z_{0,II} = 0.03$ m. The mean value of the squared roughness factor (input for the analysis) and coefficient of variation are determined by, $\mu_{c_r^2} = 0.8c_r(z_e)^2$ and $COV_{c_r^2} = 0.15$, respectively (see chapter 8). The input values for the roughness factor are given in table H.1.

Table H.1: Model parameters of the stochastic description of c_r^2

	μ [-]	COV [-]
Base moment	1.03	0.15
Base shear	0.91	0.15

H.2. Resistance

The design value of the resistance is determined from the design value of the wind loading according to EN1991-1-4, like explained in §8.2. For this the formulas in figure 2.8 on page 13 are used. Input for the procedures is given in table H.2 on the following page. A pressure distribution over the height is derived for which the corresponding base bending moment and shear force are determined.

H.2.1. Level I resistance procedure

The probability of failure belonging to the determined design resistance is calculated with $\alpha_R = -0.8$ and β the minimum required reliability index, in the case for CC2 $\beta = 3.8$. The probability of non-exceedance then equals $P_f = \Phi(-\alpha_R\beta)$. Assuming a coefficient of variation $COV = 0.1$ allows for the determination of the mean response value. These parameters are transformed to parameters belonging to the lognormal distribution. The model parameters are given in table H.3 on the next page.

Table H.2: Input parameters for the EN1991-1-4 wind load model

Parameter	Value	Unit
ρ_{air}	1.25	kg/m ³
$\rho_{concrete}$	2400	kg/m ³
c_{dir}	1.0	[-]
c_{season}	1.0	[-]
c_{prob}	1.0	[-]
$v_{b,0}$	27.0	m/s
k_I	1.0	[-]
c_o	1.0	[-]
z_0	0.5	m
$z_{0,II}$	0.05	m
$c_{p,w}$	0.8	[-]
$c_{p,l}$	-0.65	[-]
A_{ref}	Strips of 5 m over h	m ²
b	30	m
h	120	m
$n_{1,x}$	$46/h = 0.38$	Hz
δ_s	0.10	[-]
δ_a	≈ 0	[-]
k_p	3.35	[-]
z_s	$0.6h = 72$	m
G_y	1/2	[-]
G_z	3/8	[-]

Table H.3: Model parameters lognormal distribution structural resistance Level I procedure

Parameter LN(X)	μ	σ
Base bending moment	20.3	0.0998
Base shear	16.2	0.0998

